Scientific Journal

PACIFIC

OCEANOGRAPHY

Volume 1, Number 1

2003

Secretariat contact:

Elena Borozdinova, Pacific Oceanography, FERHRI,
24, Fontannaya Street, Vladivostok 690990, Russia

Email: *po@hydromet.com*   Home page: *http://po.hydromet.com*

Tel: +7 (4232) 267352   Fax: +7 (4232) 269281

TABLE OF CONTENTS

INFORMATION

ARGO News

FERHRI Studies

History

FROM EDITOR

Dear colleagues,

This is the first issue of a new international, reviewed and specialized, journal "Pacific Oceanography" published in Vladivostok. Mainly, it will publish results of the recent oceanographic researches conducted in the Northwestern Pacific and its marginal seas. It will also present results of oceanography related topics.

The journal is published in the Far Eastern Regional Hydrometeorological Research Institute (FERHRI) of the Russian Federal Service on Hydrometeorology and Environmental Monitoring. For many years Russian scientists were not actively involved in the international exchange of data and investigation results. In 1960–1990s the soviet and Russian scientists carried out thousands of research marine expeditions in the Pacific and Indian oceans and in the Far Eastern seas and fulfilled many interesting theoretical and experimental works. As a rule, all the research results were published in Russian as monographs or in the departmental proceedings that were not available for the foreign communities.

The publication of "Pacific Oceanography" in English will allow the foreign communities seeing the latest scientific results of the Russian researchers. We also incorporated the historical section in the journal that will present the old selected works of the Russian Far East oceanographers.

In recent years the Russian scientists were actively cooperating with specialists from other countries, first of all, from Republic of Korea, Japan, USA and Canada. Results of joint marine expeditions and researchers published in "Pacific Oceanography" will be a good proof of the establishing international data exchange.

We invite all Russian and foreign scientists dealing with the Pacific oceanography and related topics to contribute their results to our journal. The main criteria for publishing a manuscript or a short scientific report within "Pacific Oceanography" are high quality, simplicity and urgency. We hope our journal will serve the progress in oceanography and related topics and assist the creative cooperation between the scientists all over the world.

Yuriy Volkov

DEEP CURRENTS OF THE CENTRAL SEA OF JAPAN

M.A. Danchenkov[1], S.C. Riser[2], J.-H. Yoon[3]

[1] *Far Eastern Regional Hydrometeorological Research Institute (FERHRI), Russia*
Email: danchenk@fastmail.vladivostok.ru

[2] *School of Oceanography, University of Washington, USA*

[3] *Research Institute for Applied Mechanics (RIAM), Kyushu University, Japan*

The features of deep water circulation of the central part of the Sea of Japan at the depth of 800 m are investigated by drift of float-profilers in 1999–2001. Large-scale cyclonic gyre transporting water from Hokkaido to Peter the Great Bay was revealed. Stationary cyclonic eddies are found too. One of them located in the eastern part of gyre (with the center in 42°N, 138°E) is important for the understanding of deep water circulation of the Sea of Japan as a whole.

INTRODUCTION

In present paper the deep currents in the central part of the Sea of Japan (Figure 1) are investigated. The aim of paper is to analyze recent data of float-profilers drift.

According to the basic features of bottom relief of the Sea of Japan, it can be divided into the shelf area (southern shelf and Tatar Strait), deep-water basin and Yamato Rise. Let us note that in Russia the part of the continent that limits the researched area of the sea from the north is referred to as Primorye, though in the scientific publications this coast is often incorrectly referred to as Siberia. From the east the researched area is limited by the main Japanese islands – Honshu and Hokkaido.

Generally deep-water basin is divided into three parts: Japan Basin (to the north of Yamato Rise), Tsushima Basin (to the west) and Yamato Basin (to the east). Another important features of the Japan Basin topography are Bogorov Rise situated around 39°N and 136°E and Pervenets Rise located around 41.8°N and 132.3°E.

Vertically it is possible to divide waters of the Sea of Japan, as a first approximation, into two layers. In the

upper 200-meter layer the seasonal changes of their characteristics are well noticeable, and the so-called Sea of Japan Proper, waters lower than 200 m deep are almost homogeneous within year. The currents in the upper layer have been investigated during more than 100 years and their maps are rather numerous. The currents of the Sea of Japan lower than 200 m are investigated worse and maps of deep circulation are scarce. Nan'niti (1966) investigated 4-day drift of one float at the depth of 800 m in the western part of deep basin (39.8°N, 131.7°E) from May 30 till June 3, 1966. Average speed of drift was small (1.5 cm/s).

Some maps of geostrophic currents appeared later (Figure 2). One of them presented by Ohwada and Tanioka (1972) for 500 dB level shows cyclonic circulation in the area bordered by 40°N, 44°N, 134°E and 140°E. Its center is in the point with coordinates 41°N, 136°E. The same feature of geostrophic circulation was described (Nitani, 1972) in the same area on deeper level (1,500 dB) both in summer (July 1969) and in winter (March 1971).

Measurements of currents by anchored buoys were also used to map the deep water circulation. Duration of such observations till the 80th of the last century did not exceed 15 days and the speed of deep currents was about 3 cm/s on average with maximum up to 12 cm/s (Yurasov and Yarichin, 1991). Two continuous divergence and convergence lines are shown on the map of deep currents compiled over these data. So, any water transport between Hokkaido and Primorye is admitted to be impossible (Yarichin and Pokudov, 1982).

The first map of deep currents based on long-term (multi-month) measurements by anchored systems (Kitani, 1989) has shown appreciable movements of waters only along the borders of deep basin. The average speed of currents was 1–3 cm/s (maximum up to 21 cm/s). Subsequent measurements of deep currents in 1993–1997 under the CREAMS program (Takematsu *et al.*, 1999) have shown approximately the same values.
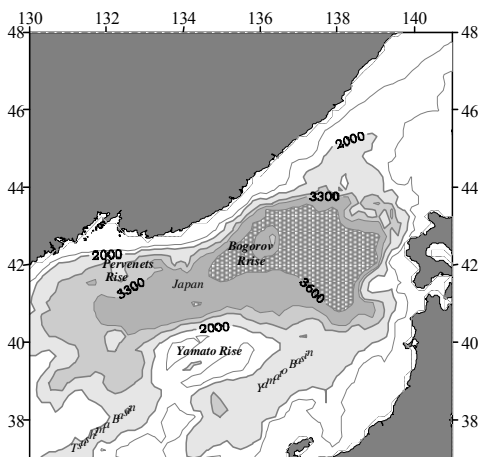
Figure 1. Bottom relief of the central Sea of Japan
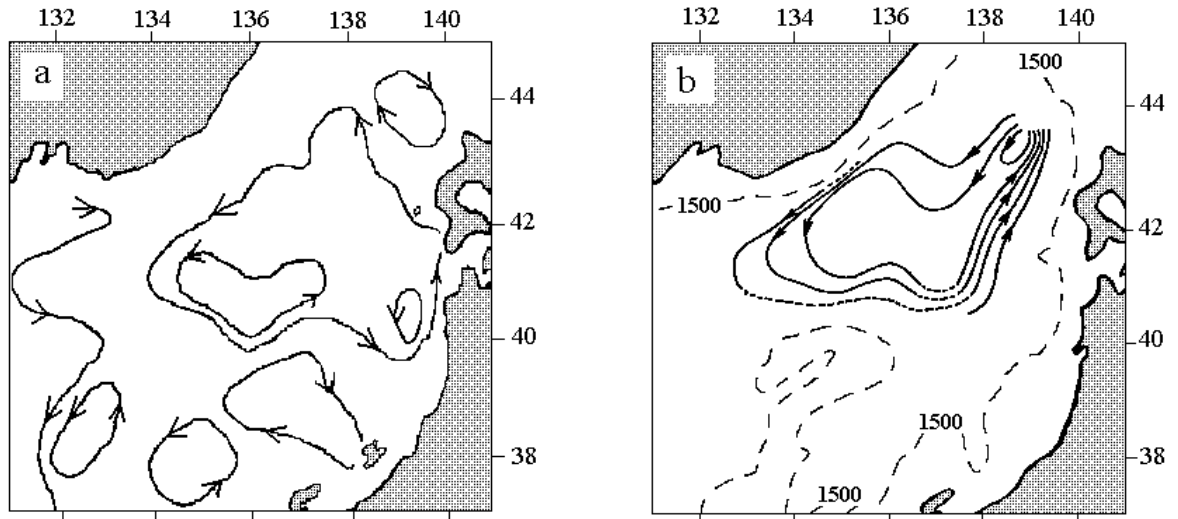
Figure 2. Geostrophic currents at 500 dB level (a) (Ohwada and Tanioka, 1972) and 1,500 dB level (b) (Nitani, 1972)

According to these data directions of deep currents (Kitani, 1989; Yurasov and Yarichin, 1991; Senjyu et al., 2001) are shown together in Figure 3. No evidence of gyre or eddies is seen.

Lagrange method of currents measurements by drifting floats was used in the Sea of Japan recently again. Drift of ALACE floats (Taira, 1997) showed two features of water dynamics at the depth of 300 m (Figure 4): southwestward current along Northwestern front (Danchenkov et al., 2000) and cyclonic eddy with the center around 42°N, 139°E. However, these features were not analyzed in details.

DATA

In the present work the data of 30 floats-profilers drifting at the depth of 800 m since August 1999 till January 2002 are used. This information is unique. The floats covered the whole researched area with a network of observations both in Russian, Korean and in Japanese economic zones. Such extensive simultaneous measurements of currents in Russian and Japanese economic zones have never been carried out before. Even the small number of floats (30) allowed to estimate deep water circulation in the largest part of the Sea of Japan during long period over 2 years.

Information on the position of floats and temperature and salinity profiles are available at the site: http://flux.ocean.washington.edu.

DEEP GYRE

The basic year-round features of deep water circulation of investigated area are basin-scale cyclonic gyre and smaller-scale cyclonic eddy in its eastern part. During two years the floats were drifting basically along the borders of cyclonic gyre (132°E–139°E, 40°N–43°N). Depending on that, floats drift to the north or to the south of Bogorov Rise
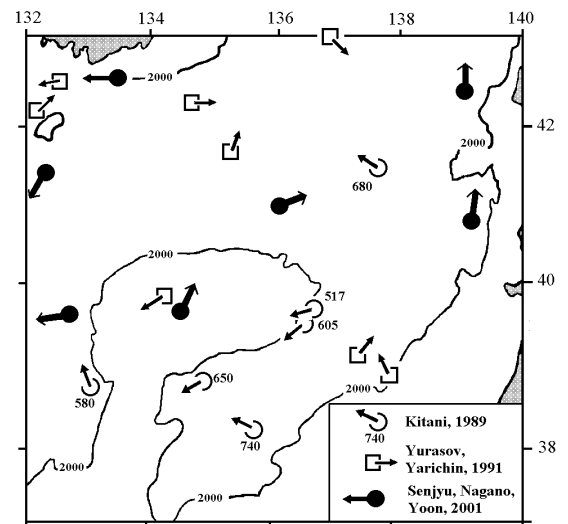
Figure 3. Average direction of residual currents in 500–1,500 m layer (the isobath of 2,000 m and the depth of measurements are indicated)
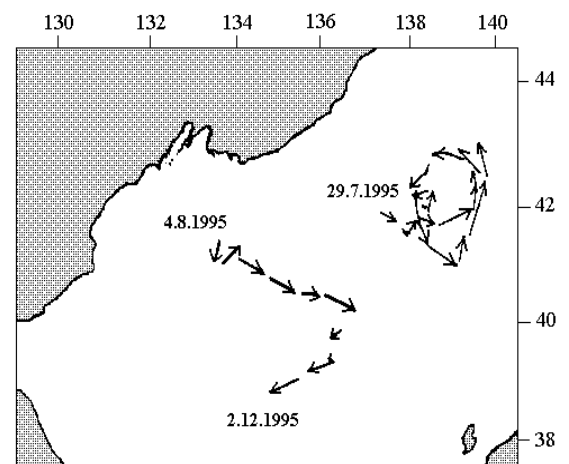
Figure 4. Drift of two ALACE floats at the depth of 300 m in 1995–1997 (Taira, 1997)
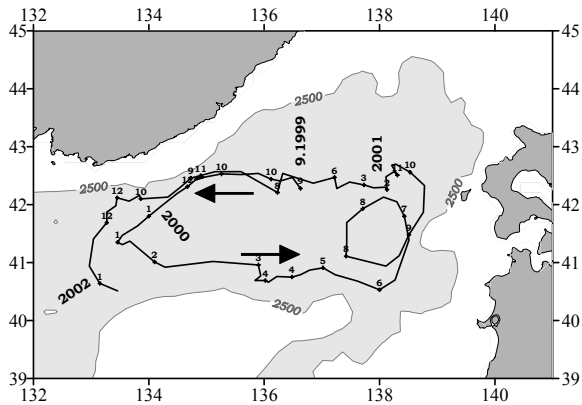
Figure 5. Trajectory of float 261 drift since September 1999 till January 2002 (monthly position of float is indicated by dots and labels)
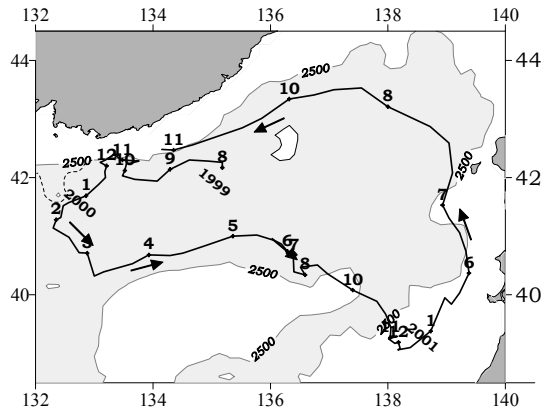
Figure 6. Trajectory of float 262 drift since August 1999 till November 2001 (isobath of 3,000 m around Pervents Rise is shown by dotted line)

where it is possible to locate the bimodality of their trajectory. The reason of two kinds of trajectory has not been clarified yet, but the eddy forcing could be one reason of it. We suppose that when the eddy is stronger, the path of float lies to the north of Bogorov Rise and when the eddy is weaker, the path lies to the south of it.

In Figure 5 the trajectory of one float drifting at the depth of 800 m during 29 months (since September 1999 till January 2002) is presented.

Two parts of deep gyre (closed circulation) can be presented as two particular deep currents: along 42.5°N (we named it "Western current") and at 41°N ("Eastern current"). The Western current transports water from Hokkaido (where the Tsushima warm current settles down at the surface) to the west while the Eastern current transports waters from Primorye to the east.

In the area between 41°N and 42°N, 137°E and 139°E a cyclonic eddy is located. The float made full rotation for 15 months (except time, when it was in the same place or bypassed the eddy). The float drifted by Western current in summer and autumn seasons while it drifted by Eastern current in spring and drifted off Primorye coast to the south only in winter. The drift of another float (Figure 6) differs from the previous one: the Western current shifted to the north (to the border of deep basin), and the Eastern current penetrated far (up to 39°N) to the south.

Superposition of 9 float trajectories shows that the cyclonic gyre can be traced to west up to 131.5°E (Figure 7). The longitude where the float trajectories turn to the southeast off Primorye coast depends on its position at the end of November.

Within the limits of considered area it is possible to allocate two areas of cyclonic activity: in the eastern and western parts of gyre (with the centers around 42°N, 138°E and 41.5°N, 133.5°E). Cyclonic eddy in the eastern part of the sea (Eastern eddy) deserves special attention.
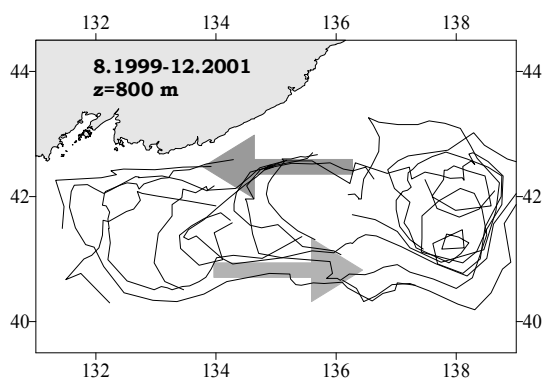
Figure 7. Trajectories of nine floats drift in 1999–2001

EASTERN EDDY

Cyclonic eddy in the eastern part of the gyre was traced by trajectories of the floats majority. Its largest diameter was about 120 miles (Figure 8).

The rotation of floats around the eddy passed within several months (from 2 up to 6). The eddy area was limited from the north, east and south by isobath of 3,500 m and by Bogorov Rise from the west. An average speed of floats drift around the eddy is about 2–3 cm/s with maximum value up to 18 cm/s observed in the southeastern part.

Sometimes the drift trajectory showed two cyclonic eddies. In this case the center of main eddy was located around 41.5°N, 138°E, and the time of the float rotation around the eddy was two months. A small eddy with diameter about 30 miles had its center located around 42°N, 138.2°E, and the time of its circulation was the same. This allows to suggest that small meanders are separated sometimes from the eddy. Eastern eddy was also presented by cyclonic circulation of ALACE float at the depth of 300 m (Figure 4) and by distribution of oceanographic parameters (Watanabe *et al.*, 2001). It was noticed in the surface layer as well.
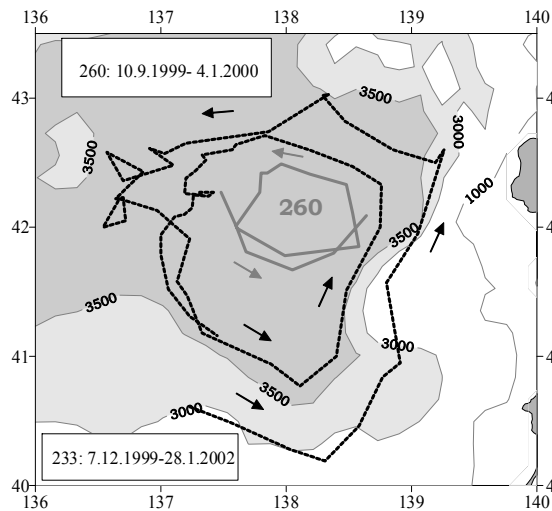
Figure 8. Drift trajectories of two floats in eastern part of the gyre

Figure 9. Trajectory of float 269 drift at 800 m deep since 20 June, 2001 till 23 January, 2002

Figure 10. Trajectory of float 266 drift since 4 August, 1999 till 12 February, 2001

On the generalized maps of surface water circulation its center is displaced to the northwest (Uda, 1934) or to the southwest (Naganuma, 1977) of the above mentioned. Last surveys (Danchenkov and Aubrey, 1999) show that the position of its center (the depth of 50 m) corresponds to the above mentioned. Thus large-scale meander of Tsushima current (for example, in September 1989) is situated to the north of the eddy.

Therefore, it is possible to conclude that the Eastern eddy is assumed to cover a layer of water at least from the depth of 50 to 800 m.

DISCUSSION

Bottom relief and trajectory of the floats. Approaching the Pervenets Rise the floats turned to the south. However, most topographic features of Japan Basin are noticeable only from the depth more than 2,500 m the floats drifting at 800 m (1,700 m higher) still follow them. In Figure 9 the turn to the south of float 269 near Bogorov Rise is evident. Similar influence of rough bottom relief was demonstrated by the drift of float 266 (Figure 10).

From the moment of its deployment the float 266 been drifting to the west before it was seized by anticyclonic movement of waters around Pervenets Rise. Having come off from it, the float followed to the south and made strange fluctuation (to the west – to the east), then it was seized by anticyclonic movement of waters toward an anonymous rise at 40°N. Having rounded it, the float followed along 2,500 m isobath. Then it stayed in the southern part of Japan Basin (at the entrance to Tsushima Basin) within 5 months and went to the southeast between two raises of bottom relief. So visually the movement of floats is strongly governed by bottom relief peculiarities.

Tongue of salt water and trajectory of drift of floats. Large-scale meander of Tsushima current off Hokkaido was revealed in distribution of water temperature and dissolved oxygen between the surface and 100 m depth (Danchenkov, Aubrey, 1999). Inside the meander waters with high temperature, high salinity and low contents of the dissolved oxygen are situated. Recently the large-scale tongue of warm and salt water was found in the central part of the Sea of Japan (between 41 and 43°N) in the layer from surface to 400 m deep (Aubrey *et al.*, 2000). Example of tongue-like distribution of sea surface temperature could be also traced on satellite images (Takematsu *et al.*, 1999). Water with higher temperature and salinity is revealed inside this tongue in winters of 1995–1999.

Presence of streams of warm deep water near southern Primorye coast was found earlier both in winter and in summer (Deryugin, 1935). Due to the influence of warm current the area to the south of Askold Island (132.3°E) is usually occupied by herds of flounder in winter (Moiseev, 1937).

Are the surface meander of Tsushima current, tongue of warm salty water and deep cyclonic gyre interconnected with each other? If to combine a position of salty tongue in March, 1999 at 50 m deep and trajectory of float 230 drift at the depth of 800 m (cyclonic rotation of float within the limits of tongue since June 2000 till April 2001 is removed), then their interconnection would be visible (Figure 11). Deep float was drifting along a periphery of the tongue. In other words, a tongue of salty water and deep gyre are under the influence of the same forces. Among possible forces the influence of bottom relief is the basic one.

Let us note that the tongue was not often traced at the surface. Usually it is traced at the depth of 50 m and below.

Many scientists concluded that Sea of Japan Proper water (JSPW) originates from southern Primorye area during the ice formation period. But no evidence of new water formation at the surface was observed. Taking into account such distribution of salt water the next mechanism of JSPW formation is possible to propose. During winter (from November till March) surface waters close to southern Primorye are cooled by strong winds from the continent. Salt subsurface waters are transported to that area by Western current. Because of heat loss the subsurface water mixed with the surface one, became colder and densee until its characteristics became the same as characteristics of JSPW (temperature is less than 0.8°C, salinity is more than 34.05 psu, density is more than 27.32).
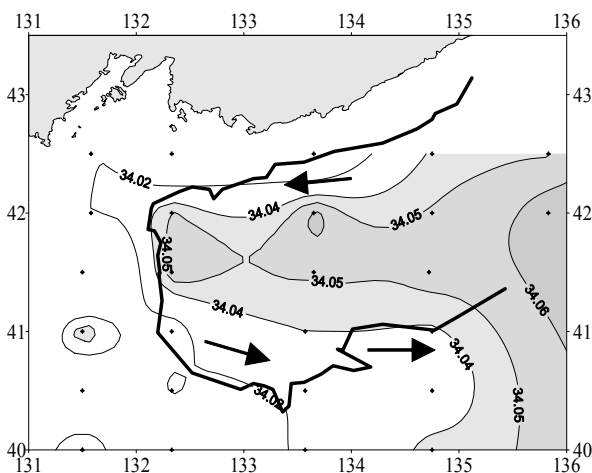
Figure 11. Tongue of salty water (depth of 50 m) in March of 1999 and trajectory (greasy line) of float 230 drift (800 m depth) since September 1999 till June 2001
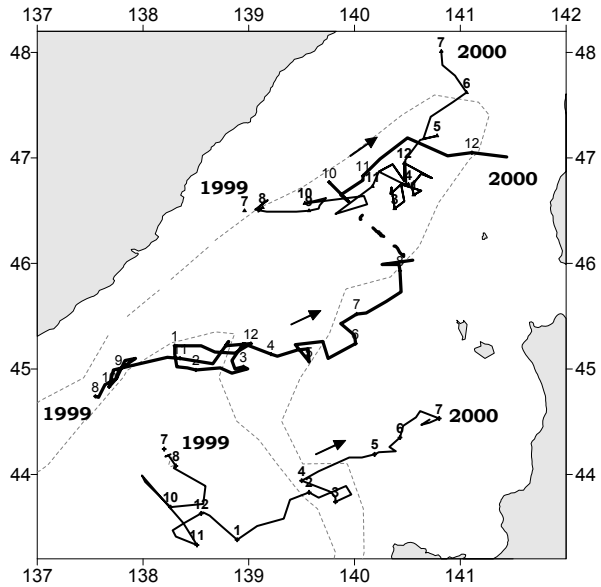
Figure 12. Drift of three floats at the depth of 800 m in the northern part of the Sea of Japan (isobaths of 1,000 m and 2,000 m are shown by dotted lines, month of eddy location is indicated)
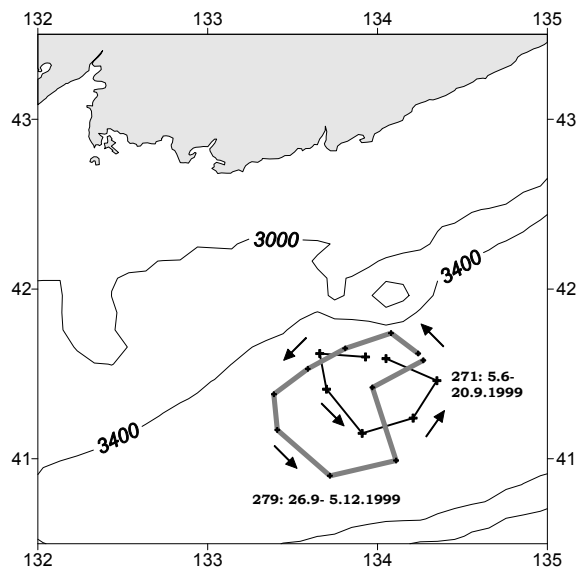
Figure 13. Cyclonic rotation of the floats in the western part of deep gyre

Northern area. To the north of considered area (between 43°N and 48°N) the floats drifted in the northeastern general direction only (Figure 12). Some northwestward drift was observed for short periods of time both during summer and winter periods. The speed of drift did not exceed 1 cm/s.

Eddies in northwestern part of the Sea of Japan. Cyclonic eddy was traced in the western part of the gyre. Its center was situated around 41.5°N, 134.0°E (Figure 13). Sometimes the size of its circulation was very large (drift of float 230 from June, 2000 till February of 2001), but usually it was about 30 miles. Another cyclonic eddy was found by drift trajectories of floats 274 and 275 from October, 1999 to March of

2000 in northwest part of the Sea of Japan. Its center was situated in point 40.7°N, 130.7°E. Some cyclonic movement was traced also around points with coordinates 40.7°N, 131.7°E (float 274 from April till July, 2000) and 41.5°N, 135.5°E (float 257 from February till August, 2000). We had no representative information to decide whether these circulations represent the same eddy or the different ones.

CONCLUSION

Large-scale cyclonic gyre and stationary eddy in its eastern part are the characteristic features of water circulation of the Sea of Japan central part. They exist throughout the year and follow the bottom relief peculiarities.

REFERENCES

Aubrey D.G., Danchenkov M.A., Riser S.C. **2001**. Belt of salt water in the north-western Japan Sea. Proc. CREAMS Int. Symposium, Vladivostok, p. 11–20.

Danchenkov M.A., **Aubrey** D.G. **1999**. Meander of the Tsushima current as possible source of the Japan Sea Proper water. CREAMS Proceedings, Fukuoka, p. 23–26.

Danchenkov M.A., Aubrey D.G., Lobanov V.B. **2000**. Spatial water structure in northwest part of the Japan Sea in winter. FERHRI Special Issue, 3, p. 92–105.

Deryugin K.M. **1935**. Works of Pacific expedition of the State Hydrological Institute in 1933. Investigations of the USSR Seas, 22, p. 5–24.

Kitani K. **1989**: Movement of the Japan Sea Proper Water. Report on Int. Conference on the Seas of Japan and Okhotsk (manuscript), Nakhodka, 5 pp.

Moiseev P.A. **1937**. Fishery of flounders by small-sizes vessels in Ussuri Bay in spring of 1935. TINRO Proceedings, 12, p. 125–158.

Naganuma K. **1977**. The oceanographic fluctuations in the Japan Sea. Kaye Kagaku, v. 9, 2, p. 137–141.

Nan'niti T., Akamatsu H., Yasuoka T. **1966**: A deep current measurement in the Japan Sea. The Oceanogr.Magazine, v. 18, p. 1–2, p. 63–71.

Nitani H. **1972**: On the deep and bottom waters in the Japan Sea. Researches in hydrography and oceanography (ed. D.Shoji). Tokyo, Hydr.Dept.of Japan, p. 151–201.

Ohwada M., **Tanioka** K. **1972**. Cruise report on the simultaneous observations of the Japan Sea in October 1969. Oceanographic Magazine, v. 23, 2, p. 47–58.

Senjyu T., Nagano Z., Yoon J.-H. **2001**. Deep flow field in the Japan Sea deduced from direct current measurements. J.Oceanography, v. 57, 1, p. 15–27.

Taira K. **1997**. Application of the ARGOS system to NEAR-GOOS. ARGOS Newsletter, 52, p. 13–15.

Takematsu M., Ostrovskii A.G., Nagano Z. **1999**. Observations of eddies in the Japan Basin interior. J.Oceanography, 55, p. 237–246.

Uda M. **1934**. Hydrographical studies based on simultaneous oceanographical survey made in the Japan Sea and its adjacent waters during May–June 1932. Records in Oceanographic Works in Japan, v. 6, 1, p. 19–107.

Watanabe T., Hirai M., Yamada H. **2001**. High salinity intermediate water of the Japan Sea. Geophysical Research, v. 106, p. 11437–11450.

Yarichin V.G., **Pokudov** V.G. **1982**. Some pecularities of water movement of the Japan Sea northward of 40°N. FERHRI Proceedings, 96, p. 111–120 (In Russian).

Yurasov G.I., **Yarichin** V.G. **1991**. Currents of the Japan Sea. 176 pp.

ON THE RELASHIONSHIP BETWEEN VOLUME TRANSPORT OF THE SUBTROPICAL AND TROPICAL GYRES IN THE NORTHWESTERN PACIFIC OCEAN

A.D. Nelezin

*V.I. Il'ichev Pacific Oceanological Institute, Far Eastern Branch of Russian Academy of Sciences
(POI FEBRAS), Russia
Email: pacific@online.marine.su*

The water transport by the main currents in the layer of 0–1,000 m is calculated by the data observed in 1967–1991 at the section of 137°E. The volume transport of the subtropical gyre (formed by the North Equatorial Current and Kuroshio) and that of the tropical gyre (formed by the North Equatorial Current and the Equatorial Counter-Current) are calculated. The trend components are distinguished. The calculated correlation coefficients show a close relationship between the volume transport of the currents forming the subtropical and tropical gyres in the Western Pacific.

INTRODUCTION

The problems of climate variability attract many researchers, including those engaged in the physical oceanography. An actual problem is the investigation of the ocean climate and its short-term variability. In the ocean there is its proper internal mechanism of redistributing the quantity of motion, heat and salt, which allows to estimate the ocean climate by the insufficiently detailed conditions on the surface (Sarkisyan, 1997). The oceans take part in forming a wide spectrum of climate variations. The climate system is most of all affected by the low-frequency variability of thermodynamic structure of waters.

The ocean climate has been studied much worse than that of the atmosphere (Monin, 1993). Today, not only a quasi-stationary long-term climate background presents interest, but also the tendencies of this background changes for several tens of years. Interdependence of the processes on a small and planetary scale is of great significance for understanding the role of the ocean trends in climate changes. Spatial-temporal diagrams (Mamaev, 1995) show that the atmosphere and the upper ocean layers present themselves the fast part of the Earth's climate system, and the deep layers – the slow one. Recently, much attention has been given to the shifts of the long-term climate parameters and their possible consequences for the marine environment. The ocean significance in the climate system is determined by the correct estimation of the meridional transport that is one of the main mechanisms of the Earth's climate formation. Thus, the monitoring of volume transport of the main currents is of great importance. With the aim of the ocean monitoring, on the basis of the available and developed methods of measurements the Global Observation System is created (Sherer and Tolkachev, 1993). Not all of the available observation data meet the needed requirements, thus making the difficulties in determining the important climate-related processes. The long-term series of oceanographic measurements are rare, and their value increases with regard to their duration (Sarkisyan, 1982).

In the Northwestern Pacific, from 1967 – in January, and from 1972 – in January and June, the regular observations have been carried out along 137°E by the Meteorological Agency of Japan from 34°N to the equator (from 1988 – to 3°N). The cross-section crosses the Kuroshio, North Equatorial Current (NEC) and Equatorial Counter-Current (ECC), which form the subtropical and tropical water gyres. The data on the spatial-temporal variability of thermodynamic structure of waters according to the regular observations along 137° are published in papers (Burkov and Kharlamov, 1985; Burkov *et al.*, 1986; Nelezin, 1981b; Nelezin, 1997; Nelezin, 1999; Kaneko *et al.*, 1998; Nagasaka, 1977; Nelezin, 1996). By the observation data of 1968–1980 the long-term variability of the water transport as a whole across the section is mainly conditioned by vibrations of the Equatorial Counter-Current (Burkov and Kharlamov, 1985). The analysis of the structure of the average long-term values of zonal constituents of geostrophic currents along 137°E for the winter and summer periods is given in (Nelezin, 1997). Calculation results (Nelezin, 1997) show the increase of the average long-term values of the main current volume transport along 137°E from winter to summer, which is manifested in less extent for the Kuroshio than for the NEC and ECC. This testifies to the strong seasonal signal of currents in the northern equatorial-tropical area of the Pacific Ocean.

It is ascertained that the subtropical and sub-arctic gyres in the Western Pacific are fluctuating in a counter-phase with the time interval of about three years, and the main components of the system vary

synchronously to each other (White, 1977). Heat inflow is the main external effect forming the rings of the general ocean circulation. Subtropical anticyclones are conditioned by the positive heat balance, and sub-polar cyclones – by the negative one. Vibrations of intensity of currents of the northern tropical gyre formed by the NPC and IPC are of great significance in the balance of the west-east water transport in a system of the equatorial-tropical circulation of the Pacific Ocean and in El-Nino formation (Nelezin, 1981a). The problem of investigating the thermodynamic parameters variability in the tropical zone of the ocean has not been solved yet by the physical oceanographers. This served the basis for the development and performance of the special TOGA Program (World Climate Research Program, 1985). Classification and generalization of the available results can be used for planning the monitoring of the most important processes in the tropical zone of the Pacific Ocean.

DATA AND METHODS

To study the variability of current volume transport of the northern tropical and sub-tropical water gyres in the Western Pacific, the data observed at the section along 137°E for the period of 1967–1991 was generalized. The observation data for the last decade are being processed. For statistical calculations two data sets were selected: for the period from 1967 to 1991 by the observation data in January, and for the period of 1972–1991 – in January and June. Results of the previous studies showed that the trend distinguishing the problem was solved in some cases quite correctly, while in most of them the initial data were not equally distributed in time. To decrease the influence of fluctuations of synoptic scale reaching considerable values along 137°E (Burkov, et al., 1986), dynamic heights calculated for the lower horizon of observations 1,000 m were smoothed by the sliding averaging. Then, the values of velocities of geostrophic currents and their volume transport were calculated in a layer of 0–1,000 m.

The margin between the gyres (being determined by the minimum of NEC velocities) is not always ascertained. So, as the value of intensity of subtropical gyre the average arithmetical value (half of a sum) of the NEC and Kuroshio volume transport was taken, and for the tropical one – the NEC and ECC. Similar approach was used in (Nelezin, 1999).

To obtain the adequate information while choosing the scales of averaging and presenting the fields as the sum of trend components and random "additions", it is necessary to know the spectral structure of hydrophysical fields of the ocean (Ozmidov, 1995). Division of hydrophysical fields into deterministic and random components is as if the studied field contains a set of structures of definite scale. Methods of spectral-correlation analysis were used to carry out studies.

RESULTS

Figure 1 presents the results of calculations of current discharges of subtropical and tropical gyres in 1967–1991. The average long-term (for the given period) value of the subtropical gyre intensity – 54.8 Sv (1 Sv = 10^6 m³/s) is higher than that of the tropical one (49.4 Sv), and the minimal values were obtained in 1972 (36 and 35 Sv correspondingly). Temporal motion of gyre volume transport for a 25-year period shows the strong relationship between them, the correlation coefficient making 0.73. The trends calculated by a linear model show the uni-directed tendencies. They are more vividly exhibited against the background of the curves smoothed according the model of sliding average (correlation coefficient makes 0.83). Residual curves, upon separation of trend components (Figure 1c), testify to the high level of correlation between the long-term changes of intensity of the sub-tropical and tropical water gyres (0.87). For the vibrations of the gyre volume transport the periods of 4.8 and 6 years were distinguished.
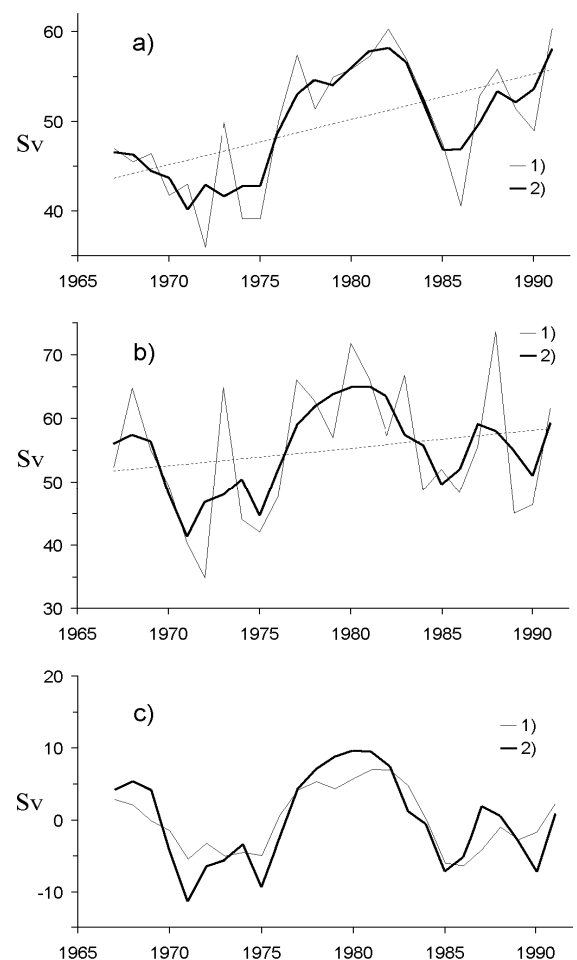
Figure 1. Temporal motion of current volume transport (10^6 m³/s) of subtropical (a) and tropical (b) water gyres at the Section of 137°E in 1967–1991; residual curves (c) of volume transport of subtropical (1) and tropical (2) gyres after filtration and separation of trend components

Figure 2 presents a temporal motion of the current volume transport of the studied water gyres by the observation data in January and June. During 1972–1991 the larger changes of the water gyres intensity were observed, they were conditioned, for the first turn by seasonal differences which were most exhibited in 1972. Total length of series made 40 realizations, with this length of series the calculated correlation coefficient (0.53) is significant. For the curves smoothed by the model of seasonal motion the correlation coefficient increases up to 0.59, but the trends calculated for the period of 1972–1991 and 1967–1991 turned out to be not uni-directional. Figure 2 shows the residual curves upon separating the trend component. They show the high (0.89) level of correlation and possess similar tendencies with the residual curves given in Figure 1c. In 1972–1975 the decreased intensity of gyres was observed, and in

1979–1982 – the increased one. According to the calculated cross-correlation function, the changes of intensity of subtropical and tropical gyres in the Western Pacific take place synchronously, as a rule. Earlier (Nelezin, 1997; Wyrtki, 1974) such tendency was established for the NEC and Kuroshio.

It is very difficult to determine the intensity of thermohaline circulation from the observations (Bryen and Griffiz, 1996). Comprehensive characteristics of changes in intensity of subtropical and tropical water gyres are limited by the used methodical approach, but the obtained results are quite grounded from the point of view of the general ocean circulation. In the Western Pacific the currents of the eastern trend: the ECC and Kuroshio are the "discharging" ones with regard to the current of the western direction – the NEC, they compensate the density advection. Figure 3

Figure 2. Temporal motion of current volume transport (10^6 m³/s) of subtropical (a) and tropical (b) water gyres at the Section of 137°E in 1972–1991; residual curves (c) of volume transport of subtropical (1) and tropical (2) gyres after filtration and separation of trend components

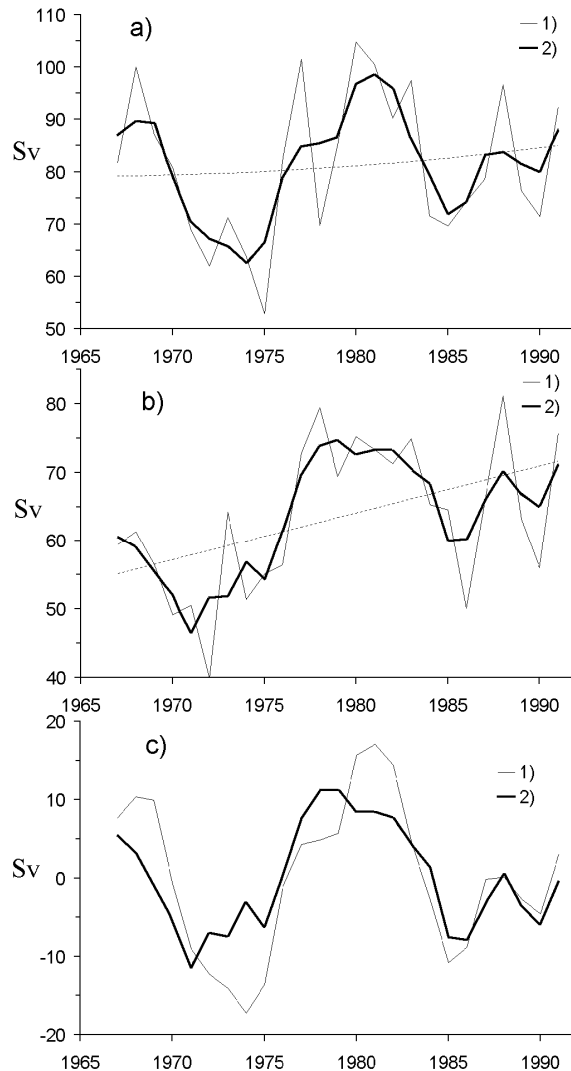**Figure 3. Temporal motion of the eastern (a) and western (b) water transport (10^6 m³/s) at the Section of 137°E in 1967–1991; residual curves (c) of the eastern (1) and western (2) water transport after filtration and separation of trend components**

presents the temporal motion (1967–1991) of the total water transport of the eastern direction (ECC and Kuroshio) and the western water transport of the NEC. This scheme does not involve the volume transport of the Northern Sub-Tropical Counter-Current, which value, as it is shown in paper (Burkov and Kharlamov, 1985) is considerably less than the discharges of the main currents at the Section of 137°E. As the Figure shows, in some years the total eastern transport reaching 100 Sv and more is larger than the western water transport of the NEC. Average for the given period, the long-term value of intensity of the eastern water transport – 81.3 Sv – appears to be higher than that of the western one (63.3 Sv). Minimal values of 53 and 40 Sv were obtained in 1975 and 1972 correspondingly, and the maximal values (105 and 81 Sv) – in 1980 and 1988. With this, the eastern transport possesses larger dispersion, and the western one – a distinctly exhibited trend to increasing. Despite the given differences in the western and

eastern water transport at the Section of 137°E, their long-term vibrations are quite well related: correlation coefficients for the initial series and for the series smoothed by the model of the sliding average made 0.62 and 0.73. Upon separating the trend component the residual curves show the high (0.8) level of the correlation between the water transports in the eastern and western directions, similarly to those ones in Figure 1c.

In conclusion we should mark that the monitoring of the volume transport of the main currents allows us to determine the informative indicators of the thermo-dynamic mode and climate tendencies in the ocean. As a result of the performed studies, the strong relationship of the long-term vibrations of the current volume transport forming the subtropical and tropical gyres in the North-Western Pacific is established. The predominant tendencies of their changes are determined.

REFERENCES

Bryen K., **Griffiz** S. **1996**. Climate variability in the Northern Atlantic on the ten-year time scale: is it predicted? Proceedings USSR Academy of sciences (FAO), v. 32, 5, p. 591–599 (In Russian).

Burkov V.A., Il'in M.B., Kharlamov A.M. **1986**. Inter-annual and synoptic variability of hydrophysical fields in the West-Northern Pacific in Winter. FERHRI Proceedings, 130, p. 67–80 (In Russian).

Burkov V.A., **Kharlamov** A.M. **1985**. Two Modes of variability of zonal barocline currents in the Equator-Japan Section. Oceanology, v. 25, 6, p. 918–925 (In Russian).

Kaneko I.Y. Takatsuki H. Kamiya and Kawae S. **1998**. Water property and current distributions along the WHP-H9 section (137–142°E) in the western North Pacific. J. Geophys. Res., 103, p. 12959–12984.

Mamaev O.I. **1995**. On spatial-temporal scales of the Ocean and Atmosphere processes. Oceanology, v. 35, 6, p. 805–808 (In Russian).

Monin A.C. **1993**. About ocean climate. Report of Academy of sciences, v. 328, 3, p. 395–398 (In Russian).

Nagasaka K. **1977**. Long-term variation of oceanographic condition along 137°E (in Japan). Mar. Sci. Mon., v. 9, 3, p. 18–22.

Nelezin A.D. **1996**. Variability of the Kuroshio Front in 1965–1991. PICES Scientific Report, 6, p. 124–130.

Nelezin A.D. **1981a**. Balance of the West-East water transport in the Equatorial system of currents of the Pacific ocean. FERHRI Proceedings, 83, p. 29–34 (In Russian).

Nelezin A.D. **1981b**. Variations of the water transport by the North Equatorial Current and the Equatorial Counter-

Current along 137°E in 1967–1980. Cruise Results of KISZ-80, p. 196–201 (In Russian).

Nelezin A.D. **1997**. On the Relationship of the North Equatorial Current and Kuroshio volume transport. Oceanology, v. 37, 4, p. 502–505 (In Russian).

Nelezin A.D. **1999**. On the possibility of the forecast of the mean location of the Kuroshio Front. Deport of Academy of sciences, v. 368, 6, p. 827–829 (In Russian).

Ozmidov R.V., **1995**. Spectral structure of hydrophysical fields in the ocean. Proceedings USSR Academy of Sciences (FAO), v. 31, 3, p. 419–426 (In Russian).

Sarkisyan A.S. **1977**. Numerical analyses and forecast of marine currents. 182 pp (In Russian).

Sarkisyan A.S. **1982**. Workshop on climate aspects of the variations of oceanographic characteristics. Tokyo, May 11–12, 1981. Proceedings USSR Academy of Sciences (FAO), v. 18, 4, p. 444–447 (In Russian).

Sherer V., **Tolkachev** A.Ya. **1993**. Construction of the Global Ocean Observing System (GOOS). VMO Bull, v. 42, 2, p. 151–158 (In Russian).

White W. **1977**: Secular variability in the baroclinic structure of the interior North Pacific Coast from 1950–1970. J. Mar. Res., 35, p. 587–607.

World climate research programme. **1985**. The Tropical Ocean. Global Atmosphere (TOGA) Programme.- Churn UGGJ, 4, p. 63–65.

Wyrtki K. **1974**. Equatorial currents in the Pacific 1950–1970 and then relation to the Trade winds. J. Phys. Oceanogr., v. 4, 3, p. 372–380.

ESTIMATION OF THE INTERANNUAL VARIABILITY OF THE SEA OF JAPAN WATER TEMPERATURE

V.A. Luchin[1], V.V. Plotnikov[1,2]

[1] Far Eastern Regional Hydrometeorological Research Institute (FERHRI), Russia
   E-mail: vluchin@hydromet.com

[2] V.I. Il'ichev Pacific Oceanological Institute, Far Eastern Branch of Russian Academy of Sciences
   (POI FEBRAS), Russia

This work is based on the most complete records of deep-water oceanographic observations (about 140,000 stations received from 1900 to 2000) that made it possible to study the Sea of Japan thermal fields structure in detail. The key areas responsible for the formation of different spatial scales variability have been singled out and the sea thermal conditions variability from 1954–1991 has been assessed. During this period neither extremely warm nor extremely cold "hydrological" winters were observed in the Sea of Japan. The warm (1954–1956, 1959, 1962, 1965, 1972, 1973, 1979, 1989, 1990) as well as cold (1963, 1968, 1981, 1984–1987) winters have been singled out. The trend line of the first component of the EOF temperature decomposition shows that the thermal state of the active layer in February–March was tending to the slow fall of temperature (approximately -0.6°C for 38 years). The information received does not confirm the previous conclusions of the lowering intensity of the active layer ventilation in the northern and northwestern parts of the Sea of Japan from 1954 to 1991.

INTRODUCTION

The interannual variability of the Sea of Japan parameters attracted attention of many researchers. However, owing to insufficiency of initial data it has been studied only in separate areas of the Sea of Japan. Several parameters were studied: water salinity (Kim et al., 1997a; Gamo and Horibe, 1983; Sudo, 1986), water temperature (Minobe, 1996; Klimov 1986; Pavlychev et al., 1989; Pavlychev and Teterin, 1996; Uranov, 1968; Riser, 1997; Lee et al., 1999; Kim et al., 1997b; Zuenko, 1994; Kim et al., 1997c), dissolved oxygen (Riser, 1997; Gamo et al., 1986; Lee et al., 1999; Kim et al., 1997b; Kim et al., 1997c), coastal waters parameters (Varlamov et al., 1997), water discharge through the Korean Strait (Pokudov, 1975; Miita and Tawara, 1984). A number of investigators (Kim, 1999; Senjyu and Sudo, 1993; Senjyu and Sudo, 1994; Seung and Yoon, 1995; Sudo, 1986) believe that the sea deep waters are formed as a result of the deep convection, the intensity of which is subject to interannual fluctuations.

The main results of the research of the Sea of Japan water parameters interannual variability presented in the previous investigations are as follows. During the second part of the XX century the air temperature at the coastal Sea of Japan stations was increasing – approximately 0.03°C per annum (Varlamov et al., 1997). There was also the rise of the water temperature, deepening of the minimum dissolved oxygen layer, and reduction of its content in the sea deep waters (Riser, 1997). As a rule, it was explained by the weakening deepwater formation in the northern part of the Sea of Japan. However, there is no common opinion on the beginning point of the deep waters warming. So, Riser (1997) considers that the process took place since 1932. Minobe (1996) asserts that the water temperature was falling up to the late 1940s. According to Kawamura et al. (1999), the temperature began rising since the end of 1960s.

Ponomarev and Salyuk (1997) note that there were two periods in the temperature rise (in the middle 1940s and early 1980s), which they connect with the climate changes. The authors (Chen et al., 1999; Gamo, 1999; Gamo et al., 1986; Kim and Kim, 1996; Mihami et al., 1999; Riser et al., 1999) also note that since 1960s or earlier the deep-water convection was less active owing to global rise in temperature. Uncommonness of conclusions is probably related to the absence of reliable assessments.

MATERIAL AND METHODS OF INVESTIGATION

The interannual variability of thermal conditions of the Sea of Japan active layer was analyzed using the deep-water oceanographic data. Most of data were provided by All-Russian Research Institute of Hydromet Information, World Data Center (VNIIGMI MCD). The data were accurately checked and supplemented. Double and doubtful data were excluded, the resulting data set consisting of 140,000 oceanographic stations that were made from 1900 to 2000. The data were submitted by scientific institutions of Russia, Japan, DPRK, Republic of Korea, and USA.

For calculation purposes data samples covering the period of 1954–1991 (period of continuous observation series) were made. They include all available data (2,672 oceanographic stations) on the water temperature distribution at the horizon of 100 m in February and March (convective cooling of the active layer finishes at this time). The set of annual water temperature anomalies registered at the horizon of 100 m in 2°×2° squares in February and March was used as initial information.

The choice of this horizon is based on the well-known fact that the intensive autumn–winter convection layer in the north and north–western part of the sea is limited by

depths of 200–250 m (*e.g.* Luchin *et al.*, 1997), and the depth of Korean Strait that is the entrance of the pacific-originated waters does not exceed 130 m. Besides, in the upper part of the active layer there is sufficiently large number of water temperature records.

At the first stage of the interannual water temperature variability analysis the hypothesis of the interannual component extraction was investigated. This task was realized by means of the factor dispersion analysis (Eliseeva and Yuzbashev, 1998). Water temperature dispersion in every square was represented as a superposition of the interannual and occasional components:

$$\sigma_{total}^2 = \delta_{int\,erannual}^2 + \overline{\sigma^2}_{occasional} \qquad (1)$$

$$\delta_{interannual}^2 = \frac{\sum_{j}^{m}(\overline{y}_j - \overline{y})^2 n_j}{\sum_{j}^{m} n_j} ; \quad \overline{\sigma^2}_{occasional} = \frac{\sum_{j}^{m}\sum_{i}^{n_j}(y_{i,j} - \overline{y}_j)^2}{\sum_{j}^{m} n_j} \qquad (2)$$

Where:

y_{ij} – is the water temperature in *i* point *j* year;

$\overline{y}_j$ – is the average temperature in *j* year;

$\overline{y}$ – is the average multi-year water temperature.

Determination coefficient (η^2) was calculated over the following formula:

$$\eta^2 = \frac{\delta_{int\,erannual}^2}{\sigma_{total}^2} \qquad (3)$$

Determination coefficient describes contribution of water temperature variability caused by interannual fluctuations. Limit of error ($\pm\Delta_\eta$) was found by Fisher tables (Eliseeva and Yuzbashev, 1998) to assess reliability of the extracted interannual variability.

Figure 1 shows marginal values of determination coefficients with 5% level of significance. As provided by results, interannual water temperature variations are reliable for the whole sea. Interannual water temperature fluctuations make the contribution of 20–80%. Therefore, it is advisable to put the initial data to the process of filtration to exclude the occasional components.

Probably, the most effective procedure is a decomposition of initial fields under EOF. Empirical orthogonal functions (EOF), being the natural functions of co-variance matrix of initial data fields, are determined by the field structure itself as well as by the dimensions of the region investigated. They give the idea of the stagnant oscillations type stationary waves induced by thermodynamic factors. Depending on its number, EOF reveals the whole series of such waves characterized by different statistic recurrence, *i.e.* they describe the spatial structure of the field investigated. EOF values marked out on the charts represent the fields where the areas of different signs are singled out. The number of such areas is increasing rapidly when increasing the orthogonal components consecutive number. It confirms the idea that higher-number orthogonal functions describe lower-scale processes. However, after comparing the manifestation scale of anomalies that have a long lifetime and are comparable with the size of the investigated area, it is advisable to have only several first EOF components to analyze interannual variability of water temperature. The first EOF components contain most of information on the sea thermal conditions.
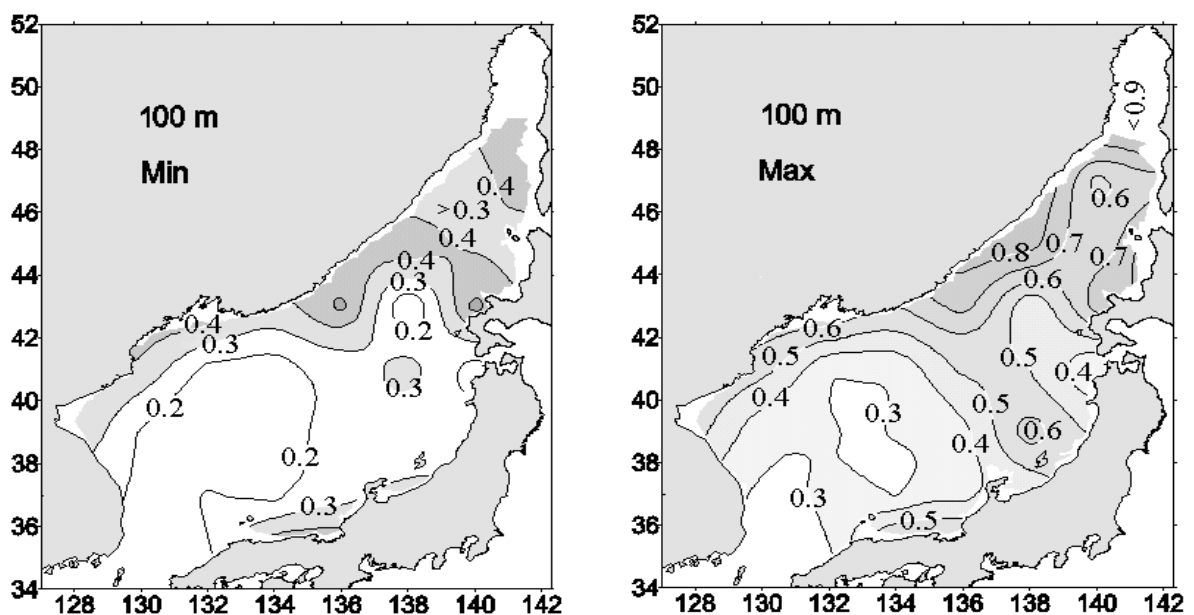

Figure 1. Marginal values of the relative contribution of interannual water temperature variability (η^2) at the depth of 100 m

RESULTS

On the whole, one can judge the interannual variability of the Sea of Japan water temperature by the standard deviation (Figure 2). Maximum standard deviation is registered in the southern and eastern parts of the sea that are under the influence of pacific-originated waters. Here standard deviation at the horizon of 100 m amounts to 0.6–0.9°C in February–March. Minimum standard deviation is observed in the northern and northwestern parts of the sea. Such distribution testifies that interaction of the warm pacific-originated waters with the cold waters of the Sea of Japan proper influences significantly the interannual variability of the subsurface water temperature. The zone with maximum spatial deviation gradients separates the cold waters to the north of Polar front and the warm pacific-originated waters.

Previously (Luchin, 2000) the first four components of EOF decomposition that accumulate 79.2% of information on the variability of the initial temperature fields were used to analyze the interannual variability of the Sea of Japan. Sea thermal fields at the horizon of 100 m. These components give the idea of the main features of the large-scale variability of the Sea of Japan thermal conditions at the depth of 100 m. It was also noted that the lower-scale components of higher levels are formed under the influence of a great number of local factors, therefore, their interpretation is usually difficult. Besides, the scales of their variability are compared with the error level of observations and the calculation process. Thus, their exclusion may be interpreted as additional data smoothing that minimizes generality of the system analyzed.

The multi-year variability of the first four temporal components of the Sea of Japan water temperature fields was analyzed at two stages. At the first stage the availability of trend component was estimated. For this purpose the filter giving the line function of time from the mixture of white noise was used. The weight function of this filter is as follows:

$$h(n-1) = \frac{6}{n^2}\left(\frac{2t}{n} - 1\right), \ t=1,2,...,n$$

And a standard error of the slope angle (α) is:

$$\sigma_\alpha = \left(\frac{12\sigma_t^2}{n^3}\right)^{1/2},$$

where:

σ_t^2 – is the dispersion of the analyzed temporal series T_t after the trend extraction.

Probability of trend extraction for the first and the second temporal function is about 80% and over 95% correspondingly. Probability of trend extraction for the rest empirical components of interannual water temperature variations is not significant.
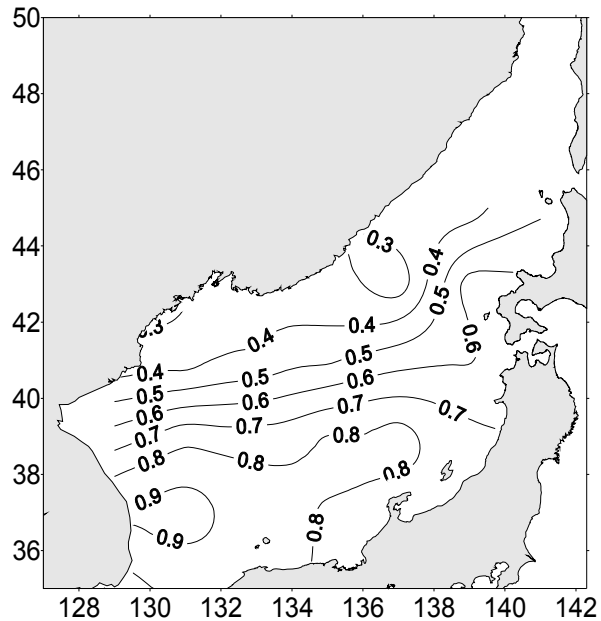
Figure 2. Standard deviation of interannual water temperature variations (°C) at the horizon of 100 m (February–March)

At the second stage the spectral analysis of the analyzed series was carried out. In order to get the correct spectral assessment we preliminary filtered trend components of the first and second EOF modes. The frequency spectra analysis $S(\omega)$ of the analyzed series received by the method of maximum entropy (Privalsky, 1985) allowed to single out (at 95% level of significance) predomination of the 17–19–, 6– and 3–4 year quasi-periodicity for the first component, 10–11– and 2–3 year for the second, approximately 22– and 2–3 year for the third, and 11–12–, 5– and 2–3 year quasi-periodicity for the fourth component (Figure 3).

Analogous periodicity is traced in the multi-year variability of other hydromet parameters. Pavlychev and Teterin (1996) found the 6 year periodicity in the interannual variability of the cold waters area in Peter the Great Bay. Zuenko (1994) noted 8–11 year periods in the interannual variability of the surface and subsurface water temperature. By the data from coastal Japanese stations Watanabe et al. (1986) found the 6 year periodicity of water temperature (especially in the southern part of the sea) and quasi-ten-year variations in the northern part of the sea. Maximum 6 year variations are registered in Tsushima Strait. Basing on the regular observations of the time section in the eastern part of Tsushima Strait for 1919–1979. Miita and Tawara (1984) singled out variations with the periods of 6–8 years and marked their possible connection with the large-scale circulation of the north Pacific waters. Klimov (1986) received predominating periods of about 2 and 5–6 years for the northern part of Tsushima current.
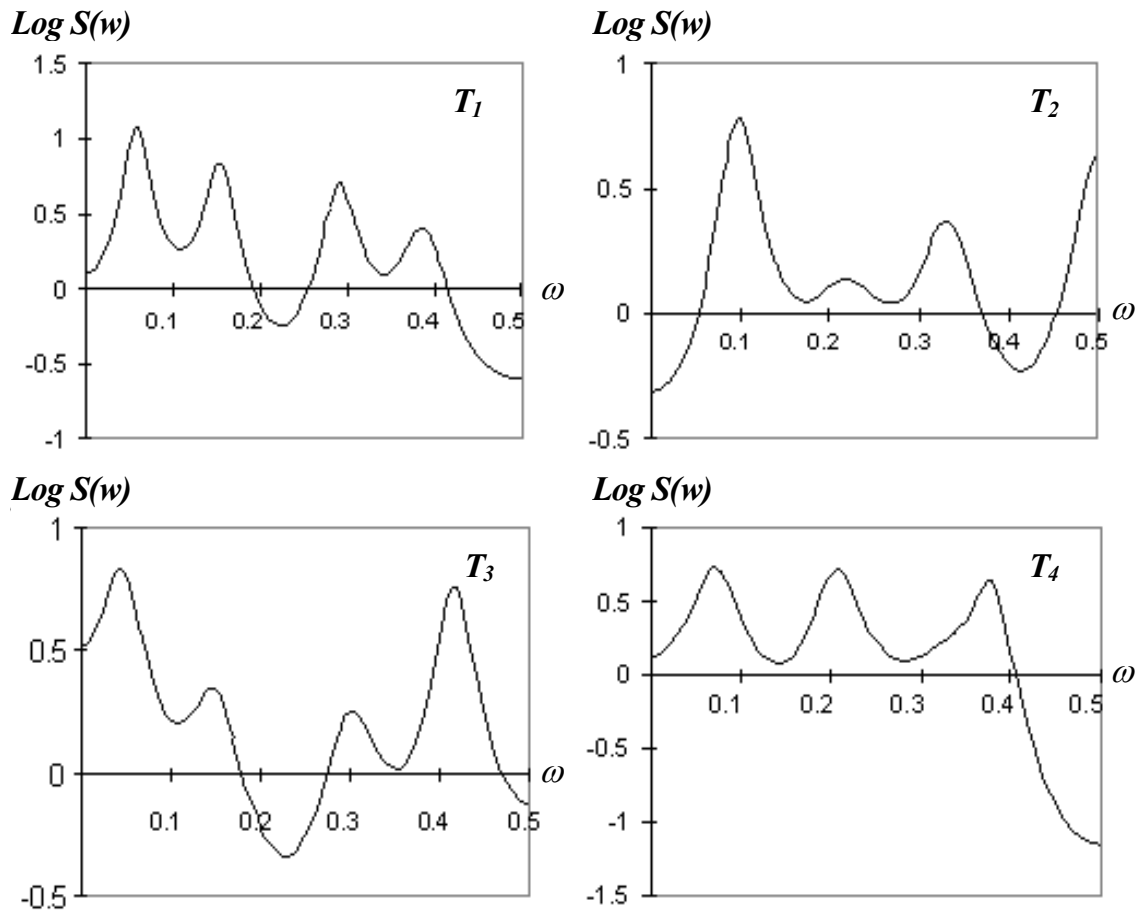
Figure 3. Estimation of frequency spectra *Log S(ω)* for the first four functions of time (*T₁–T₄*)

To single out the anomaly periods in the sea water thermal conditions which characterize the entire area in question it is sufficient to analyze the contribution of only the first component of the temperature field decomposition. This component characterizes the most large-scale processes and is responsible for the synchronic fluctuations in the water temperature within the sea (Figure 4a). The other components (*e.g.* the field of the second component in Figure 4b) characterize redistribution of the thermal potential among the separate parts of the sea. Therefore, they should be taken into account when evaluating the thermal conditions of the Sea of Japan separate regions. It is especially critical for the waters that are subject to the influence of EOF component extremes.

Taking the amount of sample into account the quantity of graduations was limited to five (Eliseeva and Yuzbashev, 1998) (extremely cold, cold, normal, warm and extremely warm years). Normal refers to the years with $|\Delta T| < 0.674\sigma$ correlation applied. Here ΔT is the product of corresponding temporal and spatial functions of water temperature anomalies decomposition and σ is the standard deviation. Other thermal gradations are distinguished by the following correlations:

- For cold years – $-2\sigma < \Delta T < -0.674\sigma$

- For extremely cold years – $\Delta T < -2\sigma$
- For warm years – $0.674\sigma < \Delta T < 2\sigma$
- For extremely warm years – $2\sigma < \Delta T$

Figure 5 shows significance of the first two components of water temperature decomposition by EOF in the interannual water temperature variability at the horizon of 100 m in February–March in the extreme points. The first component has the center in 36°N and 132°E. The second component has the center in 38°N and 130°E (Figure 4).

As it was noted above, in order to single out the anomalous periods in the sea water thermal condition which are typical for the whole area considered it is sufficient to analyze only the first component of the temperature fields decomposition which characterizes the most large-scale processes and is responsible for the synchronous water temperature variations within the sea. The analysis of the first component (within the classification proposed) shows that neither extremely warm nor extremely cold winters in the hydrological respect were observed in the Sea of Japan active layer thermal condition from 1954 to 1991. The assumptions accepted allowed to single out warm (1954–1956, 1959, 1962, 1965, 1973, 1979, 1989, 1990) as well as cold (1963, 1968, 1981, 1984–1987) winters in the thermal condition of the Sea of Japan.
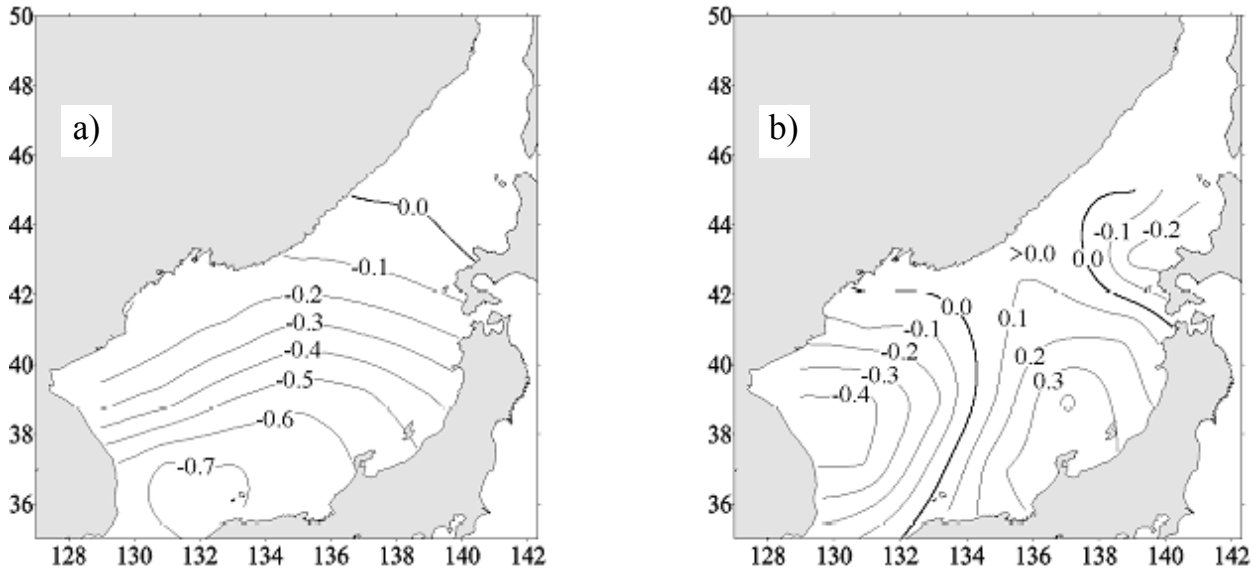
Figure 4. Distribution of the first two empirical orthogonal functions of water temperature fields in the Sea of Japan at the horizon of 100 m (*a* is EOF-1 equal to 43.8%, *b* is EOF-2 equal to 15.1%)

a)   EOF-1 (43.8%)   b)   EOF-2 (15.1%)
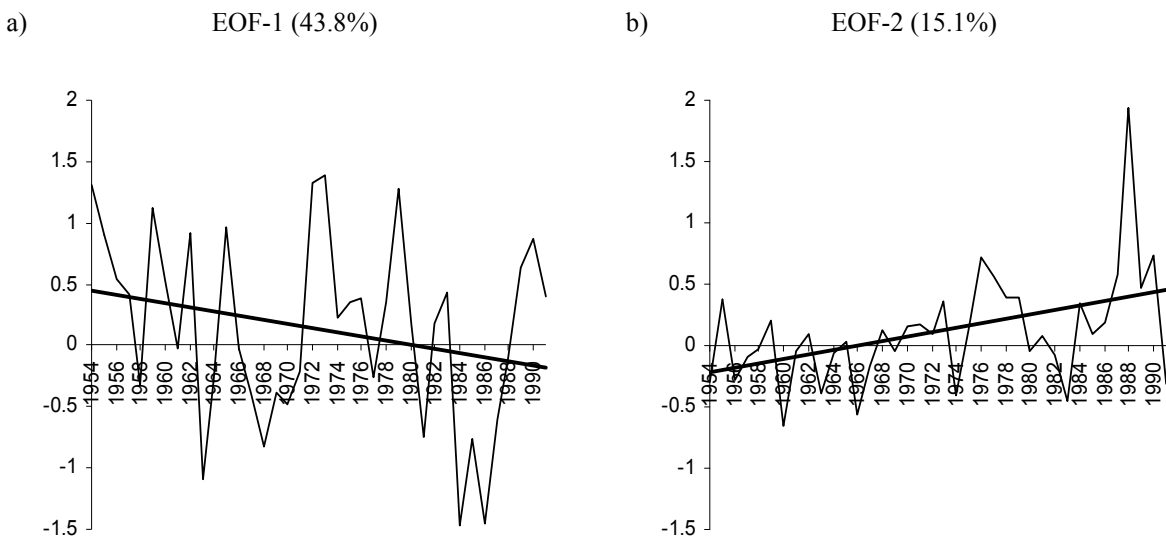
Figure 5. Significance of the first two components of water temperature decomposition by EOF (ºC) at the horizon of 100 m

The trend line in Figure 5a shows that the thermal state of the Sea of Japan active layer in February–March tended towards slow cooling (about -0.6°C for 38 years) (80% probability). In the northwestern part of the sea that is traditionally called as the source of deep waters formation the tendency towards cooling is lower (to -0.2°C).

It should be noted that the time course of the second EOF component (Figure 5b) in the western part of the sea points to the positive trend in the interannual water temperature variability at the horizon of 100 m. Thus, additional analysis of the significance of the second component of water temperature decomposition by EOF is necessary for the northwestern part of the sea. Spatial distribution

of the second EOF component (Figure 4b) reveals either zero or slightly negative values in the northern and northwestern parts of the sea where the active layer cooling in autumn and winter is significant. The positive temperature trend is traced in the time course of the second EOF component (Figure 5b) with 95% probability. It is +0.73°C (for 38 years) for the western part of the sea and about +0.2°C for the south off Peter the Great Bay.

Thus, the joint analysis of the inter-annual variants of the first two components of the EOF water temperature decomposition doesn't confirm the precedent investigators' conclusions about the cooling intensity decline in the water active layer in winter in the north and northwestern parts of the sea

in a period from 1954 to 1991 that they connect with the ventilation of the Sea of Japan deep waters.

Thus, co-analysis of interannual variations of the first two components of water temperature decomposition by EOF does not confirm previous conclusions of the lowering intensity of the active layer cooling in the northern and northwestern parts of the Sea of Japan from 1954 to 1991 due to the deep waters ventilation.

ACKNOWLEDGEMENTS

REFERENCES

Chen C.T.A., Bychkov A.S., Wang S.L., and Pavlova G.Yu. **1999**, An anoxic sea of Japan by the year 2200, Mar. Chem., p. 249–265.

Eliseeva I.I., **Yuzbashev** M.M. **1998,** The general theory of statistics. Finance and statistics press. - 368 pp. (In Russian)

Gamo T., **1999,** Global warming may have slowed down the deep conveyor belt of a marginal sea of the northwestern Pacific: Sea of Japan., Geophys. Res. Lett., 26, p. 3137–3140.

Gamo T., **Horibe** Y. **1983,** Abyssal circulation in the Sea of Japan, J. Oceanogr. Soc. Japan. v. 39, 5, p. 220–230.

Gamo T., Nozaki Y., Sakai H., Nakai T., Tsubota H. **1986,** Spacial and temporal variations of water characteristics in the Sea of Japan bottom layer, J. Mar. Res. v. 44, 4,p. 781–793.

Kawamura H., Yoon J.-H., Kim C.-H. **1999,** The formation of the intermediate and deep water in the Japan/East Sea, Proceedings of the Creams' 99 international symposium. – 26–28 January. - Fukuoka, Japan, p. 156–159.

Kim K., Kim K.-R., Takematsu M., Yoon J.-H., Volkov Y. January. **1997b,** Water masses and their vertical structure in the East (Japan) Sea; new findings from Creams, Proceedings of the CREAMS '97 international symposium. - 28–30 Fukuoka, Japan, p. 337–340.

Kim K., Kim Y.-G., Cho Y.-K., Takematsu M. and Volkov Y. January **1999,** Basin-to-basin and year-to-year variation of temperature and salinity characteristics in the East Sea (Sea of Japan), Proceedings of the CREAMS '99 international symposium. 26–28. Fukuoka, Japan, p. 3–6.

Kim K.-R., and K. **Kim**. **1996,** What is happening in the East Sea (Sea of Japan)? Recent chemical observations during CREAMS 93–96, J. Korean Soc. Oceanogr., 31, p. 164–172.

Kim K.-R., Park M.-K, Park S.-Y., Oh D.-C., Choi S.-H., Hwang J.-S., Park K.-S., Kim K., Kang D.-J. and Hong G.-H. January **1997c,** The East Sea (Sea of Japan) in changes, Resent chemical observations during CREAMS 93–96. Proceedings of the CREAMS' 97 international symposium. - 28–30. - Fukuoka, Japan, p. 237–240.

Kim Y.-G., Kim K., Kim K.-R.. January **1997a,** Intermediate and deep waters in the Sea of Japan, Proceedings of the CREAMS '97 international symposium. 28–30. - Fukuoka, Japan, p. 39–42.

Klimov S.M. **1986,** Estimation of the large-scale variability of the surface water temperature in the Tsushima Current. Proceedings of Far Eastern Regional Research Institute of State Hydromet Committee. No. 125, p. 3–10. (In Russian)

Lee C.-K., An H.-S. and Shin H.-R. January **1999,** 98 CREAMS observation and water properties of the Ulleung basin: long term change, Proceedings of the CREAMS '99 international symposium. 26–28. Fukuoka, Japan, p. 35–37.

Luchin V. A., Rykov N. A., Varlamov S. M. January **1997,** Variability of the lower boundary of the winter convection in the Sea of Japan. Proceedings of the CREAMS '97 international symposium. 28–30. Fukuoka, Japan, p. 297–302.

Luchin V.A. **2000,** Results of oceanographic researches under "Sea" program (Russia Far East). Anniversary FERHRI proceedings, Vladivostok, Dalnauka, p. 90–112. (In Russian)

Miita T., **Tawara** S. **1984,** Seasonal and secular variations of water temperature in the east Tsushima strait. J. Oceanogr. Soc. Jap., v. 40, 2, p. 91–97.

Minami H., Y. Kano, and K. Ogawa, **1999,** Long-term variations of potential temperature and dissolved oxygen of the Sea of Japan Proper Water, J. Oceanogr., 55, p. 197–205.

Minobe S. **1996,** Interdecadal temperature variation of deep water in the Sea of Japan (East Sea) Proceedings of fourth Creams workshop, R/V Okean, Vladivostok. February 12–13, p. 81–88.

Pavlychev V.P., Budaeva V.D., Khen G.V., Chernyavskiy V.I., Shatilina T.A. **1989,** Interannual variability of hydromet conditions in primary fishery areas in north-western Pacific and their forecast. Long-term variability of natural conditions and problems of fishery forecasts. Proceedings of VNIRO. Moscow, VNIRO, p. 124–141. (In Russian).

Pavlychev V. P., **Teterin** A. I. **1996,** Interannual changes of thermal conditions in the northwestern Sea of Japan, Proceedings of fourth CREAMS workshop, R/V Okean, Vladivostok. - February 12–13, p. 71–75.

Pokudov V.V., **1975,** Water and heat exchange in the Sea of Japan through the Korean Strait in summer, FERHRI Proceedings, No. 50, p. 11–23. (In Russian)

Ponomarev V. I., **Salyuk** A. N. **1997,** The climate regime shifts and heat accumulation in the Sea of Japan, Proceedings of the CREAMS '97 international symposium. - 28–30 January. Fukuoka, Japan, p. 157–161.

Privalsky V.E. **1985**, Climatic variability (stochastic models, predictability and spectra). Nauka press, Moscow, 184 pp. (In Russian).

Riser S.C. **1997,** Long – term variation in the deep ventilation of the Japan/East Sea Proceedings of the CREAMS '97 international symposium. 28–30 January, Fukuoka, Japan, p. 31–34.

Riser S.C., M.J. Warner, and Yurasov G.I., **1999,** Circulation and mixing of water masses of Tatar Strait and

the northwestern boundary region of the Sea of Japan, J. Oceanogr., 55, p. 133–156.

Senjyu, T., H. **Sudo**, **1993,** Water characteristics and circulation of the upper portion of the Sea of Japan Proper Water, J. Mar. Sys., 4, p. 349–362.

Senjyu, T., H. **Sudo**, **1994,** The upper portion of the Sea of Japan Proper Water; Its source and circulation as deduced from isopycnal analysis, J. Oceanogr., 50, p. 663–690.

Seung, Y.H., **Yoon** J.-H., **1995**, Some features of winter convection in the Sea of Japan, J. Oceanogr., 51, p. 61–73.

Sudo H. A **1986,** note on the Sea of Japan Proper Water, Prog. Oceanogr, v. 17, p. 313–336.

Uranov E.N. **1968,** Prediction of multi-year variability of the water thermal regime near the Sakhalin southwestern coast, Proceedings of TINRO, No. 65, p. 212–220. (In Russian)

Varlamov S.M., Dashko N.A., Kim Y.-S. **1997,** Climate change in the Far East and Sea of Japan area for the last 50 years, Proceeding of the CREAMS`97 International Symposium. – P. 163–166.

Watanabe T., Hanawa K., Toba Y. **1986,** Analysis of year-to-year variations of water temperature along the coast of the Sea of Japan, Progr. Oceanogr. v. 17, 3-4, p. 337–357.

Zuenko Y. I. **1994,** The year-to-year temperature variation of the main water masses in the north–western Sea of Japan // Proceedings of the CREAMS'94 international symposium. 24–26 January, Fukuoka, Japan, p. 115–118.

ESTIMATION OF CLIMATOLOGICAL SLOPE OF THE SEA OF JAPAN LEVEL AND ITS SEASONAL VARIABILITY

A.V. Saveliev

Far Eastern Regional Hydrometeorological Research Institute (FERHRI), Russia
Email: hydromet@online.ru

This study examines multiyear annual and seasonal mean sea level slope in the Sea of Japan. Non-directional method for the reduction of the level heights in the Sea of Japan to the common Unified Height System is proposed. The method is based on Zubov's equation of geostrophic ratio between flow velocity and sea level slope. Available published data on volume transport through La-Perouse (Soya) and Korea (Tsushima) Straits and historical sea level data at the tide-gauge coastal stations in Russia, Japan and Korea were used for estimation. The main feature of general climatological sea level slope in the Sea of Japan is a steady rise of the annual mean sea level towards the Japan coast and Sakhalin Island. The sea level slope magnitude varies from 60–65 cm to 75–85 cm.

The seasonal variations of the mean level do not change the main character and magnitude of mean sea level slope. Seasonal variability is spread all over the Sea of Japan, but it ranges from 10–15 cm in the north to 30–35 cm in the south with the generally higher background of mean sea level in summer and lower background in winter.

INTRODUCTION

The better understanding of the Sea of Japan water dynamics requires knowledge of the sea level slope between Japan and Russia coasts. The main obstacle here is the difference in the systems of sea level height measurement used in Russia, Japan and Korea. Unfortunately, in recent time there is no intercalibration among them. Therefore, the sea level measured in Russia, Japan and Korea cannot be directly compared. The goal of this study is to reduce all sea level observations of the Sea of Japan to the common Height System by estimation of sea level slopes across the La-Perouse (Soya) and Korea (Tsushima) Straits. The sea level slopes were estimated using available data on the volume transport through the straits. It allowed to examine the general climatic slope of the Sea of Japan level and to reveal its seasonal variability.

DATA AND METHODS

The monthly mean and mean annual sea level heights observed at 18 coastal tide-gauge stations of Russia, Japan and Korea were used (Table 1, Figure 1). The level data sets are derived from Hydrometeorological Service archive (FERHRI), Russian National Data Center (Moscow). The Russian sea level is measured in Baltic Unified Height System (UHS) relative to Kronshtadt tide gauge zero. The Sea of Japan level heights are measured in Tokyo UHS relative to the mean sea level of Tokyo Bay. Information about Japanese UHS is obtained from the journal "Tidal observations" (Japan Meteorological Agency) while Korean UHS is not available.

The sea level slopes across the straits cannot be calculated directly by differences of level heights between two coastal stations because there is no intercalibration among sea level observations in Russia, Japan and Korea. To reduce the sea level observations of the Sea of Japan to the common UHS (Baltic Height System) the sea level slopes across the straits were reconstructed on the base of geostrophic ratio between flow velocity and sea level slope (Zubov, 1935):

$$\Delta h = C / M, \qquad (1)$$

where:

Δh is the level slope in dynamic millimeters;

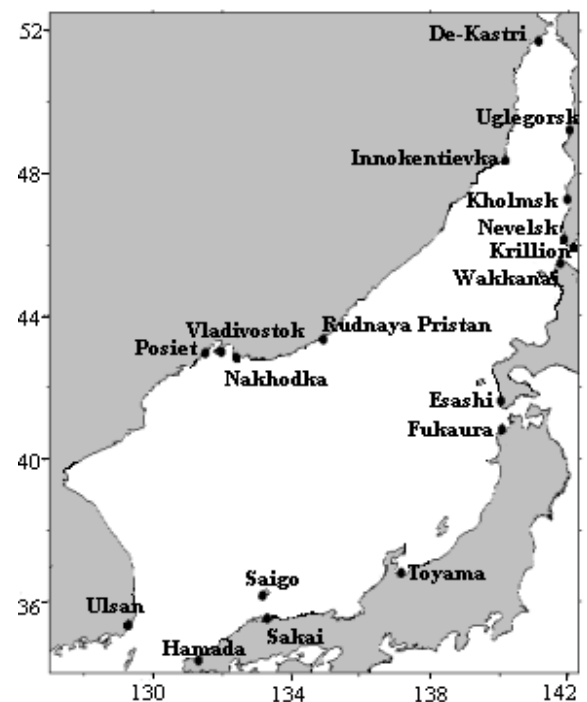C is the depth-averaged residual current velocity (without tidal component) through the strait (cm/s);

Figure 1. Location of tide-gauge stations in the Sea of Japan

Table 1

The tide-gauge stations in the Sea of Japan and their observation periods

Station	Observation period (years)	Multiyear mean annual sea level height in Unified Height System (cm)
1. Posiet	1951–1997	-104[*]
2. Vladivostok	1926–1997	-100[*]
3. Nakhodka	1948–1991	-97[*]
4. Rudnaya Pristan	1940–1996	-97[*]
5. Innokentievka	1947–1986	-98[*]
6. De-Kastri	1974–1992	-82[*]
7. Uglegorsk	1964–1992	-36[*]
8. Kholmsk	1947–1992	-40[*]
9. Nevelsk	1923–1992	-34[*]
10. Krillion	1961–1988	Unknown
11. Wakkanai	1965–1966; 1975–1994	+19[**]
12. Esashi	1983–1994	+19[**]
13. Fukaura	1973–1994	+26[**]
14. Toyama	1967–1971; 1974–1994	+21[**]
15. Saigo	1965–1994	-7[**]
16. Sakai	1958–1994	+21[**]
17. Hamada	1984–1994	+25[**]
18. Ulsan	1976–1994	Unknown

Note:

[*]   – level heights in Russian (Baltic) Height System;

[**]   – level heights in Tokyo Height System.

$M = 3.7 / L \sin \varphi$, (φ is the mean latitude of the place);

L – is the distance (in miles) between points on the section across the strait).

The current direction in (1) is connected with the sea level slope so that higher sea level is at the right hand side of the flow.

In present study we used common linear metric units instead of dynamic ones because the linear and dynamic meters differ from each other not more than 3% (Beriozkin, 1947). The depth–averaged residual current velocity C is calculated on the base of the volume transport and cross section area in the strait. Volume transport values are taken from the published sources (Table 2–3).

Finally, the estimation of sea level slopes in the straits is as follows:

$$\Delta h = V \cdot 10^2 / S \cdot M, \qquad (2)$$

where:

V is the volume transport through the strait;

S is the cross sectional area.

Proposed method is based on estimation of "basic sea level slope" (Δh) across the strait for "basic month". "Basic month" is a month when the volume transport has been measured. Evaluation of "basic sea level slope" (Δh) is made by (2). Then the monthly mean sea level deviations from mean sea level for "basic month" are determined using

historical sea level data at the opposite coasts of the straits. These deviations are the correction for calculated mean sea level slopes for other months. After that mean annual sea level slope across the strait is estimated to reduce all sea level observations in the Sea of Japan to the common HS.

In order to apply this method the reliable and accurate volume transport data should be available. As seen from Tables 2 and 3 the available volume transport estimations were largely based on the geostrophic calculations (Leonov, 1950, 1960; Vasiliev and Dudka, 1994; Misaki, 1952; Hata, 1962; Yi Sok, 1966; Pokudov, 1975; Pokudov *et al.*, 1976). Only during the last two decades the volume transport estimations were performed with the help of direct current measurements.

The most reliable values of the volume transport through the La-Perouse Strait were obtained by ADCP observations in August 8–9, 1995 (Tanaka *et al.*, 1996). All stations were located along 142°E (Figure 2), measurements were made within one day. Tanaka *et al.* (1996) calculated the volume transport through the strait using the depth-averaged residual current components perpendicular to the cross section. The cross section was also divided into subsections according to the distance between the stations. The total volume transport was estimated as the sum of the individual volume transport through the subsections and was equal 1.18 Sv (Sv = 10^6 m³/s).

<div align="right">Table 2</div>

Total volume transport (outflow in Sv) through the La-Perouse Strait by publications

Period	Authors							
	Leonov, 1950, 1960	Radzikho–vskaya, 1961	Vasiliev and Dudka, 1994	Mooers and Kang, 1996	Aota et al., 1985	Aota, 1975	Tanaka et al., 1996	Suprano-vich et al., 2001
	Methods of volume transport estimation							
	Geostrophic current	Total water Balance	Geostrophic current	Numerical modeling	Current meter	Constant current velocity through the strait	Current meter	Current meter
November	–	0.44	0.40	0.56	–	–	–	–
May–June	–	0.22	–	–	0.80	–	–	–
August	–	–	–	–	–	1.30	1.18	1.02

<div align="right">Table 3</div>

Total volume transport (inflow in S_v) through the Korea Strait obtained by publications

Period	Authors								
	Leonov, 1950, 1960	Radzikho-vskaya, 1961	Misaki, 1952 Hata, 1962	Yi Sok U, 1966	Pokudov, 1975, Pokudov et al., 1976	Mooers and Kang, 1996	Miita and Ogava, 1984	Tawara et al., 1984	Isobe et al., 1994
	Methods of volume transport estimation								
	Geostrophic current	Total water balance	Geostrophic current	Geostrophic current	Geostrophic current	Numerical modeling	Current meter	Current meter	Current meter
July	–	–	–	–	–	–	–	–	1.30
August	2.62	2.23	2,34	2.13	2.45	2,80	3.50	4.10	–
September	–	–	–	–	–	–	–	–	5.60
February-March	0.23	0.18	–	0.19	0.26	–	–	–	1.00
April	–	–	–	–	–	–	–	–	1.40
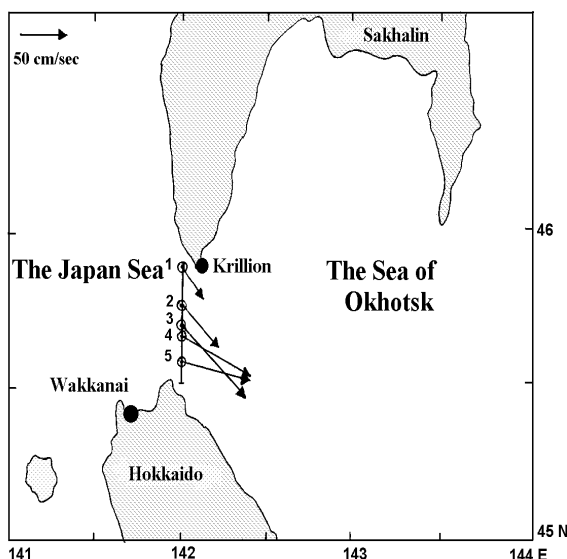
Figure 2. Location of cross section in the La-Perouse Strait and tide-gauge stations of Wakkanai (Hokkaido, Japan) and Krillion (Sakhalin, Russian Federation). (Arrows show the depth-averaged residual currents obtained by direct measuring (ADCP) in August 8–9, 1995 (Tanaka et al., 1996))

This value is considered as the "basic sea level slope" in the La-Perouse Strait in August. Cross sectional area of the strait is $S = 2.08 \cdot 10^6$ m^2. To obtain the values of sea level slopes in other months the tidal measurements in Wakkanai (Hokkaido, Japan) and Krillion (Sakhalin, Russia) for the synchronous observation period of 1975–1988 were used.

Estimations of volume transport through the Korea Strait vary over a wide range (Table 3). From our point of view the values of volume transport according to Isobe et al. (1994) are too overestimated while the volume transport obtained due to geostrophic calculations is slightly underestimated (Miyazaki, 1952; Leonov, 1960; Pokudov, 1975). We believe that more reliable estimations of volume transport through the Korea Strait based on current meter in August are 3.5 Sv (Miita and Ogava, 1984) and 4.1 Sv (Tawara et al., 1984).

In order to estimate the "basic sea level slope" in the Korea Strait we took the average value as the combined volume transport in August i.e. 3.8 Sv. This value is well agreed with the well-known ratio of the Sea of Japan water balance: climatological outflow through Tsugaru and La-Perouse Straits may account

for 70% and 30% of inflow through the Korea Strait, respectively (Leonov, 1960; Radzikhovskaya, 1961; Yasuda *et al.*, 1988; Seung and Kim, 1993; Yoon, 1991; Mooers and Kang, 1996). Taking into account this ratio and outflow value through the La-Perouse Strait in August as 1.18 Sv, the inflow through the Korea Strait in August should be equal 3.9 Sv, that is very close to our estimation. To evaluate the sea level slopes in other months the tidal measurements in Hamada (Honsu, Japan) and Ulsan (Korea) during the synchronous observation period (1984–1994) were used. The cross sectional area of the strait was made as $S = 24.0 \cdot 10^6$ m^2. Location of tide-gauge stations and cross section in the Korea Strait is shown in Figure 3.

RESULTS AND DISCUSSION

The results of estimation according to (2) are presented in Table 4. A positive sign (+) of Δh in the La-Perouse Strait corresponds to the higher sea level at Wakkanai, Hokkaido Island and outflow from the Sea of Japan into the Sea of Okhotsk (Figure 4). A negative sign (-) of Δh corresponds to the higher sea level at Krillion, Sakhalin Island and inflow into the Sea of Japan. A positive sign (+) of Δh in the Korea Strait corresponds to the higher sea level at Hamada, Honsu Island and inflow into the Sea of Japan. Estimations of multiyear mean annual sea level slopes in the straits (Table 4) and multiyear mean annual level height in Baltic UHS at Nevelsk, Sakhalin Island (nearest to the La-Perouse Strait Russian tide-gauge station) were performed to reduce the level heights (Table 1) at all Japanese stations and at Ulsan (Korean Peninsula) to the common HS (Figure 4). Standard deviation does not exceed ±3 cm.

According to Figure 4 the main feature of general climatological sea level slope in the Sea of Japan is a steady rise of average sea level towards the Japan coast and Sakhalin Island. The sea level slope magnitude varies from 60–65 cm in the Tatar Strait (between Asian and Sakhalin Island coasts) to 75–85 cm between Russia and Japan coasts. In general this climatological slope depends on the static influence of the sea level atmospheric pressure and water density distribution. Their role in different parts of the Sea of Japan may change. However, Nomitsu and Okamoto (1927), Galerkin (1960), Saveliev (1983), Oh *et al.* (1993) believe that about 20–25% of mean sea level deviations are caused by atmospheric pressure and 75–80% depend on variations of water density. At the same time temperature, salinity and density distribution in the Sea of Japan are determined by prevailing currents and volume transport through the straits. Consequently, the main reason of general slope of mean sea level (Figure 4) is the well-known prevailing cyclonic circulation in the Sea of Japan. It is responsible for the spread of warm water along the Japan coast by Tsushima Current and cold water along the Asian coast resulting in the sea level rise in the
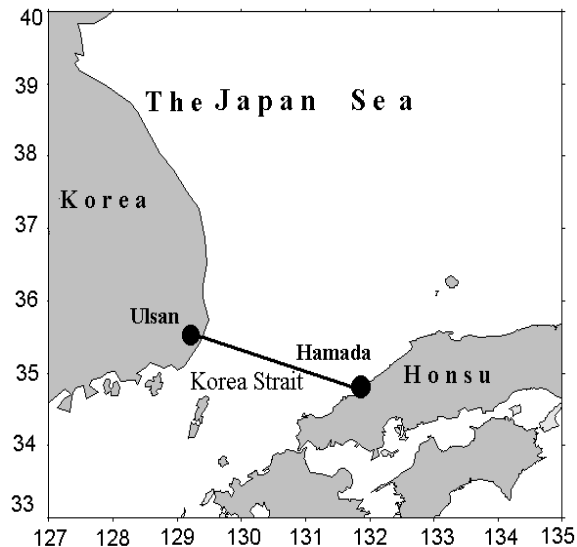
Figure 3. Location of cross section in the Korea Strait and tide-gauge stations of Hamada (Honsu, Japan) and Ulsan (Korea)
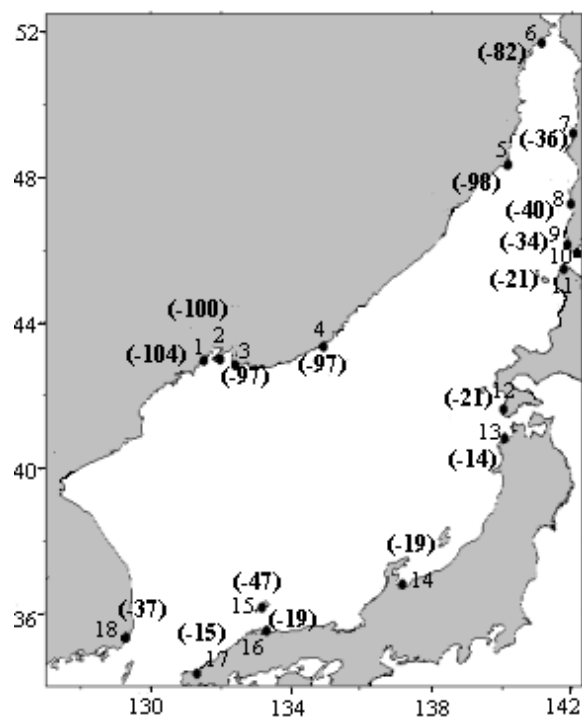
Figure 4. Multiyear mean annual level heights in the Sea of Japan (cm) expressed in Russian (Baltic) UHS (in brackets). (Ordinal numbers of tide-gauge stations correspond to Table 1)

eastern part (Japan, Sakhalin) and low background of the level at the western coast of the sea.

Using available monthly mean sea level data at tide-gauge stations the seasonal variations of the Sea of Japan level slope were examined. Figure 5 shows the multiyear monthly mean sea level heights for winter (February) and summer (August). It is evident that seasonal variations practically do not change the above-mentioned general character and magnitude of
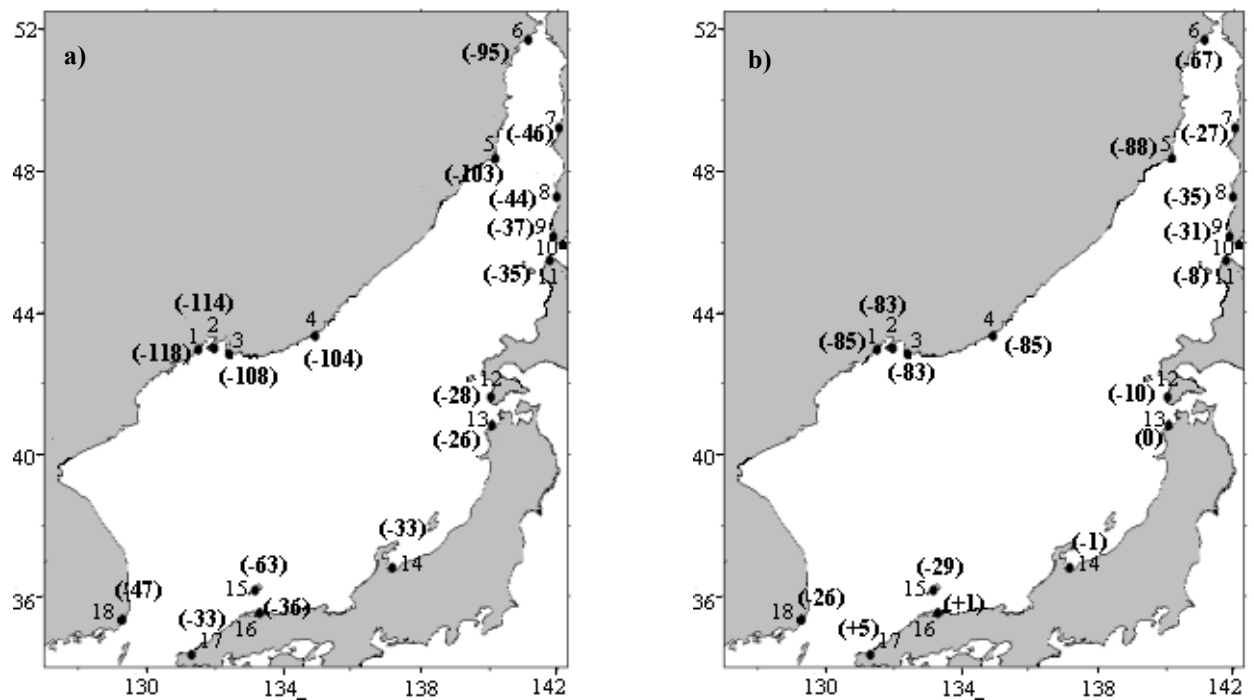
Figure 5. Multiyear monthly mean level heights in the Sea of Japan (cm) in February (a) and August (b) expressed in Baltic UHS (in brackets). (Ordinal numbers of tide-gauge stations correspond to Table 1)

the mean sea level slope between the western and eastern coasts of the sea. At the same time the changes of sea level height are visible and caused by seasonal variations of water density and inflow through the Korea Strait. These changes spread all over the Sea of Japan, but their range is smoothly increased towards the south from 10–15 cm to 30–35 cm with higher background of mean sea level in summer and lower background in winter.

CONCLUSIONS

In this study for the first time the reduction of the level heights in the Sea of Japan to the common UHS was made basing on available published data on volume transport through La-Perouse (Soya) and Korea (Tsushima) Straits and historical sea level data at the tide-gauge coastal stations in Russia, Japan and Korea. The general slope of multiyear annual and seasonal mean level in the Sea of Japan were estimated.

The main feature of general climatological sea level slope in the Sea of Japan is a steady rise of annual mean sea level towards the Japan coast and Sakhalin Island. The sea level slope magnitude varies from 60–65 cm in the Tatar Strait (between Asian and Sakhalin Island coasts) to 75–85 cm between Russia and Japan coasts.

The seasonal variations of the mean level practically do not change the general character and magnitude of the mean sea level slope. Seasonal variability is spread all over the Sea of Japan, but it ranges from 10–15 cm in the north to 30–35 cm in the south with the generally higher background of the mean sea level in summer and lower background in winter.

This study is the first step to find the climatological slope of the Sea of Japan level. The lack of information in the open part of the Sea of Japan makes it impossible to execute more detailed analysis.

REFERENCES

Aota M. **1975**. Studies on the Soya warm current. J. Low Temperature Sci., A33, p. 151–172.

Aota M., Nagata Y., Inaba H., Matsuyama Y., Ono N., Kanari S. **1985**. The Soya Warm Current – A typical oceanic current flowing over shelf region. Ocean Characteristics and Their Changes, p. 164–187.

Beriozkin B.A. **1947**. Dynamics of the sea. 683 pp. (In Russian).

Galerkin L.I. **1960**. About physical bases of the forecast of seasonal oscillations of the Japan Sea level. POI Proceedings, v. 37, p. 73–91.

Hata K. **1962**. Seasonal variation of the volume transport in northern part of the Japan Sea. J. Oceanogr. Soc. Jap. 20-th Anniv., Vol., p. 168–179.

Isobe A., Tawara S., Kaneko A. and Kawana M. **1994**. Seasonal variability in the Tsushima Warm Current.

Tsushima-Korea Strait. Continental Shelf Research, v. 14, 1, p. 23–35.

Leonov A.K. **1950**. Experience of application of the Bierknes circulation theory for definition of water balance of the Japan Sea. To memory of Shokalsky, p. 83–183 (In Russian).

Leonov A.K. **1960**. Regional Oceanography. Part I. 765 pp. (In Russian).

Miita T., **Ogava** Y. **1984**. Tsushima currents measured with current meters and drifters. Ocean Hydrodynamics of the Japan and East China, p. 67–76.

Miyazaki M. **1952**. The heat budget in the Japan Sea. Bull. Hokkaido Reg. Fish. Res. Lab., v. 4, p. 4–45.

Mooers C.N.K., **Kang** H.S. **1996**. A note on some aspects of the spin-up of the Japan (East) Sea circulation model (SOJ-POM). CREAMS Proceedings, Vladivostok-Seul, p. 123–132.

Nomitsu T., **Okamoto** M. **1927**. The causes of annual variation of the mean sea level along the Japanese Coast. Mem. Coll. Sci.Univ. Kyoto., A, 10, p. 28–36.

Oh I.S., Rabinovich A.B., Park M.S., Mansurov R.N. **1993** Seasonal sea level oscillations in the East Sea (Sea of Japan). Oceanological Society of Korea, v. 28, 1, p. 1–16.

Pokudov V.V. **1975**. Water and thermal exchange of the Japan Sea through the Korean Strait in summer. FERHRI Proceedings, 50, p. 11–23 (In Russian).

Pokudov V.V., Man'ko A.N., Khlusov A.N. **1976**. Features of hydrological regime of the Japan Sea in winter. FERHRI Proceedings, 60, p. 74–115

Radzikhovskaya M.A. **1961**. Water and thermal balance of the Japan Sea. The basic features of geology and hydrology of the Japan Sea, p. 132–145 (In Russian).

Saveliev A.V. **1983**. About influence of atmospheric pressure and wind on mean level oscillations in the Japan Sea along the Primorye Coast. FERHRI Proceedings, 100, p. 83–86.

Seung Y.H., **Kim** K. **1993**. A numerical modeling of the East Sea circulation. Oceanol. Soc. Korea., v. 28, 4, p. 292–304.

Supranovich T.I., Yurasov G.I., Kantakov G.A. **2001**. Unperiodical currents and volume transport in the La Perouse Strait. Meteorology and Hydrology, 3 p. 80–84 (In Russian)

Tanaka I., Nakata A., Yagi H., Samatov A.D., Kantakov G.A. **1996**. Result of direct current measurements in La Perouse Strait (the Soya Strait) in 1995–1996. Presentation at the 5-th Annual PICES Meeting. Nanaimo, Japan, p. 1–13 (the manuscript).

Tawara S., Miita T., Fujiwara T. **1984**. The hydrography and variability in the Tsushima Straits. Bull. Coast. Oceanogr. v. 22, p. 50–58.

Vasiliev A.S., **Dudka** K.V. **1994**. About water exchange of the Japan Sea and the Sea of Okhotsk with Pacific Ocean. Meteorology and Hydrology, 10, p. 56–64 (In Russian).

Yasuda I., Okuda K., Hirai M., Ogava Y., Kudoh H., Fukushima S.I., Mizuno K. **1988**. Short-term variations of the Tsugaru Warm Current in Autumn. Bull. Tohoku Region. Fish. Res. Lab., 50, p. 153–191.

Yi Sok U. **1966**. Seasonal and secular variations of the water volume transport across the Korea Strait. Oceanogr. Soc. Korea., v. 1, p. 1–2, p. 7–13.

Yoon J.H. **1991** The branching of the Tsushima Current. Rep. Res. Inst. Applied Mech. v. 37, 108, p. 1–21.

Zubov N.N. **1935**. Dynamic method of processing of oceanological observations. 104 pp. (In Russian).

MARINE INTERNAL WAVES OF THE RAYLEIGH TYPE

I.Ya. Tyukov

retired, V.I. Il'ichev Pacific Oceanological Institute, Far Eastern Branch of Russian Academy of Sciences (POI FEBRAS), Russia

The forced seismic gravitational internal waves occurring in the bottom layer under the sea floor deformations are considered. In their turn, the sea floor deformations are induced by the earth's vibration or pulsations of external pressure (connected with the sea level variations) that are immediately transmitted to the sea floor by the vertical incompressible water column. The problem is based on the linear Euler equation and incompressibility equation with consideration of continuity of the vertical velocity component at the deformed sea floor. The continual deepening of the ocean is in linear dependence on the rate of bottom hydrodynamic pressure rise. The coefficient of proportionality is represented by the dimensionless deformation function N that is calculated in every point of the oceanic crust over experimental data. The absence of vertical or horizontal motion is the kinematic feature of the upper boundaries $z = z_0$, $z = z_1$ of the bottom layer where low-frequency ($w = w_1$) and high-frequency ($w = w_2$) seismic gravitational waves are induced. If $N \to 1$, the upper boundaries $z = z_0$ and $z = z_1$ are approaching each other. If $N = 1$, the upper boundaries are merging into the single surface. Kinematics of internal seismic gravitational waves is analogous to kinematics of the surface seismic Rayleigh-type waves existing in the upper earth layer. When the long seismic gravitational waves with T_2 pendulum periods belonging to $0 < T_2 < 2\pi\sqrt{\dfrac{H}{g}} = 3.5\,\text{min}$ interval spread, the sea floor deformations are reflected at the sea surface without any changes.

INTRODUCTION

When studying the wave motion in the ocean, the sea floor is usually considered to be absolutely rigid. Therefore, a vertical component of the water flow velocity at the horizontal sea bottom is accepted to be zero $\left(\dfrac{\partial H}{\partial t} = 0\right)$. If we ignore the sea floor deformation vibrations, it may lead to diverging physical properties of the surface gravitational waves and corresponding real wave motion. Then, the whole class of wave motion – the forced seismic gravitational internal waves – may be eliminated. Evidently, these waves are also existent since the deformation vibrations in the Earth's crust are an experimental fact (Dolgikh, 2000; Monakhov, 1977).

The motive for the present investigation is that different theoretical wave motion models do not contain large enough pulsations of the bottom hydrodynamic pressure that can induce prominent microseisms in the oceanic earth's crust. The physical reason is the ignorance of existing deformation vibrations of the sea floor. The absolutely rigid sea floor eliminates the mechanism of energy interchange between the ocean and upper earth mantle (Tyukov, 2001) and does not allow developing reliable theoretical models of underwater earthquakes and tsunami.

BASIC EQUATIONS

Let us regard the following linear wave solutions:

$$u, w, \widetilde{P}, h = R_e\{u_0(z), w_0(z), P_0(z), \\ h_0 x \exp i(wt - kx + \alpha)\} \tag{1}$$

$$\frac{\partial \vec{V}}{\partial t} = -\frac{1}{\rho}\nabla P + \vec{g}, \ \nabla \cdot \vec{V} = 0, \ \rho = const \tag{2}$$

$$z = 0, \ \widetilde{P} = \widetilde{P}_a + \rho g h \equiv \widetilde{P}_0(x,t), \ w = -\frac{\partial h}{\partial t} \tag{3}$$

$$z = \overline{H} = const, \ w = \frac{\partial H}{\partial t} = q\frac{\partial \widetilde{P}}{\partial t} \equiv \frac{N}{\rho g}\frac{\partial \widetilde{P}}{\partial t} \tag{4}$$

where:

$\vec{V}(u, w)$ – is a vector velocity of homogeneous water and its projections on x, z axes of rectangular coordinate system. *X0Y* plane coincides with non-disturbed ocean surface and *Z* axle is directed vertically down;

$\vec{g}$ – is a constant gravity;

∇ – is the Hamilton operator;

$P_a, \widetilde{P}_a$ – is an atmospheric pressure constant and its pulsations;

$z = -h(x,t)$ – is a desired equation of the ocean disturbed surface, the initial position ($t=0$) of the ocean disturbed surface in $x=0$ point coincides with coordinate origin $z=0$, that is:

$$h(x,t) = 0, \ x = 0, \ t = 0 \tag{5}$$

$$P(x,z,t) = \overline{P}_a + \rho g z + \widetilde{P}(x,z,t)$$

where:

P, ρ – are the hydrodynamic pressure and water density;

$\widetilde{P}$ – are the hydrodynamic pressure pulsations;

$h_0 = h_1 + ih_2$, $w = w_0 + t\mu$, $k = k_1 + ik_2$ – are the complex wave numbers.

The dynamic boundary condition (4), according to which the continual ocean deepening is proportionate to the rate of bottom hydrodynamic pressure rise, is the analogue of the Hook's law on the proportional dependency of the relative body deformation on the imposed tension. The deformation function $q = \dfrac{N}{\rho g}$ describes the elastic gravitational properties of the top rocks of the oceanic earth's crust and is proportional to the rocks compressibility coefficient $\beta_2 = \dfrac{1}{\rho_c} \dfrac{\partial \rho_e}{\partial P}$.

Deformation function is defined in a point (x, y) by instrumental data and accepted to be constant during the forecast period of time. $q = N = 0$ is in case when the oceanic rocks do not become deformed and behave like absolutely rigid body.

It should be noted that the wave problem stated in (1)–(4) is analogous to a simpler classical Rayleigh problem about internal waves at the border of different environments and a rapid density change. The complexity of problem (1)–(4) follows from the fact that the underlying layer of the upper earth mantle H_g thick is very heavy and viscous. Therefore, there are significant elastic and shear forces at $Z = \overline{H}$ border in addition to quasi-elastic forces (for example, the resultant of gravity and Archimedes forces).

The dynamic boundary condition (4) causing the change in physical properties of the surface gravitational waves and generation of forced seismic gravitational waves is typical for any bottom topography. In case of viscous flow the condition (4) is met precisely due the fluid adhesion to the bottom. In case of ideal flow the condition (4) is met with an accuracy up to $|\nabla H| = 10^{-3}$ as it follows from the streamline condition.

When introducing solutions of (1) for $\widetilde{P}_a = 0$ into equations (2)–(6), we can get the following equations for the amplitude factors and dispersion relation $w = w(k, n)$:

$$u_0(z) = \frac{k}{\rho w} \widetilde{P}_0(z), \ w_0(z) = \frac{i}{\rho w} \frac{\partial \widetilde{P}_0(z)}{\partial z} \tag{6}$$

$$P_0(z) = P_g \left(\cos hkz - \frac{w^2}{gk} \sin hkz \right), \ P_g = \rho g h_0$$

$$w^2 = w_{1,2}^2 = gk \times$$

$$\times \left\{ \frac{1+N}{2N \tan hk\overline{H}} + \left[\left(\frac{1+N}{2N \tan hk\overline{H}} \right)^2 - \frac{1}{N} \right]^{1/2} \right\} > 0 \tag{7}$$

They can be implied as well in implicit form:

$$N(w^4 \tan hk\overline{H} - w^2 gk) = gk(w^2 - gk \tan hk\overline{H}) \tag{8}$$

If we take account of the sea water compressibility ($\rho = \rho(P)$) and try to solve the problem (1)–(5) with consideration of continuity equations again, the resultant dispersion relation will be almost the same as relations (7) and (8). This is connected with the fact that the squared Brunt-Vaisalla frequency $w_{VB}^2 = \dfrac{\overline{g}\nabla\rho}{\rho}$ describing the proper inertial variations of the vertical heterogeneous flow is one or two order less than the squared seismic gravitational frequency w_2^2. The latter is not connected with the ordinary internal waves of the heterogeneous flow at all, thus, we do not give the solution of this complex problem here.

DISCUSSION

Let us regard the case when h_0, w, k, and α are the real numbers, though the case with complex numbers h_0, w, and k with $\mu < 0$ is of more interest.

When separating the real components in (1) with the help of (5)–(8) solutions, we find the following expressions for desired functions u, w, $\widetilde{P}$, and h:

$$u(x,z,t) = \frac{k}{\rho w} P_1(z) \sin(wt - kx)$$

$$w(x,z,t) = w_1(z) \cos(wt - kx) \tag{9}$$

$$P(x,z,t) = P_1(z) \sin(wt - kx)$$

$$H(x,t) - \overline{H} \equiv \widetilde{H}(x,t) = \frac{N}{\rho g} \widetilde{P}(x, \overline{H}, t) \tag{10}$$

Here:

$$P_1(z) = -\widetilde{P}_0(z) \equiv P_g \left(\frac{w^2}{gk} \sin hkz - \cos hkz \right)$$
$$w_1(z) = wh_f \left(\cos hkz - \frac{gk}{w^2} \sin hkz \right) \tag{11}$$

Equalities (9)–(11) describe distribution of velocity fields and hydrodynamic pressure pulsations within the oceanic layer and define the laws of its external boundaries $z = 0$, $z = \overline{H}$ variability. The dispersion relation (7) with a minus sign describes the low frequency ($w = w_1$) surface gravitational waves with consideration of the sea floor deformation variations. The dispersion relation (7) with a plus sign describes the high-frequency ($w = w_2$) forced seismic gravitational waves that exist only under the sea floor deformations ($N \neq 0$).

From the dispersion relation (8) resulting from the dynamic boundary condition (4) it follows that in case of absolutely rigid sea floor ($N = 0$) the low-frequency surface gravitational waves occur in the ocean. The waves have the following dispersion relation:

$$w^2 = w_1^2 = gk \tan hk\overline{H} \qquad (12)$$

From here the following equations can be written down for the short ($kH \geq 2$) and long ($kH \leq 0.3$) surface gravitational waves:

$$w_1^2 = gk , \ w_1^2 = k^2 g\overline{H} \qquad (13)$$

The changes in physical properties of the surface gravitational waves occurring under the sea floor deformations ($N \neq 0$) can be studied over relation (7) written down for the short and long waves with an accuracy up to $\varepsilon = 0.05$:

$$w_1^2 = gk , \ w_1^2 = \frac{k^2 g\overline{H}}{1+N} , N>0 \qquad (14)$$

When comparing the relations (13) and (14) we can state that:

1. The frequency and phase velocity of the short surface gravitational waves do not depend at all on the sea floor dynamics, as according to (6), (10) and (11) the inertial hydrodynamic pressure variations are attenuating with depth by the exponential law and produce no impact on the deformed sea floor.

2. The sea floor deformations ($N \neq 0$) produce the stabilizing effect on low-frequency long waves $w = w_1$. The waves frequency and phase velocity decrease.

3. The horizontal component of the long surface gravitational waves velocity

$$u(x,t) = \left(\frac{g(1+N)}{\overline{H}} \right)^{1/2} h(x,t) \qquad (15)$$

is almost the same at any depth. If we take account of the sea floor deformations ($N \neq 0$), its amplitude will increase $(1+N)^{1/2}$ times.

4. The vertical component of the long surface gravitational waves velocity:

$$w(x,z,t) = w_1 h_f (1 - \frac{z}{\overline{H}}(1+N)) \cos(w_1 t - kx) \qquad (16)$$

when equal to zero and changing its sign at the horizon, $z_0 = \dfrac{\overline{H}}{1+N}$ divides the oceanic layer into upper ($0 < z \leq \overline{H}$) and lower ($z_0 < z \leq \overline{H}$) active parts with no water interchange between them. If the horizon $z = z_0$ with no vertical motion survives in real conditions, there will be no convective heat exchange. Thus, the geothermic heat flows will partly accumulate in the lower layer accounting for a slight temperature rise with depth in the lower layer of the ocean (Zhukov, 1976; Istomin, 1969).

In the upper layer $0 < z < z_0$ the particles move clockwise by elliptical orbits ($h_f > 0$). When in the upper orbit points, the particles velocity coincides with the wave direction.

In the bottom layer $z_0 < z < \overline{H}$ with $\overline{H} - z_0 = \dfrac{N\overline{H}}{1+N}$ thick, that is existent under the sea floor deformations only ($N \neq 1$), the opposite things are observed like in case of the surface seismic Rayleigh waves (Zharkov, 1983). When in the upper orbit points, the particles velocity does not coincides with the wave direction. At the horizon $z = z_0$ the elliptical orbits change into horizontal sections.

5. Long-wave pulsations of external pressure $\tilde{P}_1$ (induced by the passing surface wave and becoming the driving force with w_1 frequency) and forced seismic gravitational Rayleigh-type sea floor (and adjacent bottom layer) deformations occur in the opposite phases:

$$\tilde{z}(x,t) = h_f \sin(w_1 t - kx)$$

$$\tilde{H}(x,t) = -Nh_f \sin(w_1 t - kx)$$

It means that the local sea level rise ($\tilde{z} < 0$) corresponds to the sea floor lowering ($\tilde{H} > 0$). Such behavior of the deformed surface under the low-frequency ($w = w_1$) is usually called a meteorological tide.

The dispersion relation (7) with a plus sign describes a new class of high-frequency forced seismic gravitational variations that are existent only the sea floor deformations ($N \neq 0$). Disappearance of the leading term $Nw_2^4 \tan hk\overline{H}$ in the dispersion relation (8) under absolutely rigid sea floor ($N = 0$) testifies to it.

Let us mark the primary features of high-frequency forced seismic gravitational waves.

A. Long waves ($\lambda_1 \equiv \dfrac{2\pi\overline{H}}{0.3} \leq \lambda \leq \lambda_2 \approx 500 \ km$)

The dispersion relation (7) may be in the following approximate form:

$$w^2 = w_2^2 = \frac{g(1+N)}{N\overline{H}} = \left(\frac{2\pi}{T_2} \right)^2 > 0 \qquad (17)$$

1. Pendulum seismic gravitational variations (Tyukov, 2001) are in the interval of

$$0 < T_2 < 2\pi \sqrt{\frac{\overline{H}}{g}} = 3.5 \ min \qquad (18)$$

The accepted upper limit for the long waves is $\lambda < \lambda_2 = 500 \ km$ and connected with impact produced on the features of super-long seismic

gravitational waves ($\lambda > \lambda_2$) by the Earth's curvature.

2. The vertical component of the forced seismic gravitational waves velocity

$$w(x,t) = w_2 h_f \cos(w_2 t - kx) \qquad (19)$$

is the same at any depth.

3. Variations of the sea level and bottom that reflect each other identically are described by one equation:

$$\widetilde{z}(x,t) = \widetilde{H}(x,t) = h_f \sin(w_2 t - kx) \qquad (20)$$

4. When the long high-frequency ($w = w_2$) seismic gravitational waves spread – $\dfrac{w_2^2}{gk} = \dfrac{1+N}{NkH} > 1$ according to (17) – the oceanic layer is divided into the upper ($0 < z < z_1$) and bottom ($z_1 < z \leq \overline{H}$) layers with opposite directions of horizontal motion.

5. The horizon $z = z_1$ with zero velocity ($u(z_1) = 0$) according to (8), (9) and (11) is connected with deformation function N by general relations:

$$w_2^2 = \frac{gk}{\tan hkz_1}, \ N = \frac{\tan hkz_1}{\tan hk(\overline{H} - z_1)} \qquad (21)$$

For the long wave proper:

$$w_2^2 = \frac{z_1}{\overline{H} - z_1} \qquad (22)$$

If we exclude the zero horizon z_1 from equation (22), we will get the dispersion relation (17).

It should be noted that if $N \to 1$, the zero horizons z_0 and z_1 are approaching to each other. If $N = 1$, the zero horizons are merging into one surface.

6. Kinematics of high-frequency ($w = w_2$) long waves is analogous to kinematics of low-frequency long waves.

B. Short waves ($k\overline{H} \geq 2.0$)

1. Frequency and phase velocity of the forced seismic gravitational waves

$$w_2^2 = \frac{gk}{N}, \ c_2 = \left(\frac{g}{Nk}\right)^{1/2} \qquad (23)$$

are dependent on deformation function of the oceanic rocks.

2. Variations of the sea level and bottom

$$\widetilde{z}(x,t) = h_f \sin(w_2 t - kx)$$
$$\qquad (24)$$
$$\widetilde{H}(x,t) = (1-N)h_f \cos hk\overline{H} \sin(w_2 t - kx)$$

occur either in the same (if $N < 1$) or opposite (if $N > 1$) phases. Thus, against the long-wave case, the length $H(x, t)$ of non-equilibrium column of incompressible fluid changes due to displacement or inclusion of new particles.

Why the progressive waves with w_1 and w_2 frequency occurring in the bottom layers $z_0 < z \leq \overline{H}$, $z_1 < z \leq \overline{H}$ are called the forced seismic gravitational internal waves?

First, there are no sea floor deformation variations if the external pressure pulsations $\widetilde{P}_1$ transferred by incompressible oceanic layer from the sea surface to the bottom are completely compensated by $\widetilde{P}_2$ pressure pulsations coming from inside the earth to the surface. $\widetilde{P}_1$ pulsations are connected with wind activity and consequences of typhoons and storms, while $\widetilde{P}_2$ pulsations are linked to the earth's vibration and consequences of underwater earthquakes.

Second, the external pressure $\widetilde{P}_1$, $\widetilde{P}_2$ pulsations representing the driving forces of w_1 and w_2 frequency have the gravitational origin ($\vec{g} \neq 0$).

Third, the mechanism of transfer of the external pressure pulsations $\widetilde{P}_1$, $\widetilde{P}_2$ from the sea surface to the bottom and vice versa is not of inertial character typical for the surface gravitational waves, but of seismic gravitational or percussion character. Pressure pulsations $\widetilde{P}$ hit the end of incompressible water column and cause the forced deformed motion of the opposite column end.

Thus, we can solve two problems by equation (10). The direct problem is to define the sea floor deformation variations $\widetilde{H}$ (microseisms) by the given external pressure pulsations $\widetilde{P}$. The reverse problem is to define the forced variations of the sea level $\widetilde{Z}$ (tsunami waves) by the given sea floor deformations $\widetilde{H}$.

In order to solve these two problems it is necessary:

First, to replace the partial solutions of (10) type with the general solution of (1)–(5) that includes the whole spectrum of the free ($\widetilde{P} = 0$, $\widetilde{g} = 0$) and forced ($\widetilde{P} \neq 0$, $\widetilde{g} \neq 0$) wave frequencies $w_1(N, k)$, $w_2(N, k)$, ($-\infty < k_0 < \infty$).

$$\widetilde{z}_t(x, y, t) = A_i(t) \sin(\sigma_i t - k_{0i}(x \cos\theta_i + y \sin\theta_i)) \quad (25)$$

Second, to define deformation function N of rocks for a specific surface point (x, y) taking account of starting conditions.

Here:

$k_0 \cos\theta$ and $k_0 \sin\theta$ – are the projections of wave vector $\vec{k}_0$;

θ – is the angle between the wave vector and positive x axle.

In general case the free vibrations (25) in any point of the ocean surface are formed out of surface gravitational vibrations

$$\widetilde{z}_1 = h_f \sin(w_1 t - k_0(x\cos\theta + y\sin\theta))$$

and seismic gravitational vibrations

$$\widetilde{z}_2 = h_f \sin(w_2 t - k_0(x\cos\theta + y\sin\theta)) \ .$$

Therefore, for any free progressive wave of (25) type we have:

$$\widetilde{z}_1 + \widetilde{z}_2 = \widetilde{z}(t) = A(t)\sin(\sigma t - k_0(x\cos\theta + y\sin\theta)) \quad (26)$$

where:

$$A(t) = 2h\cos\frac{(w_2 - w_1)}{2}t \ , \quad \sigma = \frac{w_1 + w_2}{2}$$

The first theoretical part of the problem (1)–(5) can easily be solved. The second practical part requires many efforts since there are only disembodied data on microseisms at the surface of continental crust.

Let us make some quantitative assessments using the data (Dolgikh, 2000) of laser deformograph with horizontal arm S_0=52.5 meters located on the coast of Gamov peninsula. According to data, the amplitude of horizontal microseismic vibrations caused by the change of atmospheric pressure amounts to about $\left|\widetilde{S}\right| = 10^{-6}\ m$. If assume R_0=6.371×10⁶ meters and use the following equality line $\alpha = \frac{S_0}{R_0} = \frac{S(t)}{R(t)} = \frac{\left|\widetilde{S}\right|}{\left|\widetilde{H}\right|}$, we can calculate

$\left|\widetilde{H}\right| = \frac{S_0}{R_0}\left|\widetilde{S}\right| = 0.12\ m$. Here, α is the central angle at which the arm of laser deformograph is seen from the earth's center. The corresponding change of atmospheric pressure $\left|\widetilde{P}_a\right| = 15\ mmHg$ turned into meteorological tide equals $h_f = \frac{\left|\widetilde{P}_a\right|}{\rho g} = 0.2\ m$. In this case using equation (10) we get the deformation function for the rocks of continental crust:

$$N = \frac{\left|\widetilde{H}\right|}{h_f} = N_M = 0.6 \quad (27)$$

Unfortunately, this result cannot be immediately used for the oceanic crust with completely different elastic and deformation properties. We can only assume the deformation function N_0 of oceanic

rocks does not exceed $N_m = 0.6$, as a compressibility coefficient $\overline{\beta}_{ro}$ of oceanic rocks saturated with water is always lower than a compressibility coefficient of continental rocks $\overline{\beta}_{rc}$.

For example, if we assume $N_0 = 0.5$, $\overline{H} = 4\ km$ and $h_f = 1\ m$, we can get the following results for the long forced seismic gravitational internal waves from (9), (17), (19), (21), and (22): $|u| = 1.7$, $|w| = 8.6\ cm/s$, $w_2 = 0.086\ s^{-1}$, $T_2 = 1.2\ min$, $z_1 = 1333\ m$, $\left|\widetilde{H}\right| = h_f = 1\ m$.

The obtained results confirm the general conclusion that a horizontal component of the wave motion velocity is $\frac{1+N}{k\overline{H}}$ times lower than a vertical component. Therefore, it is almost impossible to define the location of the zero horizon z_1 and use equation (22) for calculating N function. It is much easier to calculate the deformation function N by means of equating theoretical variations of the sea level $\widetilde{z}(x, y, t, N)$ with the real ones $\widetilde{z}_f(x, y, t)$ obtained experimentally.

Let us use the least square method and generate the function

$$\Phi(N) = \sum_{j=1}^{m}\left(\widetilde{z}(x, y, t_j, N) - \widetilde{z}_f(x, y, t_j)\right)^2 = \min$$

and demand it will take the possible minimum value at a specified time section $t = m\Delta t$. In this case we can calculate deformation function N using the extreme condition $\frac{\partial Q}{\partial N} = 0$.

CONCLUSIONS

1. The forced low-frequency ($w = w_1$) and high-frequency ($w = w_2$) seismic gravitational waves occur in the bottom layer $z_0 < z \le \overline{H}$, $z_1 < z \le \overline{H}$ under the influence of the sea floor deformation vibrations ($N \ne 0$).

2. Kinematics of the forced low-frequency ($w = w_1$) and high-frequency ($w = w_2$) waves caused by the sea floor deformations in the bottom layer is analogous to kinematics of the surface seismic Rayleigh-type waves existing in the upper layer of oceanic crust.

3. When the long surface gravitational waves of low frequency ($w = w_1$) spread, the sea level $\widetilde{z}(t)$ and bottom $\widetilde{H}(t)$ variations occur in antiphase as the local level rise corresponds to the sea floor lowering.

4. When the long seismic gravitational waves of T_2 pendulum periods belonging to

$$0 < T_2 < 2\pi\sqrt{\frac{\overline{H}}{g}} = 3.5 \text{ min}$$

interval spread, the sea floor deformations are reflected at the sea surface without any changes.

5. Absence of vertical or horizontal motion is the kinematic feature of the upper boundaries $z = z_0$, $z = z_1$ of the bottom layer where low-frequency ($w = w_1$) and high-frequency ($w = w_2$) seismic

gravitational waves are induced. If $N \rightarrow 1$, the upper boundaries $z = z_0$ and $z = z_1$ are approaching each other. If $N = 1$, the upper boundaries are merging into single surface.

6. The sea floor deformations cause the possible increase of the frequency of free progressive waves from w_1 to $\dfrac{w_1 + w_2}{2}$ and temporal variability of their amplitude $A(t)$.

REFERENCES

Dolgikh G.I. **2000**. Research of ocean and lithosphere wave fields by laser-interference methods, Vladivostok, Dalnauka, 160 pp. (In Russian).

Istomin Yu.V. **1969**. Oceanology, Leningrad, GIMIZ, 470 pp. (In Russian).

Monakhov F.I. **1977**. Low-frequency seismic noise of the Earth, Moscow, Nauka, 96 pp. (In Russian).

Tyukov I.Ya. **2002**. About Mechanism of appearance of Rayleigh type FSGW waves. Proceedings of XLV All-Russian Inter-college research conference, Vladivostok, v.1, p. 158–163. (In Russian).

Tyukov I.Ya. **2001**. About Mechanism of appearance of seismic-gravitation waves in the ocean and Earth mantle. Proceedings of 2nd All-Russia Symposium "Seismo-acoustic of transition zones", p. 53–55. (In Russian).

Zharkov V.N. **1983**. Internal structure of the Earth, Moscow, Nauka, 416 pp. (In Russian).

Zhukov L.A. **1976**. General Oceanology, Leningrad, GIMIZ, 376 pp. (In Russian).

ASSESSMENT OF LARGE-SCALE CONNECTION BETWEEN THE ATMOSPHERE AND ICE COVER IN THE SEA OF OKHOTSK

L.N. Vasilevskaya[1,2], N.I. Savelieva[1], V.V. Plotnikov[1,3]

[1] *V.I. Il'ichev Pacific Oceanological Institute, Far Eastern Branch of Russian Academy of Sciences (POI FEBRAS), Russia*
Email: arctic@online.marine.su

[2] *Far Eastern State University (FESU), Russia*

[3] *Far Eastern Regional Hydrometeorological Research Institute (FERHRI), Russia*

Long-term and seasonal variability of ice cover in the Sea of Okhotsk from the 1929 to 2000 is investigated. The relationship between ice cover and parameters of the Siberian High, Aleutian Low and Hawaii High is examined on the base of analysis of cumulative curve of their anomalies. The long-term variability of ice cover in the Sea of Okhotsk reveals two periods with tendency to reducing ice cover (1929–1957 and 1982–1998) and one period with tendency of increasing ice extent (1958–1982). The ice conditions depend on the complex relations between three centers of action of the atmosphere (CAA) over the Asian-American sector of the Northern Hemisphere. The mild ice conditions in the Sea of Okhotsk till the early 1980s are accompanied by weakening Siberian High. Heavy ice cover coincides with the greater-than-normal development of the Siberian High. The ice cover and pressure difference between the Siberian High and Aleutian Low shows the same relation. Otherwise, the Aleutian Low itself does not reveal good correlation to the ice cover. During the last two decades the relationship between ice cover in the Sea of Okhotsk and these two CAA changed. The main reason of these changes is connected to the influence of the Hawaiian High ridge on the cyclone trajectory over the Sea of Okhotsk.

INTRODUCTION

The estimation of the ice cover variability is important for better understanding of some basic climatic variables. Ice cover is assumed to be a sensitive indicator of climate conditions. Regional sea ice variations are generally consistent with air temperature anomalies and modes of atmospheric circulation (Chapman and Walsh, 1993; Power and Mysak, 1994).

The Sea of Okhotsk is the one of the southernmost ice covered seas in the Northern Hemisphere. Relationship between the regional oceanography and meteorology and sea ice cover in the Sea of Okhotsk have been examined in several studies (Watanabe, 1972; Parkinson and Gratz, 1983; Cavalieri and Parkinson, 1987; Plotnikov, 1981; Muktepavel *et al.* 2001) The results of all previous investigations suggest a large-scale atmospheric control of ice cover in the Okhotsk region.

Parkinson and Gratz (1983) examined the seasonal cycle of the ice cover in the sea for 4 years (1973–1976). They found that unusually heavy ice conditions in 1973 are associated with greater than normal impact of the Siberian High while in 1974–1976 the Aleutian Low produced greater influence on the sea level pressure over the Sea of Okhotsk. Cavalieri and Parkinson (1987) investigated relations between atmospheric circulation and the fluctuations in the sea ice extent in the Bering Sea and Sea of Okhotsk for four winters 1972–1973 through 1975–1976 on the short-term, seasonal, and interannual time-scales and defined those periods when there is the out-of phase relationship between the fluctuations of ice cover in these seas. It was shown that sea ice fluctuations were

related to changes in the position and intensity of Aleutian Low and Siberian High. Shatilina *et al.* (2001), Muktepavel *et al.* (2001) investigated abnormal ice conditions in the Sea of Okhotsk and came to the conclusion that extreme ice conditions are characterized by intensive troposphere polar whirl over the Sea of Okhotsk.

The Sea of Okhotsk is one of the most productive areas of the World Ocean. Severe weather conditions form a seasonal ice cover reaching sometimes 100% area of the sea surface (Plotnikov, 1985). The atmospheric circulations over Eastern Asia and the northwestern part of the Pacific Ocean during the cold period of the year determines the hydrometeorological and, in particular, ice conditions.

In this paper we study connection between the large-scale circulation associated with centers of action of the atmosphere (CAA) (the Siberian High, Aleutian Low, and Hawaiian High) and ice cover in the Sea of Okhotsk on the base of all available historical data on ice conditions and large-scale circulation in the Asian-American sector of the Northern Hemisphere for 1929–2000.

DATA AND METHODS

Data set of the averaged monthly and maximum ice extent over the Sea of Okhotsk is used for the study (unpublished data of Plotnikov's archive). This archive is created out of data obtained during the regular aircraft observations of 1957–1981 (carried out by Hydrometeorological Service), ship observations over the ice conditions since early 1950s published by Krydin (1964). Data for the early 1930–1960 and

satellite data were collected in TINRO Center for 1979–2000. Initial data consist of 10-day mean values of ice cover, which are calculated on the base of all available information. Here ice cover (%) is the area of sea surface covered with ice relative to the total area of the Sea of Okhotsk.

The time series of geographical coordinates and sea level pressure (hPa) in the centers of the Siberian High, Aleutian Low (for 1890–2000), and Hawaiian High (1929–1994) were created from three sources. The first one is data sets taken from "Catalogue of atmospheric circulation" (1988), the second one is from the proceedings of Maximov and Karklin (1969) and Smolyankina (1999) and the one third is the additional data presented kindly by the department of long-term weather forecasts of FERHRI.

The area of Siberian High for 1955–1989 period (January through March) was calculated using the method offered by Il'inskiy (1965). It is a part (%) of Asian continent northward 40°N enclosed by the 1020 hPa anticyclonic isobar contour. This parcel of the Siberian High is the most variable (Figure 1) and produces strong influence on the synoptic processes over the Sea of Okhotsk.
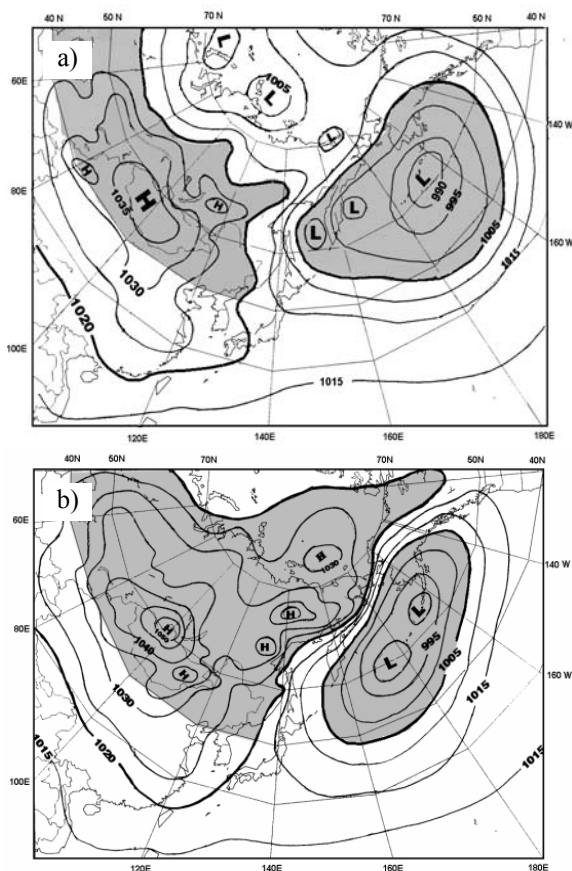
Figure 1. Examples of minimum (a) (60% of the Asian area to the north of 40°N in December, 1963) and maximum (b) (100% in December, 1976) development of Siberian High (Savelieva *et al.*, 2000)

To estimate the long-term connection in the atmosphere-ice system the analysis of cumulative curves of seasonal ice cover in the Sea of Okhotsk and large-scale atmospheric circulation (the Siberian High, Aleutian Low and Hawaii High parameters) was used. The cumulative curves allow identifying the long-term tendencies of the parameters investigation. This approach was applied for the study of the long-term variability of circulation patterns in the Northern Hemisphere by Girs (1960). The method is as follows: the monthly mean value of a parameter is compared with the multi-year monthly averaged value and anomalies are calculated. The cumulative curve is obtained by consecutive summing of these anomalies. If the anomalies are positive (value is higher than the multi-year mean) during any period of time, the cumulative curve goes upward. It means that the process under consideration has anomalous development. When cumulative curve is downward (negative anomalies prevail) the process is weak. The turning point on the cumulative curve is the moment when processes change their tendencies. It is important that cumulative curves allow analyzing the data without smoothing.

RESULTS

Long-term variability of ice cover in the Sea of Okhotsk. Variations in the ice extent in the Sea of Okhotsk are dominated by the growth and decrease associated with the seasonal cycle. The seasonal ice cover begins to appear as the earliest in the end of November–December. The January is characterized by the highest speed of ice field formation. March is the month of maximum ice cover when only the waters near the Kuril Island are ice-free. In April the ice melting and break are the dominating processes and the most area of the sea becomes free of ice. In June only the little amount of ice can be found except for the trace amounts in the coastal regions.

We examined the cumulative curves of ice cover (IC) during the cold months of the year (December through May) where the periods of abnormal growth and decrease of IC are clearly revealed. The cumulative curves of IC appear to vary on a time scale of approximately 45 years period (1957–2000) as a long wave similar century solar cycle (Girs and Kondratovitch, 1978)

The cumulative curves of seasonal IC show variability of IC on many time scales (Figure 2). We found that during 1957–1980 in December the IC was above average with the positive anomalies prevailing. The next 19 years are characterized by negative anomalies (curve falls). The background of long-term variability is the short-time fluctuations of 5 years.

In January there is a uniform upward of cumulative curve, as in December, till the 1980 (positive anomalies accumulate), and then rather steady downward till 1997 (negative anomalies prevailed). The duration of short-term fluctuations is 2–3 years.
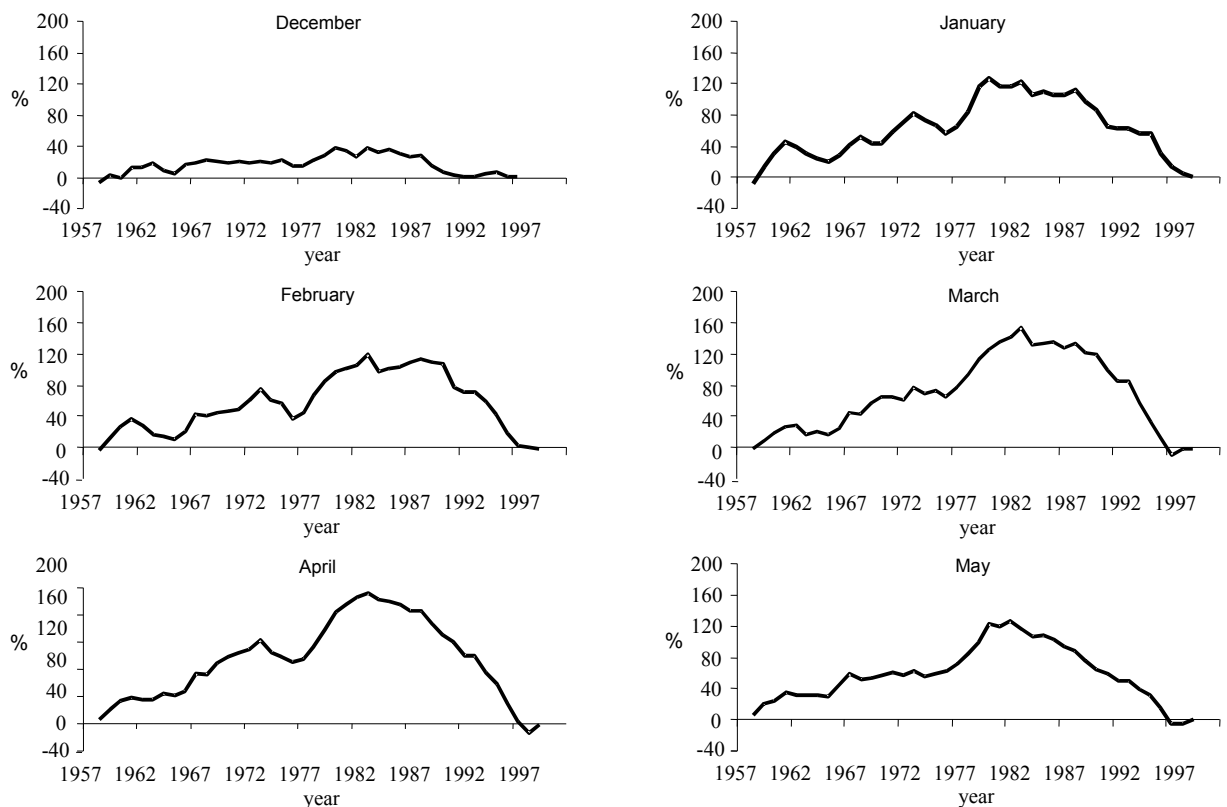
**Figure 2. Cumulative curves of ice cover anomalies in the Sea of Okhotsk
in different months of the year (1957–1999)**

In February 1983 the growth of cumulative curve changed from upward to downward. The duration of positive anomaly accumulation is 26 years and 16 years for negative ones. The short-term change in tendencies is 7–8 and 11 years.

In March, April, and May the cumulative curves have the same tendencies: increase to 1983 and then decrease through 1997.

Therefore, the main feature of the long-term variability of IC in the Sea of Okhotsk for 1957–1997 is the period of positive anomalies (1957–1983) and the next shorter period (about 14 years) of negative anomalies in the cold part of the year.

The maximum IC in the Sea of Okhotsk is in March (Hydrometeorological…, 1998). We obtained high correlation ($r = 0.92$) between seasonal IC (December through April) and maximum IC for 1957–2000. There is the data of maximum IC since 1929. Based on high correlation between seasonal and maximum IC for 1957–2000 we suggest that a mode of the seasonal IC for previous years (1929–1957) is similar. So we can discuss the seasonal variability of IC for 1929–2000 using maximum IC cumulative curve (Figure 3).

Muktepavel *et al.* (2001) analyzed the changed ice conditions in the Sea of Okhotsk and found that peak ice cover was recorded in 1970s amounting to 70% in February and to more than 80% in March.
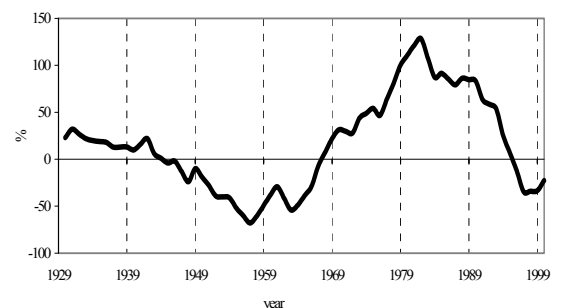
**Figure 3. Cumulative curve of maximum
ice cover anomalies (%) in the
Sea of Okhotsk (1929–2000)**

Low-ice periods occurred in 1952–1958, 1976 and 1990–1997. Starting from 1998, the ice cover began to grow and by 2000 it exceeded the standard rate.

As shown in Figure 3, in the Sea of Okhotsk the light ice conditions for 1929–1957 (recession of a curve) were observed. On the contrary, 1957–1982 period reveals a positive IC anomaly. So the turning point on the cumulative curve is obtained for the early 1980s. The difference peaks of cumulative curve in 1920s and 1980s might be connected with different macro-circulation epoch in the troposphere (Dmitriev, 1996). 1930–1950s are characterized by zonal fluxes in the atmosphere and low-than-normal Siberian High development while 1970–1980s, which coincide with

the growth of ice extent and harsh ice conditions, by meridional fluxes and enhance of the Siberian High. It should be noted that in 1976–1977 there was the well-known shift in both the climate and ecosystem of the North Pacific (Minobe, 2000; Hare *et al.*, 2000), which resulted in reorganization of the whole climate system.

After 1980s the observed decrease of IC through 1997 testifies to the milder ice conditions in the Sea of Okhotsk during the last decades. In 1997 the ice cover amounted to 44% of the sea area. Since 1999 there is the upward tendency in the cumulative curve and in 2001 93% of the sea were covered with ice (Muktepavel *et al.*, 2001). In the end of 1990s (1998–1999) there was a phase when lighter ice conditions began to change (slight positive anomalies appeared).

During 1997 and 1998 in the southeastern Bering Sea unusual conditions were observed: the highest sea surface temperature, the change in the timing of the last winter storm, strong winds in May and decreasing onshore transport of slope water (Stabeno *et al.*, 2001). As previous investigations showed (Plotnikov, 1996), the evolution processes of ice conditions in the Bering Sea and Sea of Okhotsk are closely related to each other (inverse relation). Against the background of general rules there are cases of their violation, with their number essentially increasing for the last decade, which points to the possible climate changes of hydrometeorological and, in particular, ice conditions on all the Far Eastern seas. After the climate shift mentioned above 'out-of-phase' ice conditions between the Bering Sea and Sea of Okhotsk changed and 'in-phase' ice conditions appeared. We can consider this phenomenon in the context of linkage inside the Northern Pacific climate system.

Long-term variability of the CAA. According to the recent point of view, the direct influence of atmospheric circulation on the sea ice cover in winter is caused by interaction of the Siberian High and Aleutian Low. The strengthened zonal air fluxes over Asia result in the weakening of the Siberian High and creation of western cyclones over the Far East. On the back edge of western cyclones there is a restoration of the Siberian High and large flux of cold air mass from Eastern Asia. The high-altitude frontal zone strengthens, and marine cyclones form, which composite in the Aleutian Low. As a result the Kamchatka, Chukotka peninsulas, and the Sea of Okhotsk are under the influence of warm air of the pacific origin moving to the eastern periphery of southern cyclones. But the trajectory of this warm air flux is in turn determined by a location of the blocking ridge of the Hawaiian High. In these cases the amplification of the Siberian High is carried out as the consequence of the stability of meridional atmospheric circulation.

The Siberian High. The geographical location of the Siberian High (SH) and its intensity play the important role in formation of atmospheric processes over the Asian continent and in general circulation of atmosphere in the Northern Hemisphere.

The SH begins to develop in September in the mountainous regions of Siberia and Central Asia and reaches maximum development in winter. It disappears in May–June. The center of the SH is located between 49° and 52°N and from 88°E up to 98°E. It is formed in low layers of the troposphere near the Earth's surface and disappears at 3 km height. The pressure in the center of the SH varies from 1007 up to 1060 hPa.

As our calculation shows in the process of development the SH at first occupies about 40% of the Northern Asia in September (to the north of 40°N on the average long-term data). Then it is gradually increases in size till December–February when more than 80% of the northern Asian area is under the influence of high pressure. In March it is still significant (75%) decreasing through April (35%) till May when it covers less than 14% (Figure 4).

The negative pressure anomalies were observed during 1891–1957 and then there was a sharp increase between 1960 and 1980s (Figure 5). The short-term variability is from 3 to 10 years. The significant positive anomalies since 1960s are connected with enhance of this center of action. The background of this variability of sign anomalies is about 90 years long-term climate wave (Luchin and Saveliev, 1999).
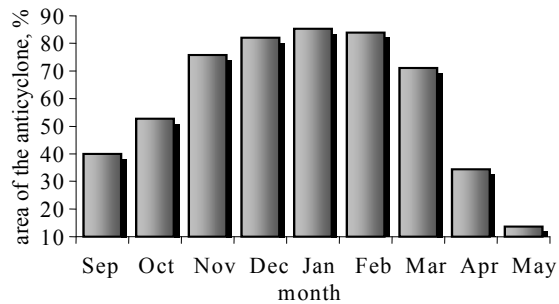
Figure 4. The averaged seasonal values of relative size (%) of the Siberian High square for 1958–1990 period
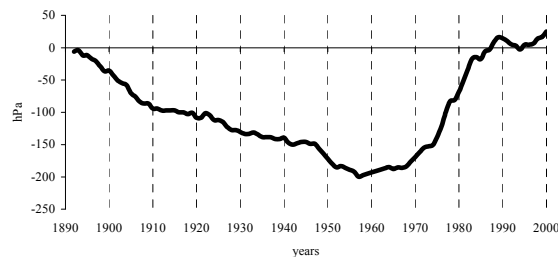
Figure 5. Cumulative curve of the Siberian High pressure anomalies (hPa)

The analysis of coordinates of the SH for 1947–1994 showed that from the end of 1950s up to the middle 1980s the SH was to the east of the normal location (Vasilevskaya *et al.*, 2002). In the first half of this period the SH was situated to the southeast of usual, and in the second half to the northeast of the averaged multi-year location. In 1958–1990 the SH was displaced to the north, the area occupied by it (north of 40°N) increased, and then SH displaced southward and its area decreased.

Aleutian Low (AL) develops over the North Pacific simultaneously with the development of the SH above the Asian continent. As a rule, AL has two centers. One center is situated to the southeast of the Kamchatka Peninsula and the second one is over the Gulf of Alaska (Figure 1).

The average latitude of the AL varies from 50°N (February) to 60°N (August) that is the displacement in the south-north direction within the year is 10°. In some years the AL in summer is located as far north as 75°N and in winter as far south as 31°N (Perevedentsev, 1994). For the last five decades the latitudinal position of AL varied from 40° up to 66°N. The pressure in the center of AL has strong seasonal variability and varied from 982 up to 1016 hPa. According to the long-term monthly average, the minimum pressure (997 hPa) is observed in January and the maximum one in June (1010 hPa) (Pervedentsev, 1994). During the 1890–1910s (about 25 years) the AL positive anomalies grew. From the beginning of 1920s till the end of 2000 (~80 years) the AL deepened accompanied by the small rise of pressure in the end of 1940–1950s and the early-middle 1970s (Figure 6). As shown in the previous investigations (Overland *et al.*, 1999), over one-third of winter interannual variability of the Aleutian Low since 1900 is on time scale greater than 5 years.

Hawaiian High (HH) plays a key role in the teleconnection between low and moderate latitude. The average monthly values of pressure in the HH changed from 1013 hPa up to 1033 hPa and displaced from 18° up to 48°N, and from 151°E up to 117°W. Volkov *et al.* (1990) found that in most cases weakening of HH occurred during El-Niño phenomena. Saveliev (1999) examined that this accompanies by south or southwest HH displacement and resulted in less advection of warm air mass from low to moderate latitudes. The negative air temperature anomalies appeared over northwestern Pacific.

The analysis of long-term (1929–1994) variability of HH pressure showed that in 1929–1940s the HH was in its active state, which was replaced by 7 years with low pressure. Since 1948 to 1977 the pressure in the HH was above norm, and in 1977–1994 its pressure became abnormally low (Figure 7). The 1977 and 1982–1983 periods coincided with El-Niño and HH

was characterized by very low pressure anomalies (-6.4 and -6.7 mb, correspondingly). The main periodicity of multi-year variation of HH is close to the South Oscillation (Saveliev, 1999).

DISCUSSION

The joint analysis of cumulative curves of IC (Figure 3) and the SH pressure (Figure 5) showed that in 1929–2000 the light ice conditions in the Sea of Okhotsk coincided with the weak development of the SH. The period of the IC rise coincides with the period of intensive development of the SH. However, during the last two decades there is a shift in the maximum of cumulative curves of the IC and the SH pressure by approximately 7 years. In previous period their extremes coincided. In 1982 the IC became to reduce whereas the SH begins to weaken only since 1989.
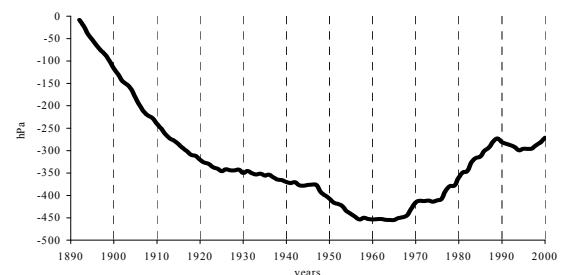
To understand the reason of this shift we estimated the joint influence of the SH and AL in the formation of ice conditions in the Sea of Okhotsk using pressure differences (PD) between these centers (Figure 8).
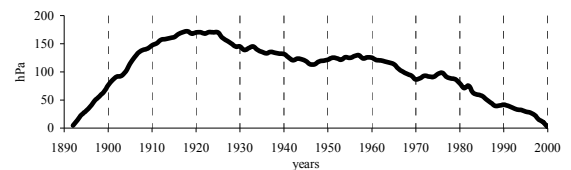
Figure 6. Cumulative curve of the Aleutian Low pressure anomalies (hPa)
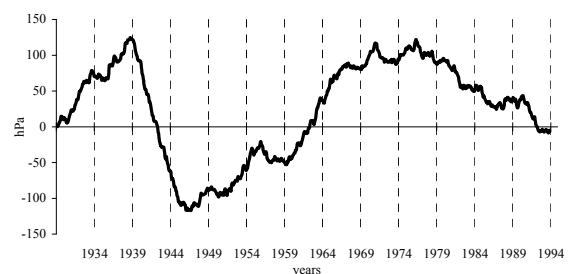
Figure 7. Cumulative curve of the Hawaiian High pressure anomalies (hPa)

Figure 8. Cumulative curve of pressure differences between the Siberian High and Aleutian Low (hPa)

It is important that of PD determine type of atmospheric air fluxes. As the previous studies showed (Savelieva *et al.*, 2000), the pressure difference between these centers increased 5.1 hPa since 1970s when the Siberian High intensity increased 3.5 hPa and the Aleutian Low deepened 1.6 hPa. The horizontal gradient of pressure between the Siberian High and Aleutian Low increased from 0.41 hPa/longitude degree before 1970s to 0.46 hPa/longitude degree after that. The maximum gradient was observed in 1977 (0.65 hPa/long. degree) when Siberian High reached extreme development, and in 1983 (0.54 hPa/long. degree) when Aleutian Low was the deepest. Increasing PD induces the strengthening of meridional fluxes.

The PD influences the intensity of atmospheric circulation over the Sea of Okhotsk. The PD from the end of the 19th century to the beginning of the 20th century remained abnormally low. In the next four decades (till 1967) its anomalies remained close to the norm. Since the end of 1960s (1967–1989) the anomalous PD are positive. During 22-year period there was a simultaneous activity in the both centers of action.

The comparison of cumulative curves of maximum IC and PD showed that in 1929–1982 the variability of IC (Figure 3) and PD anomalies (Figure 8) is the same. The IC increase is accompanied by increase of PD and vice versa. However, the turning point of IC cumulative curve took place for about 7 years earlier (in 1982) than on PD curve (in 1989). On the other hand the weakening of the HH became in 1977 (Figure 7), *i.e.* 5 years earlier than reduction of ice cover in the Sea of Okhotsk. At the same time the AL does not have such relationship (Figure 8).

The connection between IC and PD might be explained in the following way. The increase of PD influences the strengthening cyclone activity over northwestern Pacific and, as a consequence, the storm activity over the Far Eastern seas (Bering, Okhotsk and Japan seas). In storm case the sea surface in the back edge of cyclones cools down faster than under calm weather conditions (Vasilevskaya, 2000). Why in 1982–1989 this connection was fell apart?

We suppose that it is connected with the HH influence on a trajectory of cyclones (mainly to the Okhotsk or Bering Sea), which also plays an important role in the formation of ice cover in the Sea of Okhotsk. If the HH is located to the west of North Pacific the cyclones move to the Sea of Okhotsk. In the case of eastward location of HH the cyclones displace to the Bering Sea. Therefore, the location of HH is a very important factor for ice conditions in the both seas.

Estimation of the contiguity of ice conditions in the Sea of Okhotsk and Bering Sea shows different tendencies in ice cover variability. For example, when ice conditions in one of the sea increase, the decrease is expected in the other one in most cases. Nevertheless, sometimes these out-of-phase episodes disturb in particular during the last decade (Plotnikov, 1996).

CONCLUSION

The long-term variability of ice cover in the Sea of Okhotsk (1929–2000) reveals two periods when negative anomalies (light ice conditions) dominate (1929–1957 and 1982–1998) and one period of heavy ice conditions with prevailing positive anomalies (1958–1982). Close to half-century cycle in ice cover variability exists.

The connection between ice cover in the Sea of Okhotsk and atmosphere processes over Asia-Pacific region is found. The ice conditions depend upon the complex relationship between three CAA: the Siberian High, Aleutian Low and Hawaiian High. The variability of ice cover, parameters of CAA have the same duration (2–4, 5–7, 11–16, 21–29 years).

The heavy ice cover in the Sea of Okhotsk is accompanied by greater-than-normal development of the Siberian High and mild ice conditions coincide with the weakening of Siberian High, accordingly. The pressure difference between the Siberian High and Aleutian Low shows the same dependence. Otherwise, the Aleutian Low itself does not reveal close relation to the ice cover.

During the last two decades the relationship between ice cover in the Sea of Okhotsk and two CAA changed. From our point of view the main reason of these changes is connected to the influence of the Hawaiian High ridge that determines the cyclones trajectory over the Sea of Okhotsk.

Extrapolation of cumulative curves of ice cover makes it possible to forecast future scenario of ice conditions in the Sea of Okhotsk as following. The cold seasons of 2003–2004 are expected to reveal mild ice conditions, and starting from 2005 to 2020 a prevalence of greater-than-norm ice cover should be observed. Nevertheless, during the first months of the latter period (December–February) rather light ice conditions with the duration of 2, 5 and 7 years could be expected. However, in March, April and May ice conditions should be hard, as a rule.

REFERENCES

Catalogue of parameters of atmospheric circulation. Northern Hemisphere: the centers of action of an atmosphere. A planetary high-altitude frontal zone. Blocking anticyclones. **1988**. RIHMI-WDC. (In Russian)

Cavalieri D.J., **Parkinson** C.L. **1987**. On the relation between atmospheric circulation and the fluctuations in the sea ice extents of the Bering and Okhotsk seas. J.Geophys.Res., 92, p. 4141–7162.

Chapman W.L., **Walsh** J. **1993** Recent variations of sea ice and air temperature in high latitudes. Bull.Am.Met.Soc., v.74, 1, p. 33–47.

Dmitriev A.A. **1994**. Variability of atmospheric processes over the Arctic and its taking into account in long-term forecasts. St-Petersburg: Hydrometeoizdat. (In Russian)

Girs A.A., **Kondratovich** K.V. **1978**. Methods of long-term weather forecasts. Leningrad: Hydrometeoizdat (In Russian)

Girs A.A. **1960**. The base of long-term forecasting. Leningrad: Hydrometeoizdat. (In Russian)

Hare S.R., **Mantua** N.J. **2000**. Empirical evidence for North Pacific regime shifts in 1977 and 1989. Progr.Oceanogr., 47, pp. 103–147

Hydrometeorological conditions. **1998**. In Hydrometeorology and hydrochemistry of the seas. The Okhotsk sea. V.1 St.-Petersburg:Hydrometeiizdat (In Russian).

Krydin A.N. **1964**. Seasonal and interannual changes of ice conditions and position of ice edge in the Far Eastern seas because of the peculiarities of atmospheric circulation. GOIN Proceedings, 71, p. 5–83. (In Russian).

Il'inskiy O.K. **1965**. Synoptic processes and weather forecasting in the east region of the USSR. In The manual on short-term weather forecasts. Part 3, v.4, Leningrad: Hydrometeoizdat. (In Russian).

Luchin V.A. **Saveliev** A.V. **1999**. Interannual and long-period variability of waters in the west part of the Bering Sea. J.Met. i.Hydr.. 5, p. 91–99. (In Russian).

Maximov I.V. **Karklin** V.P. **1969**. Seasonal and long-term changes of a geographical location and intensity of the Siberian maximum of atmospheric pressure. Proc. of Vsesouznogo Geograficheskogo obschestva, 4. (In Russian).

Minobe S. **2000**. Spatio-temporal structure of the pentadecadal variability over North Pacific Progr.Oceanogr., 47, p. 381–408.

Muktepavel L.S., Plotnikov V.V., Colony R.L. **2001**. The cause of anomalous ice conditions in the Okhotsk (Bering) Sea. Proc. of Arctic Regional center v.3, p. 29–41.

Overland J.E., **Adams** J.M., Bond, N.A. **1999**. Decadal variability of the Aleutian Low and Its relation to high-latitude circulation. J. Climate, 12, p. 1542–1556.

Parkinson C.L, **Gratz** A.J. **1983**. On the seasonal sea ice cover of the Sea of Okhotsk. J.Gephys. Res., 88, p. 2793–2802.

Perevedentsev U.P., Ismailov I.V., Shantalinskiy K.M. **1994**. The centers of action of an atmosphere in the Northern Hemisphere. 4–15, Kazan, (In Russian).

Plotnikov V.V. **1981**. Investigation and forecast of ice condition in the Sea of Okhotsk. Ph.D.Thesis, Far Eastern Hydromet. Research Inst., Vladivostok, Russia.

Plotnikov V.V. **1985**. The statement and perspectives of development of methods of the ice forecasts in the Far Eastern seas. J.Met.i.Hydr., 10, p. 114–118. (In Russian).

Plotnikov V.V **1996**. Space-time relations between ice conditions in the Far Eastern seas. J.Met. i.Hydr., 3, p. 71–78. (In Russian).

Power S.B., **Mysak** L.A. **1994**. On the interannual variability of Arctic sea-level pressure and sea ice. Atmos.–Ocean., 30, p. 1–23.

Saveliev A.V. **1999**. Japan Sea response to El-Niño. FEHRI Special Issue, 2, p. 54–70.

Savelieva N.I., Semiletov I.P., Vasilevskaya L.N., Pugach S.P. **2000** A climate shift in seasonal values of meteorological and hydrological parameters for Northeastern Asia. Progr.Oceanogr., 47, p. 279–297.

Shatilina T.A., Nikitin A.A., Muktepavel L.S. **2001**. Peculiarities of atmospheric circulation in abnormal oceanological conditions in the Japan, Okhotsk seas and adjacent part of the Pacific. TINRO Proceedings, (in press). (In Russian).

Smolyankina T.V. **1999**. Long-term variability of anomalies of pressure, latitude and longitude of the centers of action of an atmosphere Asian-Pacific region // FERHRI Proceedings, thematic issue, 2, p. 10–16. (In Russian).

Stabeno P.J, Bond N.A., Kachel N.B., Salo S.A., Schumacher J.D. **2001**. On the temporal variability of the physical environment over the south-eastern Bering Sea. Fish. Oceanogr., 10, 1, p. 81–98.

Vasilevskaya L.N. **2000**. The strong winds in the Sakhalin Island. In Abstr. of the 2nd ice scoure and arctic marine pipelines workshop, 264, Mombetsu, Hokkaido, Japan.

Vasilevskaya L.N., Zhuravleva T.M., Manko A.N. **2002**. Seasonal and long-term variability of the Siberian High parameters. FERHRI Proc., 150, (in press). (In Russian).

Volkov Yu.N., **Kalashnikov** B.M. **1990**. El-Niño: identification and possibility of forecasting. FERHRI Proceedings, 136, p. 158–172. (In Russian).

Watanabe K., **1972**. An average pattern of extending and retreating of an ice area in the Sea of Okhotsk. In Sea Ice, National Research Council, Reykjavik, Iceland.

MONITORING OF POTENTIAL ENVIRONMENTAL EFFECTS OF OIL EXPLORATION IN THE SEA OF OKHOTSK AND DISTRIBUTION OF ARTIFICIAL RADIONUCLIDES IN THE SEA OF JAPAN

A.V. Tkalin[1], T.S. Lishavskaya[1], T.A. Belan[1], E.V. Karasev[1], O. Togawa[2]

[1] *Far Eastern Regional Hydrometeorological Research Institute (FERHRI), Russia*
   Email: ATkalin@hydromet.com

[2] *Japan Atomic Energy Research Institute (JAERI), Japan*

An extensive ecological survey was conducted to investigate possible environmental effects of offshore oil drilling activities in the Sea of Okhotsk in 1998. Marine environmental impact of appraisal well drilling and production platform installation in the NE Sakhalin Island shelf appeared to be present in less than a month in the water column and also limited to the immediate surrounding bottom sediments within 250 m of the center of activity.

As a follow up of the 1994–1995 intergovernmental investigation on the consequences of radioactive waste dumping and accidents in the Sea of Japan proper and its coastal zone, two sampling expeditions were carried out in 1999–2000 period. Activities of gamma emitters, ^{90}Sr and ^{239,240}Pu in seawater and bottom sediments were low and caused by global atmospheric fallout of radionuclides. Data obtained in these expeditions are quite close to the results of previous investigations by different research groups. In Peter the Great Bay, the main sources of radionuclides appeared to be still their global atmospheric fallout and the discharge of freshwater and suspended sediments from river runoff. There is no clear indication of the impact of navy facilities on radioactive contamination of Peter the Great Bay except elevated ^{60}Co activities resulting from 1985 accident in Chazhma Bay. ^{60}Co released during this accident is still present in bottom sediments of Strelok Bay at significant levels (up to 150 Bq/kg). In fishing and recreational areas of Peter the Great Bay (Amurskiy and Ussuriyskiy bays), levels of radionuclide activities in seawater and bottom sediments are low and caused mainly by global atmospheric fallout.

INTRODUCTION

The northwest Pacific marginal seas are characterized by reach biological resources which might be threatened by coastal urbanization and industrial development, by oil and gas exploration, extraction and transportation, by radioactive waste dumping and other anthropogenic factors. In order to forecast and mitigate possible negative effects to the marine environment, FERHRI in collaboration with the Japanese, Korean and US research centers has implemented a series of marine pollution surveys in the Sea of Japan and the Sea of Okhotsk. This review paper is intended to give a summary of the recent results. Sakhalin shelf surveys were performed in 1998–2002, the Sea of Japan expeditions in 1999–2000. Radionuclides in Peter the Great Bay were studied in 1994–1997.

SAKHALIN ISLAND SHELF OF THE SEA OF OKHOTSK

Introduction. Oceanographic observations along the NE Sakhalin Island shelf have started in 1930s as a part of large-scale investigations of the Far Eastern seas of Russia. Comprehensive ecological studies began in late 1980s because of possible offshore oil and gas exploration activities. Since 1990, several expeditions were implemented by FERHRI specialists at the Piltun-Astokh area (approximately 52–53ºN, 143–144ºE) in order to assess baseline environmental characteristics. Parameters of plankton and benthos communities as well as background concentrations of different classes of

contaminants in seawater and bottom sediments were investigated (Belan *et al.*, 1996; Tkalin, 1993; Tkalin and Belan, 1993). Sakhalin Energy Investment Company Ltd. (SEIC) has also organized a few baseline ecological surveys at the Piltun-Astokh field in 1992, 1995 and 1996 (see, for example, CSA, 1996; CSA, 1997). In 1998, the first stationary platform Molikpaq has been installed at the Piltun-Astokh field by SEIC and FERHRI was responsible for environmental impact monitoring.

Installation of platform and appraisal well drilling. In July–September 1998, oil production platform, Molikpaq, has been installed by SEIC (52°42'55N, 143°33'59E) and one appraisal well, AW16, was drilled in August–October (52°54'39N, 143°29'36E). In order to install the Molikpaq platform, about 800,000 m³ of bottom sediments were dredged and relocated. During the drilling of AW16, about 1,000 m³ of drilling mud and cuttings and similar amount of wastewaters were discharged to the sea. In June and October, two ecological surveys were implemented by FERHRI to characterize marine environment conditions before and after Molikpaq installation as well as before and after AW16 drilling. In August–September, ecological observations were carried out from the AW16 drilling rig.

Monitoring parameters and sites. Monitoring parameters for June and October surveys are presented in Table 1; number of samples (measurements) is given in Table 2. Monitoring parameters were chosen according to anticipated

impacts associated with bottom sediment dredging and relocation and with the discharge of drilling mud and cuttings. The following polygons were sampled:

- AWRSGSS (Appraisal Well Regional Survey Grid Sediment Stations), 24 stations
- AWRSEDS (Appraisal Well Reference Sediment Stations), 3 stations
- MOLSEDS (Molikpaq Sediment Stations), 22 stations
- MOLRSEDS (Molikpaq Reference Sediment Stations), 3 stations
- MOLSSASS (Molikpaq Sand Source Area Sediment Stations), 15 stations
- MOSSRASS (Molikpaq Sand Source Reference Area Sediment Stations), 15 stations
- MOLDDASS (Molikpaq Dredge Disposal Area Sediment Stations), 15 stations
- MODDRASS (Molikpaq Dredge Disposal Reference Area Sediment Stations), 15 stations

In addition to polygons, 9 stations were sampled around AW16 drilling site (central site and two cross-sections from west to east and from south to north). At the cross-sections, the distances from central site to sampling stations were 250 and 500 m respectively. Similar cross-sections were sampled around Molikpaq site, the distances along the west-east transect were 125, 250, 500, 1,000 and 3,000 m from Molikpaq, along the south-north transect the distances were 125, 250, 500, 1,000, 3,000 and 5,000 m from Molikpaq. Four grabs were taken at each station around Molikpaq (one grab at every other station).

Effects of dredging and relocation of dredged material. Water column parameters measured in June and October demonstrated usual seasonal variability and were within their natural range. No anthropogenic influences were detected also in distribution of phenols and trace metals in seawater. Due to activities of supporting ships around the Molikpaq platform, concentrations of petroleum hydrocarbons in seawater in the vicinity of the platform were 3 times higher than at other locations.

Table 1

Monitoring parameters at the Piltun-Astokh area in 1998

Seawater	Bottom sediments
• Temperature (T) • Salinity (S) • pH • Turbidity • Suspended solids (SS) • BOD_5 • Dissolved oxygen (DO) • Nutrients (nitrite, nitrate, phosphate, silica) • Chlorophyll *a* • Petroleum hydrocarbons (PHC) • Trace metals (TM) • Phenols	• Grain size • Trace metals (TM) • Petroleum hydrocarbons (PHC) • Polynuclear aromatic hydrocarbons (PAH) **Biota** • Phytoplankton • Zooplankton • Ichtyoplankton • Benthos • Birds and mammals

Table 2

Number of samples (measurements) in June and October 1998

Parameters	Polygons			
	AWRSGSS, AWRSEDS	MOLSEDS, MOLRSEDS	MOLSSASS, MOLSSRASS	MOLDDASS, MODDRASS
Seawater and plankton				
T, S, turbidity	7 profiles	10 profiles		
pH, DO, SS, nutrients	21 samples	30 samples		
PHC, BOD_5, chlorophyll, phytoplankton	21 samples	30 samples		
TM, phenols		30 samples		
Zoo- and ichtyoplankton	7 samples	10 samples		
Bottom sediments, benthos, birds and mammals				
Grain size (0–2 cm)	90 samples	200 samples		
Grain size (bulk)	90 samples	200 samples	60 samples	60 samples
TM	90 samples	200 samples		
PHC	90 samples	200 samples		
PAH	12 samples	3 samples		
Benthos	90 samples	200 samples	60 samples	60 samples
Birds and mammals	Continuously at daytime	Continuously at daytime	Continuously at daytime	Continuously at daytime
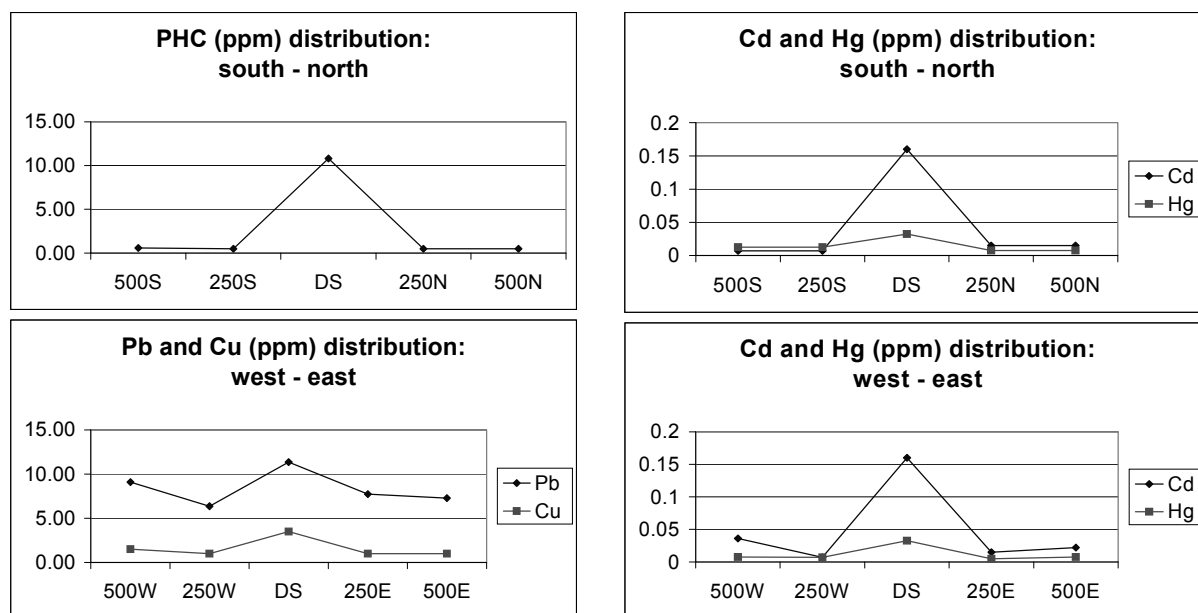
Figure 1. Distribution of some metals and petroleum hydrocarbons along the east-west and south-north transects around AW16 in October 1998

Lithological characteristics of bottom sediments at the Piltun-Astokh area are very variable. Nevertheless, some changes of bottom sediment grain size were detected near the Molikpaq platform due to dredging and replacement/relocation of sediments (the platform core was filled by fine sediment transported from different location). The increased percentage of fine fractions of bottom sediments was observed also around the AW16 (within 125 m from the drilling site). Outside this zone, no effects of drilling were detected.

Due to sediment replacement at the Molikpaq site, the concentrations of Al and Fe in bottom sediments in October decreased comparing to June values. Contents of other metals correlate with Al and Fe quite well and were also different in June and October. This effect was more pronounced within the 125–250 m zone around the platform.

At the AW16 drilling site, concentrations of almost all trace metals in bottom sediments in October were significantly higher than in June. Concentration of petroleum hydrocarbons in bottom sediments at the AW16 drilling site in October (10.8 ppm) was ten times higher than in June (1.0 ppm). The only reason of these differences can be the discharge of drilling mud and cuttings. Distribution of some metals and petroleum hydrocarbons along the east-west and south-north transects around AW16 in October is shown on Figure 1. Nevertheless, even the maximum concentrations of trace metals in bottom sediments in October were less than those causing negative ecological effects (Long *et al.*, 1995).

Benthic communities at the study area were characterized by high values of biomass, density and species diversity. In the local areas around the Molikpaq platform (within the 125 m zone), decrease of benthos biomass was observed. This effect is connected with the replacement of bottom sediments around the platform. Nevertheless, species richness and diversity did not change at the stations close to the platform.

Visual observations from the AW16 drilling rig have shown that areas of increased turbidity or oily sheen which were observed from time to time (no more than 9% and 26% of total observations respectively) were of limited size (up to 200 m) and duration (in most cases less than 2 hours). No negative effects of drilling on birds or mammals were observed.

Conclusions. Thus, observations carried out in 1998 clearly demonstrated that ecological consequences of Molikpaq installation and AW16 drilling were limited in space to about 125–250 m and are expected to be short-term. Ecological monitoring at the Piltun-Astokh area in 1999–2002 has confirmed these conclusions. The detailed information on the environmental impact assessment for the Molikpaq installation and AW16 drilling site can be found in FERHRI reports prepared for SEIC.

RADIONUCLIDES IN THE SEA OF JAPAN PROPER

Introduction. In 1999–2000, two joint Japanese–Russian expeditions to study radionuclide behavior in the Sea of Japan were implemented aboard FERHRI research vessel "Professor Khromov". During these expeditions, specialists from FERHRI and JAERI performed CTD casts with measurements of temperature, salinity, dissolved oxygen and nutrients from the surface to the bottom, deployed PALACE drifters and moorings with current meters and

sediment traps, took samples of seawater from the surface, bottom layer and three intermediate layers, and took samples of surface and subsurface sediments. Activities of gamma emitters, ^{90}Sr and ^{239,240}Pu were measured in samples of seawater and bottom sediments.

Location of sampling stations in 1999 is shown on Figure 2 as an example. Water samples from near-bottom layer (100–150 m over the bottom) and intermediate layers (200, 1000, 2000 m) were taken by special large-volume water sampler. Surface water samples were taken by submersible pumps and hoses. Bottom sediment samples were taken by the Petersen grab. The surface layer (about 3 cm) and residual subsurface layer of bottom sediments were used to measure radioactivity separately. Water and bottom sediment samples were preserved as required (when necessary) and stored for further analysis in shore laboratories. Techniques used for radionuclide activity measurements in shore laboratories were described earlier (Joint Expedition, 1995; Joint Expedition, 1997).

Radionuclides in seawater. Typical vertical distribution of radionuclides in 1999 is shown in Table 3. According to data collected in 1999–2000, activities of ^{137}Cs and ^{90}Sr decreased with depth and became less then detection limit below 2000 m, ^{137}Cs/^{90}Sr ratio varied from 1.43 to 1.77 (global fallout value is 1.57). Well-known feature of vertical distribution of ^{239,240}Pu activities is the subsurface maximum between 400 and 1000 m depth (*e.g.*, Nagaya and Nakamura, 1984; 1987; Hirose *et al.*, 1999). During 1999–2000 expeditions, maximum ^{239,240}Pu activities were observed at 1000 m depth. Elevated ^{239,240}Pu activities at the surface at some stations located to the north of Polar front (*e.g.*, station E-10 in 1999) probably resulted from winter convection (Hirose *et al.*, 1999).

The results on ^{137}Cs activities in seawater obtained during the 1999–2000 expeditions are presented in Table 4 along with the data of Japanese–Korean–Russian joint expedition, 1994 and 1995, for the Sea of Japan (median values). The results of independent measurements of Japanese (Miyao *et al.*, 1998) and Korean (Kang *et al.*, 1997) researchers are also given for comparison. The data for 1999–2000 are equal or below values measured in 1995, 1994 or earlier.

Similar comparative data for ^{90}Sr are given in Table 5. Again, 1999–2000 data are equal or below the results of 1994 and 1995 cruises. It should be taken into account that geographically the study area in 1994 was located between 41 and 42°N, while in 1995, observations were carried out in the southern part of the Sea of Japan (about 37°N).

Data on activities of ^{239,240}Pu in seawater measured in 1999–2000 are presented in Table 6 along with the results of Japanese–Korean–Russian joint expedition, 1994 and 1995 (median values). The results of
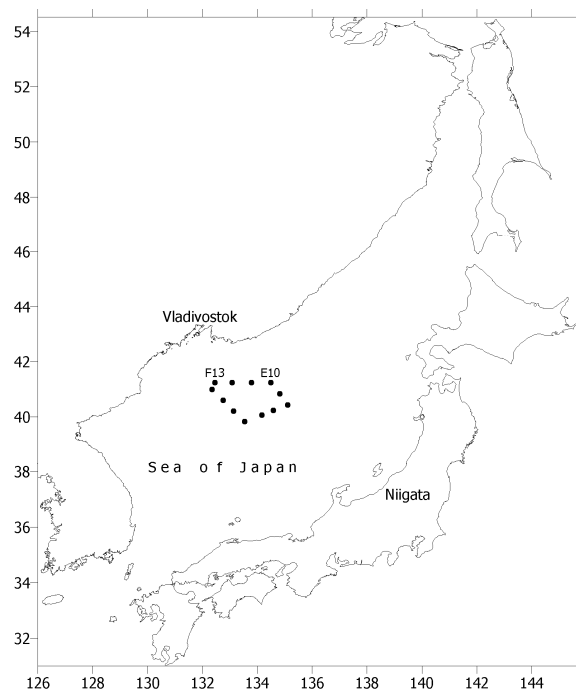

Figure 2. Location of sampling stations, May 1999

independent measurements of Korean (Kang *et al.*, 1997) and Japanese (Miyao *et al.*, 1998; Yamada *et al.*, 1996) researchers are also given for comparison. The data for 1999–2000 are close to values measured previously in the Sea of Japan.

Radionuclides in bottom sediments. The results of activity measurements of some natural and anthropogenic radionuclides in surface and subsurface bottom sediments in 1999 are shown in Table 7 for two stations, F-13 and E-10. Measured activities of natural radionuclides are typical for marine sediments, similar values of ^{40}K (590–684 Bq/kg), ^{226}Ra (28.1–37.8 Bq/kg), ^{232}Th (43.1–51.8 Bq/kg) and ^{238}U (38.8–53.7 Bq/kg) were observed, for example, in the South-China Sea (Yu *et al.*, 1994).

In 1999–2000, ^{90}Sr activities in bottom sediments were below 1.0 Bq/kg, activities of ^{137}Cs were also extremely low, especially in subsurface layer of bottom sediments. The results on ^{137}Cs activities in bottom sediments in 1999–2000 are presented in Table 8 along with the data of previous joint cruises, 1994 and 1995, for the Sea of Japan (median values). Data of Korean researchers (Lee *et al.*, 1998) are given for comparison. The data of 1999–2000 expeditions are well below the values measured before. Similar activities of ^{137}Cs in bottom sediments (1.52–3.11 Bq/kg) were observed in Hong Kong (Yu *et al.*, 1994) as well as in the Yellow and the East China Seas (0.35–6.11 Bq/kg; Nagaya and Nakamura, 1992). Comparison of 1999–2000 data with the previous results on ^{90}Sr is shown in Table 9. Recent data are fairly similar to 1994–1995 results.

The results on ^{239,240}Pu activities in bottom sediments in 1999–2000 are presented in Table 10 along with the

Activities of some radionuclides in seawater of the Sea of Japan, May 1999

Depth	^{137}Cs, Bq/m^3	^{90}Sr, Bq/m^3	^{239,240}Pu, mBq/m^3
Station F–13			
Surface	2.44±0.40	1.38±0.33	22.5±2.7
200 m	2.15±0.32	1.50±0.38	22.6±4.2
1000 m	1.77±0.51	1.14±0.22	30.9±5.0
2000 m	0.31±0.10	<0.49	25.7±3.4
3350 m	<0.69	<0.47	32.6±2.9
Station E–10			
Surface	2.38±0.32	1.44±0.22	44.0±4.0
200 m	2.22±0.44	1.50±0.23	19.4±4.0
1000 m	1.57±0.27	1.04±0.23	44.0±4.0
2000 m	<0.69	<0.34	38.6±5.7
3480 m	<0.69	<0.33	21.9±3.8

Note:

the errors given are ±1 σ counting statistics

Activities of 137Cs (Bq/m^3) in seawater of the Sea of Japan

Period of observations (number of stations)	Surface waters	Bottom waters
2000 (3)	2.5–2.8	<0.3
1999 (2)	2.4	<0.7
1995 (2)	2.5–2.9	1.1–1.3
1994 (9)	2.8–3.6	0.6–2.0
1993 (19)*	2.6–3.3	–
1986–1993 (6)**	2.7–9.9	–

Note:

*Kang et al., 1997

**Miyao et al., 1998

Activities of ^{90}Sr (Bq/m^3) in seawater of the Sea of Japan

Period of observations (number of stations)	Surface waters	Bottom waters
2000 (3)	1.6–1.8	<0.3
1999 (2)	1.4	<0.5
1995 (2)	2.0	0.4–0.7
1994 (9)	1.6–2.0	0.4–1.2

Activities of ^{239,240}Pu (mBq/m^3) in seawater of the Sea of Japan

Period of observations (number of stations)	Surface waters	Bottom waters
2000 (1)	7.0	3.5
1999 (2)	22.5–44.0	21.9–32.6
1995 (2)	8.6–16.0	25.0–27.0
1994 (9)	8.0–25.0	15.0–29.0
1993 (3)*	6.0–10.0	–
1993 (2)**	7.4–9.5	26.1–33.0
1986–1994 (10)***	1.3–14.0	–

Note:

*Kang et al., 1997

**Yamada et al., 1996

***Miyao et al., 1998

Table 7

Activities of some radionuclides (Bq/kg) in bottom sediments of the Sea of Japan, May 1999

Radionuclides	Station F–13		Station E–10	
	Surface sediment (0–3 cm)	Subsurface sediment (> 3 cm)	Surface sediment (0–3 cm)	Subsurface sediment (> 3 cm)
^{137}Cs	1.60±0.53	<1.1	1.27±0.92	<1.0
^{90}Sr	<0.3	<0.3	<0.3	<0.3
^{239,240}Pu	0.32±0.06	0.003±0.001	0.19±0.05	<0.003
^{40}K	600±20	560±30	660±30	580±30
^{226}Ra	32±5	28±7	42±8	27±6
^{232}Th	42±5	38±6	47±6	35±5
^{238}U	34±31	113±29	69±31	73±30

Table 8

Activities of ^{137}Cs (Bq/kg) in bottom sediments of the Sea of Japan

Period of observations (number of stations)	Surface sediment	Subsurface sediment
2000 (3)	1.9–2.6	0.9–1.2
1999 (2)	1.3–1.6	<1.1
1995 (2)*	7.2	7.2
1994 (9)	1.0–2.8	<2.3
1995 (2)**	11.0–13.1	0.9–1.8

Note:

at the station BG4 sediment sample was not divided to surface and subsurface

**Lee et al., 1998, 0–2 cm and 8–10 cm layers*

Table 9

Activities of ^{90}Sr (Bq/kg) in bottom sediments of the Sea of Japan

Period of observations (number of stations)	Surface sediment	Subsurface sediment
2000 (3)	0.2–0.3	<0.3
1999 (2)	<0.3	<0.3
1995 (2)*	0.2–0.8	0.2–0.8
1994 (9)	0.1–0.2	<0.3

Note:

at the station BG4 sediment sample was not divided to surface and subsurface

Table 10

Activities of ^{239,240}Pu (Bq/kg) in bottom sediments of the Sea of Japan

Period of observations (number of stations)	Surface sediment	Subsurface sediment
2000 (3)	0.34–1.04	<0.01–0.12
1999 (2)	0.19–0.32	<0.01
1995 (2)*	0.33–1.80	0.13–1.33
1994 (9)	0.01–1.03	<0.01–0.76
1995 (2)**	2.00–3.73	0.13–0.55

Note:

at the station BG4 sediment sample was not divided to surface and subsurface

**Lee et al., 1998, 0–2 cm and 8–10 cm layers*

data of previous joint expeditions, 1994 and 1995 (median values). Data of Korean researchers (Lee *et al.*, 1998) are given for comparison. The data of 1999–2000 expeditions are very close to the values measured before. Similar activities of ^{239,240}Pu (0.107–0.467 Bq/kg) were observed in bottom sediments in the Yellow and the East China Seas (Nagaya and Nakamura, 1992).

Conclusions. According to the results of 1999–2001 expeditions, activities of gamma emitters, ^{90}Sr and ^{239,240}Pu in seawater and bottom sediments were low and caused by global atmospheric fallout of radionuclides. Data obtained in these expeditions are quite close to the results of previous investigations by different research groups. For better understanding of radionuclide inputs, distribution, transport and possible effects, further studies in the Sea of Japan are necessary.

RADIONUCLIDES IN PETER THE GREAT BAY

Introduction. Peter the Great Bay is divided into two secondary bays by peninsula: Amurskiy to the west and Ussuriyskiy to the east (Figure 3). Vladivostok, the largest port and city in Russian Far East, with population of about 1 million people, is situated along the peninsula between these two bays. The main sources of radionuclides in Peter the Great Bay are as follows: 1) global atmospheric fallout; 2) river input; 3) discharges from navy facilities situated around Peter the Great Bay. Other sources of radionuclides can be considered as of less importance at present.

One of navy facilities, shipyard "Zvezda", is located in Bolshoy Kamen (Figure 3). Repair and decommissioning of nuclear submarines are carried out at this shipyard (Handler, 1995). Refueling facility for nuclear submarines is situated in Chazhma Bay (Figure 3). In 1985, the accident with the reactor of nuclear submarine took place at this facility with the total activity release of about 260 PBq of short-living isotopes, ^{60}Co and ^{54}Mn (Sivintsev *et al.*, 1994). As a result, Chazhma Bay itself was contaminated by ^{60}Co as well as local areas in Ussuriyskiy and Strelok bays.

Peter the Great Bay is well known by its high biological productivity and recreational potential. Therefore, radioactive contamination of the marine environment and seafood is of great concern to local authorities, environmental organizations and general public. In September–October 1994, the comprehensive investigation of radionuclides in Peter the Great Bay was implemented. The following organizations participated in the survey: 1) FERHRI; 2) Regional Radiochemical Laboratory, Hydrometeorological Office of Primorsky Kray; 3) Service of Radiological, Chemical and Biological Safety, Pacific Fleet, Russian navy; 4) State Environmental Committee of Primorsky Kray. The expedition was carried out aboard FERHRI R/V "Akademik
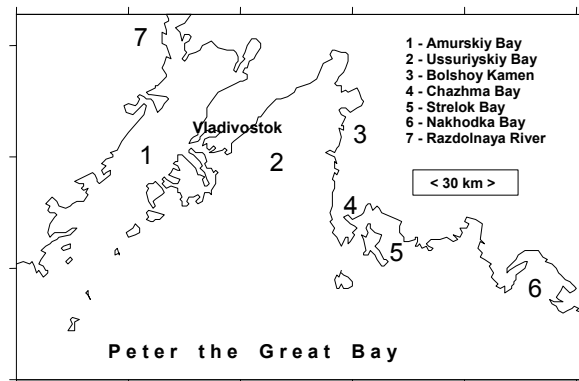
Figure 3. Peter the Great Bay

Shokalsky" and two smaller boats (to collect samples in shallow areas). Seawater samples (100 liters) were taken by 10-liter plastic water bottles (Hydro–Bios), sediment samples were collected by a van Veen grab sampler. At most of the stations, water samples were taken from the surface. Sub-samples of surface (0–2 cm) and subsurface (2–10 cm) sediments were used for analysis. Sampling stations were located close to potential radioactivity sources (Bolshoy Kamen, Chazhma Bay, etc.) as well as in recreational and fishing areas (Amurskiy and Ussuriyskiy bays). Techniques of radionuclide preconcentration and analysis were described in detail elsewhere (Tkalin and Chaykovskaya, 2000).

Radionuclides in seawater. Mean activities of ^{137}Cs and ^{90}Sr and their ratios for different areas of Peter the Great Bay are presented in Table 11 (± one standard deviation). Spatial distributions of these radionuclides in surface seawater are shown on Figures 4, 5. During the expedition, there were heavy rains in Primorsky Kray (250 mm in September 18 to September 30) which could affect the distribution of radionuclides in surface seawater. Heavy rains caused also high floods in the rivers entering the bay. Because of fresh water input with river runoff, activities of ^{137}Cs were lower in upper parts of Amurskiy and Ussuriyskiy bays as well as in Nakhodka Bay (Figure 4). While salinity in the open Peter the Great Bay varied in the range 31~33PSU, surface seawater salinity values decreased in the upper parts of the bays as follows; Amurskiy Bay: 28.05, Ussuriyskiy Bay: 26.39, Nakhodka Bay: 24.90PSU. There are no major rivers entering Strelok Bay and therefore mean activity of ^{137}Cs is higher there (Table 11). ^{137}Cs/^{90}Sr ratio was also affected by freshwater input: lower values were observed in upper parts of Amurskiy and Ussuriyskiy bays.

For all stations in Peter the Great Bay, mean activities of ^{137}Cs and ^{90}Sr in surface waters were 3.9 and 2.7 Bq/m^3 respectively. These activities are quite low and comparable with the open Sea of Japan values. For example, in 1999, the following values were obtained for surface seawater: ^{137}Cs: 2.4, ^{90}Sr: 1.4 Bq/m^3 (Tables 4, 5). Mean ^{137}Cs/^{90}Sr ratio for surface seawater of Peter the Great Bay (1.50) is close to the ratio for global fallout (1.57).

Mean activities of ^{137}Cs and ^{90}Sr in seawater at the surface in 1994
(and range of activities in parentheses)

Area	Number of samples	^{137}Cs (Bq/m^3)	^{90}Sr (Bq/m^3)	^{137}Cs/^{90}Sr
Amurskiy Bay	3	3.0 ± 0.3 (2.8–3.4)	2.5 ± 0.2 (2.3–2.6)	1.2 ± 0.1 (1.1–1.4)
Ussuriyskiy Bay	14	3.9 ± 1.2 (1.7–5.7)	2.7 ± 1.2 (1.7–6.6)	1.5 ± 0.5 (0.8–2.4)
Nakhodka Bay	3	3.4 ± 0.3 (3.1–3.6)	2.6 ± 0.5 (2.0–2.9)	1.4 ± 0.2 (1.2–1.6)
Strelok Bay	4	4.9 ± 0.3 (4.4–5.2)	3.0 ± 0.5 (2.7–3.5)	1.7 ± 0.3 (1.4–2.1)

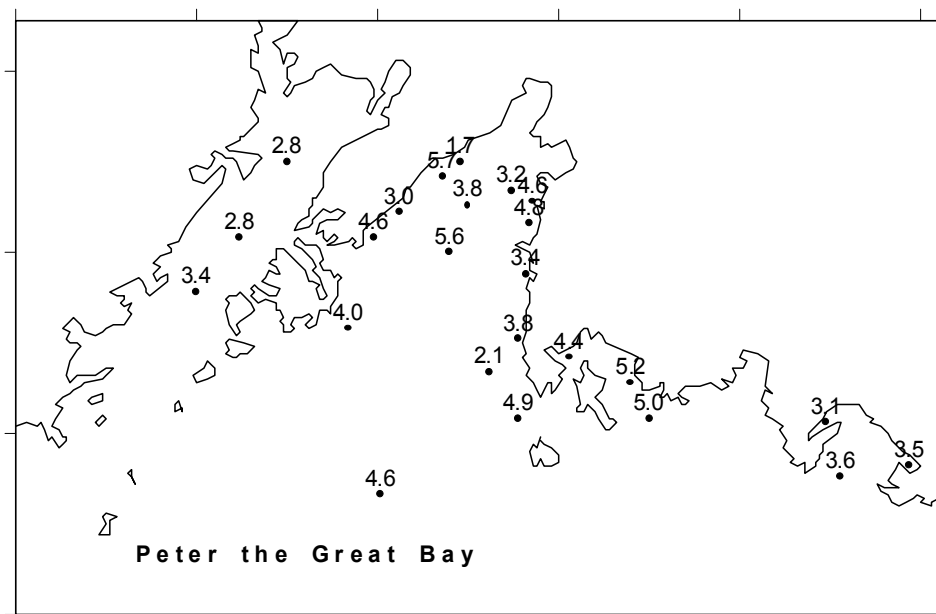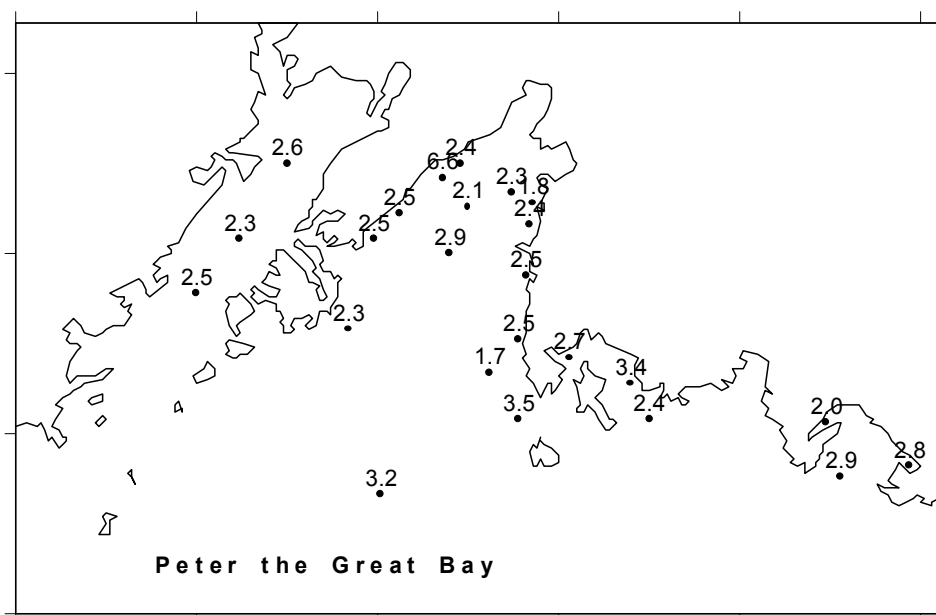**Figure 4. Distribution of ^{137}Cs (Bq/m^3) in seawater at the surface, 1994**

Figure 5. Distribution of ^{90}Sr (Bq/m^3) in seawater at the surface, 1994

Radionuclides in bottom sediments. Data on activities of γ-emitting radionuclides in bottom sediments of different areas of Peter the Great Bay are presented in Tables 12 and 13. ^{60}Co was detected only in Strelok Bay (close to Chazhma Bay entrance, up to 150 Bq/kg) and in very limited area in Ussuriyskiy Bay, up to 21.6 Bq/kg. In other areas of Peter the Great Bay, activities of ^{60}Co were below the detection limit (1.7 Bq/kg). Even highest detected activity was a few orders of magnitude lower than the maximum permissible level (150,000 Bq/kg) in the Russian Federation. In 1985, just after the accident, maximum activities of ^{60}Co in Chazhma Bay sediments were as high as 77,700 Bq/kg and this isotope was distributed over the Strelok Bay sediments (Sivintsev *et al.*, 1994). In 1990, maximum activity of ^{60}Co in surface sediments was about 400 Bq/kg (dry) and total inventory of ^{60}Co in Chazhma and Strelok bays was estimated as 185 GBq (Sivintsev *et al.*, 1994). The results of 1994 expedition show that ^{60}Co contamination of bottom sediments in Strelok Bay still exists.

Distribution of ^{137}Cs in surface bottom sediments of Peter the Great Bay was affected by the discharge of suspended matter with rivers: maximum activities of ^{137}Cs were observed in upper parts of Amurskiy and Ussuriyskiy bays. Razdolnaya river which enters Amurskiy Bay drains large territory of China and Primorsky Kray of Russia collecting radionuclides derived from atmospheric fallout. Mineral soil particles derived from river runoff can effectively absorb ^{137}Cs. This effect may lead to elevated activities of ^{137}Cs near river mouths as it was observed elsewhere (*e.g.*, Baskaran *et al.*, 1996; Cooper *et al.*, 1995).

In the open areas of Peter the Great Bay, activities of ^{137}Cs in bottom sediments were lower than 5 Bq/kg or even below the detection limit (1.1 Bq/kg). Variations of activities with sediment depth (*i.e.* 0–2 cm or 2–10 cm) are not statistically significant (Table 13). There is no clear indication of any significant influence of navy facility operations on activities of ^{137}Cs in bottom sediments of Peter the Great Bay. Similar elevated activities of ^{137}Cs (up to 12.9 Bq/kg) were observed in coastal areas of the Bering and Chukchi seas due to freshwater runoff (Cooper *et al.*, 1995). Close to the mouths of Yenisey and Ob rivers, activities in bottom sediments were even higher: up to 50–70 Bq/kg (Baskaran *et al.*, 1996).

Table 12

**Mean activities of ^{60}Co in bottom sediments in 1994
(and range of activities in parentheses)**

Area	Number of samples	Surface layer, 0–2 cm (Bq/kg, dry)	Subsurface layer, 2–10 cm (Bq/kg, dry)
Ussuriyskiy Bay	23/19	1.2 ± 4.6 (ND–21.6)	0.9 ± 2.8 (ND–10.0)
Strelok Bay	9/9	21.5 ± 49.1 (ND–150)	11.1 ± 16.2 (ND–45.5)

Note:

ND – not detected. Detection limit for ^{60}Co is 1.7 Bq/kg; values below the detection limit were assumed to be zero for calculation of means.

Table 13

**Mean activities of ^{137}Cs in bottom sediments in 1994
(and range of activities in parentheses)**

Area	Number of samples	Surface layer, 0–2 cm (Bq/kg, dry)	Subsurface layer, 2–10 cm (Bq/kg, dry)
Amurskiy Bay	9/7	13.7 ± 4.9 (2.8–19.1)	17.5 ± 5.4 (6.2–22.9)
Ussuriyskiy Bay	23/19	4.9 ± 5.1 (ND–14.8)	5.2 ± 5.7 (ND–17.4)
Nakhodka Bay	3/3	5.8 ± 0.6 (5.1–6.2)	7.4 ± 1.2 (6.1–8.4)
Strelok Bay	9/9	3.9 ± 3.1 (ND–8.5)	2.8 ± 3.7 (ND–9.1)
All stations	44/38	6.6 ± 4.5 (ND–19.1)	7.1 ± 5.0 (ND–22.9)

Note:

ND – not detected. Detection limit for ^{137}Cs is 1.1 Bq/kg, values below the detection limit were assumed to be zero for calculation of means.

In 1996, activities of γ-emitters were measured in a few samples of surface bottom sediments taken along the west and east coasts of Amurskiy Bay (8 stations) as well as along the west coast of Ussuriyskiy Bay (3 stations). While ^{60}Co and ^{134}Cs were not detected, activities of ^{137}Cs ranged in 1.9~16.1 Bq/kg (Tkalin et al., 1998). In 1997, surface layer samples of bottom sediments were collected along the west coast of Amurskiy Bay (6 stations) and along the west coast of Ussuriyskiy Bay (6 stations). Again, ^{60}Co and ^{134}Cs were not detected and ^{137}Cs activities were in the range of <0.7~19.6 Bq/kg, which are very close to the results obtained in 1994. Along the east coast of Ussuriyskiy Bay (at 7 stations), surface and subsurface layer samples of bottom sediments were collected. Activities of ^{137}Cs were 3.1~7.6 Bq/kg. Activities of ^{60}Co were in the range of ND~96 Bq/kg in surface layer and ND~14.4 Bq/kg in subsurface layer. So, the consequences of the Chazhma Bay accident still exist in the limited area of Ussuriyskiy Bay.

Conclusions. The results of comprehensive investigation of radionuclide distributions in seawater and bottom sediments of Peter the Great Bay have shown that the main sources of radionuclides in Peter the Great Bay are still their global atmospheric fallout and the discharge of freshwater and suspended sediments from river runoff. There is no clear indication of the impact of navy facilities on radioactive contamination of Peter the Great Bay except elevated ^{60}Co activities resulting from 1985 accident in Chazhma Bay. ^{60}Co released during this accident is still present in bottom sediments of Strelok Bay at significant levels (up to 150 Bq/kg). In fishing and recreational areas of Peter the Great Bay (Amurskiy and Ussuriyskiy bays), levels of radionuclide activities in seawater and bottom sediments are low and caused mainly by global atmospheric fallout. Regular observations of radioactive contamination of Peter the Great Bay (including marine biota) are necessary to assure safety of local population and tourists.

REFERENCES

Baskaran M., Asbill S., Santschi P., Brooks J., Champ M., Adkinson D., Colmer M., Makeyev V. **1996**. Pu, ^{137}Cs and excess ^{210}Pb in Russian Arctic sediments. Earth and Planetary Science Letters, 140, 243–257.

Belan T.A., Oleynik E.V., Tkalin A.V., Lishavskaya T.S. **1996**. Characteristics of pelagic and benthic communities on the North Sakhalin Island shelf. PICES (North Pacific Marine Science Organization) Scientific Report No. 6, 227–229.

Cooper L.W., Grebmeier J.M., Larson I.L., Solis C., Olsen C.R. **1995**. Evidence for re-distribution of ^{137}Cs in Alaskan tundra, lake, and marine sediments. The Science of the Total Environment, 160/161, 295–306.

CSA 1996. Environmental survey report for the Piltun-Astokhskoye field offshore Sakhalin Island, Russia (the results of 1995 observations). Continental Shelf Associates, November 1996.

CSA 1997. Environmental survey report for the Piltun-Astokhskoye field 1996 survey offshore Sakhalin Island, Russia. Continental Shelf Associates, June 1997.

Handler J. **1995**. The radioactive waste crisis in the Pacific area. Arctic Research of the United States, 9, 105–108.

Hirose K., Amano H., Baxter M.S., Chaykovskaya E., Chumichev V.B., Hong G.H., Isogai K., Kim C.K., Kim S.H., Miyao T., Morimoto T., Nikitin A., Oda K., Pettersson H.B.L., Povinec P.P., Seto Y., Tkalin A., Togawa O., Veletova N.K. **1999**. Anthropogenic radionuclides in seawater in the East Sea/Sea of Japan: results of the first stage of Japanese–Korean–Russian expedition. Journal of Environmental Radioactivity, 43, 1–13.

Joint Expedition 1995. Investigation of Environmental Radioactivity in Waste Dumping Areas of the Far Eastern Seas. Results from the First Japanese–Korean–Russian Joint Expedition, 1994. 64 pp.

Joint Expedition 1997. Investigation of Environment Radioactivity in Waste Dumping Areas in the northwest Pacific Ocean. Results from the Second Stage of Japanese–Korean–Russian Joint Expedition, 1995. 57 pp.

Kang D.J., Chung C.S., Kim S.H., Kim K.R., Hong G.H. **1997**. Distribution of ^{137}Cs and ^{239,240}Pu in the surface waters of the East Sea (Sea of Japan). Marine Pollution Bulletin, 35, 7–12.

Lee M.H., Lee C.W., Moon D.S., Kim K.H., Boo B.H. **1998**. Distribution and inventory of fallout Pu and Cs in the sediment of the East Sea of Korea. Journal of Environmental Radioactivity, 41, 99–110.

Long E.R., Macdonald D.D., Smith S.L., Calder F.D. **1995**. Incidence of adverse biological effects within ranges of chemical concentrations in marine end estuarine sediments. Environmental Management, 19, 81–97.

Miyao T., Hirose K., Aoyama M., Igarashi Y. **1998**. Temporal variation of ^{137}Cs and ^{239,240}Pu in the Sea of Japan. Journal of Environmental Radioactivity, 40, 239–250.

Nagaya Y., **Nakamura** K. **1984**. ^{239,240}Pu, ^{137}Cs and ^{90}Sr in the central North Pacific. Journal of the Oceanographical Society of Japan, 40, 416–424.

Nagaya Y., **Nakamura** K. **1987**. Artificial radionuclides in the western Northwest Pacific. II. ^{137}Cs and ^{239,240}Pu inventories in water and sediment columns observed from 1980 to 1986. Journal of the Oceanographical Society of Japan, 43, 345–355.

Nagaya Y., **Nakamura** K. **1992**. ^{239,240}Pu and ^{137}Cs in the East China and the Yellow Seas. Journal of Oceanography, 48, 23–35.

Sivintsev Yu.V., Vysotsky V.L., Danilyan V.A. **1994**. Radioecological consequences of nuclear submarine accident in Chazhma Bay. Nuclear Power, 76, 158–160 (In Russian).

Tkalin A.V. **1993**. Background pollution characteristics of the NE Sakhalin Island shelf. Marine Pollution Bulletin, 26, 704–705.

Tkalin A.V., **Belan** T.A. **1993**. Background ecological conditions of the NE Sakhalin Island shelf. Ocean Research, 15, 169–176.

Tkalin A.V., **Chaykovskaya** E.L. **2000**. Anthropogenic radionuclides in Peter the Great Bay. Journal of Environmental Radioactivity, 51, 229–238.

Tkalin A.V., Lishavskaya T.S. Shulkin V.M. **1998**. Radionuclides and trace metals in mussels and bottom sediments around Vladivostok, Russia. Marine Pollution Bulletin, 36, 551–554.

Yamada M., Aono T., Hirano S. **1996**. $^{239+240}$Pu and ^{137}Cs distributions in seawater from the Yamato Basin and the Tsushima Basin in the Sea of Japan. Journal of Radioanalytical and Nuclear Chemistry, 210, 129–136.

Yu K.N., Guan Z.J., Stokes M.J., Young E.C.M. **1994**. Natural and artificial radionuclides in seabed sediments of Hong Kong. Nuclear Geophysics, 8, 45–48.

NEW VERSION OF CONTAMINANT TRANSPORT MODEL IN SEA

I.E. Kochergin, A.A. Bogdanovsky

Far Eastern Regional Hydrometeorological Research Institute (FERHRI), Russia
Email: ikochergin@hydromet.com

The application of models that adequately describe transport and sedimentation of contaminants in the marine environment is critical for the ecological studies and the impact assessment within the shelf exploration and development projects. The VOSTOK model is one of the commonly used models under the Russian Far East conditions. The model was used to assess water and sea-bottom pollution zones in the course of the oil and gas production facilities construction and operation on Sakhalin shelf as well as for hydro-construction activities in coastal zones. This work describes the latest version VOSTOK 8.9 model for calculation of contaminant transport and sedimentation in the sea water.

The VOSTOK model is a 3D diffusive-advection model developed on the basis of the particle method with the use of random number generator for the simulation of nondeterministic processes. The distinguishing features of a new version are the setting of boundary conditions at water-air and water-bottom boundaries, description of three turbulence scales, account of flocculation effect and jet sinking effect, and account of contaminant non-conservativity.

Results of only two main verification tests presented in this paper. The first one is the discharge experiment organized by Exxon Neftegas Ltd. company in 1998. The second is the comparative simulation on AKS model developed in Computing Centre of the Russian Academy of Sciences in 2002.

INTRODUCTION

The application of models that adequately describe transport of contaminants in the marine environment is critical for the environmental studies and the impact assessment within the shelf exploration and development projects. The VOSTOK model (including all its versions 1.0–8.9), developed by FERHRI specialists, is one of the commonly used models under the Russian Far East conditions. All model versions were used to estimate the zones of contaminants transport and sedimentation in the course of the oil and gas production facilities designing and operation on Sakhalin shelf: starting from 1992 for Sakhalinmorneftegas company (Kochergin, 2000) and then from 1995 to present day under Sakhalin 1, 2, 3, and 4 projects (Bogdanovsky and Kochergin, 1998; Bogdanovsky and Kochergin, 1999; Kochergin *et al.*, 2000). The modeling technique and the model itself were constantly updated to take advantage of newer computer technology, complex calculation requirements, and availability of new data coming from analysis of other models and verification tests. This paper provides a description of the latest version VOSTOK 8.9 model for calculation of contaminant transport and sedimentation in the marine environment. This is the latest version of the model; however, additional improvements will be incorporated in the future.

VOSTOK 8.9 model is a 3D diffusive-advection model developed on the basis of the particle method with the use of random number generator for the simulation of nondeterministic processes according to the general approach of Ozmidov (1986). Analogous models with either a direct calculation of particle movement (Lagrange approach) or a diffusion equation calculation (Euler approach) were used to estimate the suspended solids transport and described in the papers (Astrakhantsev *et al.*, 1988; Voltsinger *et al.*, 1990; Dmitriev and Dvurechenskaya, 1994; Zaytsev and Zaytseva, 1984; Korotenko and Lelyavin, 1990; Kochergin and Bokovikov, 1980; Nikolskiy *et al.*, 1990; Ozmidov, 1986; O'Reilly *et al.*, 1989; Patania *et al.*, 2000; Sharp and Moore, 1989; Zagar *et al.*, 2000; Arkhipov *et al.*, 2000). The models based on the particle method have a number of practical advantages allowing the numerical implementation of the applied tasks being described in the papers by (Dmitriev and Dvurechenskaya, 1994; Ozmidov, 1986; Kochergin and Bogdanovsky, 1999; Kochergin *et al.*, 2000).

The latest version of VOSTOK 8.9 is based on the general theoretical approaches described by Ozmidov (1986) but is distinguished from analogous models of (Dmitriev and Dvurechenskaya, 1994; Zaytsev and Zaytseva, 1984; Korotenko and Lelyavin, 1990; Ozmidov, 1986; O'Reilly *et al.*, 1989; Sharp and Moore, 1989). The distinguishing features are the setting of boundary conditions at water-air and water-bottom boundaries, description of different scales of turbulence, account of flocculation effect and jet sinking effect, and account of non-conservative contaminants. The complete version of VOSTOK 8.9 model is described for the first time.

MAIN EQUATIONS

Contaminants discharged into marine environment are simulated as a quantity of markers that preserve the characteristics of mass, buoyancy, fractional distribution etc. The markers interact with marine environment and water-air and water-bottom boundaries. When mixing begins, the markers may interact with each other, sometimes they are destroyed

due to non-conservative contaminants. The general equations that describe the markers trajectory in a water column are as follows:

$$\frac{dx_i}{dt} = u(x_i, y_i, z_i, t) + u'_{0.5-15}(x_i, y_i, z_i, t) +$$
$$+ u'_{15-60}(x_i, y_i, z_i, t) + u'_{60-360}(x_i, y_i, z_i, t)$$

$$\frac{dy_i}{dt} = v(x_i, y_i, z_i, t) + v'_{0.5-15}(x_i, y_i, z_i, t) +$$
$$+ v'_{15-60}(x_i, y_i, z_i, t) + v'_{60-360}(x_i, y_i, z_i, t)$$
<div align="right">(1)</div>

$$\frac{dz_i}{dt} = w(x_i, y_i, z_i, t) + w_{S+Fl}(x_i, y_i, z_i, t) +$$
$$+ w_{JS}(x_i, y_i, z_i, t) + w'(x_i, y_i, z_i, t)$$

where:

x_i, y_i, z_i – are the coordinates of i marker;

u, v, w – are the components of advective transport influenced by the fluid flow velocity (tidal and non-tidal currents)

u', v', w' – are the components of the turbulent pulsation velocity; 0.5–15 minute, 15–60 minute and 60–360 minute range of the turbulent pulsation spectrum are distinguished for u' and v' in the shelf waters;

w_{S+Fl} – is the velocity of vertical marker motion (S from "settling") under the influence of gravity force for the contaminants with a neutral, positive or negative floatability. If the drilling effluents are discharged, there is an account of settling velocity correction due to adhesion or flocculation effect (Fl from "flocculation"). Under certain conditions the nonzero vertical motion may be registered even for markers with neutral bouyancy;

w_{JS} – is the additional velocity of the marker vertical motion at the beginning of the jet destruction. It results from the difference between the jet density and the sea water density (*e.g.* if heavy drilling mud are discharged, the jet sinking (JS) effect is observed).

The choice of the time step here is of great importance. Among the criteria limiting the calculation interval there are the typical frequency of the highest mode of current velocity turbulent pulsations and requirements to the effect account at the beginning of the jet destruction. In practice the time step ranges from ten seconds to several minutes.

Among the input parameters for equations (1) there are coordinates of markers issued by sources x_{0i}, y_{0i}, z_{0i} and the corresponding start time t_{0i}. The number of markers N, that describe the contaminant field in moment t_{0i} is the sum of issued markers n_s minus the markers taken out of calculations (these are the markers beyond the calculation field or the markers that disappear due to the non-conservative contaminats). The contaminant concentration is calculated by the number of markers describing a pollutant, markers volume ΔV and summary weight, and a background concentration:

$$C = C_b + \frac{\sum_{i=1}^{N} n_i m_i (for \rightarrow n_i \in \Delta V)}{\Delta V}$$
<div align="right">(2)</div>

where:

C_b – is the background concentration;

n_i – are the markers in ΔV volume;

m_i – is the mass of i marker.

The accuracy of concentration calculation over (1) depends on ΔC_b error in (2) and $m_i/\Delta V$ ratio, that is $\Delta C = \Delta C_b + m_i/\Delta V$.

BOUNDARY CONDITIONS

Boundary conditions specify the effects occurring at the boundary of different environments and the calculation field. Boundary conditions are presented as a logical operator $\hat{B}$ (B from *boundary*):

- if the markers are beyond the calculated horizontal field [0,X], [0,Y], they are excluded by operator $\hat{B}$ from further calculations;

- boundary conditions at water-air boundary $Z = <0$ show no-leaking of the solid phase and the partial evaporation for the dissolved contaminants and films (evaporation coefficient K_{Ev} ranges from 0 to 1). If a marker gets to the surface, $\chi < K_{Ev}$ condition is checked (χ is a random value that is evenly distributed in [0,1] interval). If the evaporation condition ($\chi < K_{Ev}$) is observed, a marker is excluded from further calculations. If a marker does not evaporate ($\chi > K_{Ev}$ is observed every time the evaporation coefficient equals 0), $\hat{B}$ operator demands observance of the following conditions for vertical velocities:

  $w = w$,   if $w > 0$
  $w = 0$,   if $w = < 0$
  $w_{S+Fl} = w_{S+Fl}$, if $w_{S+Fl} > 0$
  $w_{S+Fl} = 0$,   if $w_{S+Fl} = 0$ (1)
  $w_{JS} = 0$,
  $w' = |w'|$ (for all contaminants except for the surface films)

- if the boundary is solid, that is $Z => h(x_i, y_i)$ (where $h(x_i, y_i)$ is the depth in x_i, y_i point), the condition of the dissolved contaminants no-leaking and partial sedimentation or reflection of markers that simulate the solid phase is set. The markers settled at the bottom are not excluded from further calculations. The extent of a marker reflection/adhesion depends on the adhesion coefficient K_{Ad} that ranges from 0 to 1. If a markers gets to the bottom, $\chi < K_{Ad}$ condition is checked (χ is a random value that is evenly distributed in [0,1] interval). If the adhesion condition ($\chi < K_{Ad}$) is observed, $\hat{B}$ operator demands equality of both horizontal and vertical velocities to 0 till the next checking. If a marker is reflected ($\chi > K_{Ad}$ is observed every time the adhesion coefficient equals 0), $\hat{B}$ operator demands the compliance of horizontal velocities to the ones calculated for

bottom conditions and observance of the following conditions for vertical velocities:

$$
\begin{aligned}
w &= w, & &\text{if } w < 0 \\
w &= 0, & &\text{if } w >= 0 \\
w_{S+Fl} &= w_{S+Fl}, & &\text{if } w_{S+Fl} < 0 \\
w_{S+Fl} &= 0, & &\text{if } w_{S+Fl} >= 0 \qquad (3) \\
w_{JS} &= 0, \\
w' &= -|w'|
\end{aligned}
$$

Adhesion coefficients for different fractions are estimated over engineering equations from (Kurganov and Fedorov, 1973) or investigation results of (Beloshapkova and Beloshapkov, 1994a; Beloshapkova and Beloshapkov, 1994b). There are adhesion coefficients for fine and coarse solid particles. Coefficients are standardized per a time unit not to be dependent on the calculation discreteness. The physical meaning of adhesion coefficients is the probability that particles of a given size stay on the bottom for a while under the medium current velocity.

ADVECTIVE TRANSPORT

For practical purposes u, v, w components of current velocities in equation (1) can be specified for the source area in the following way:

1) When the real discharges are modeled within environmental monitoring studies for example, the series of instrumental observations over horizontal currents are used. This kind of modeling provides the most objective results of retrospective modeling of the contaminant plume statistics in case of availability of the reliable analogous series of current observations in the region. In the operative calculations the automated current observations near the discharge point at different horizons also allows getting the high-quality modelling results of the marine environment impact. As there are usually no observations over vertical current component, w component is taken equal to 0. This is quite correct for the impacts that do not exceed about several hundred meters across and dozens meters in depth if there are no identified upwelling/downwelling zones. The vertical current component is taken into account when calculating the turbulent pulsations.

2) The 95% probability current velocity profile that is not promoting the mixing process can be used to assess the static contamination field. As a rule, this profile is constructed for discharge standardization purposes to define the control section. Current velocity profiles are constructed over the frequency tables of instrumental or calculated current series.

3) The model fields of tidal and non-tidal currents are calculated to forecast the discharged contaminants transport using the near-surface wind characteristics. Tidal currents are calculated over harmonics constructed by instrumental series. Non-tidal currents are calculated over both diagnostic and prognostic models. For example, the application of the Ekhman-type diagnostic model to simulate the sea currents at the north-eastern Sakhalin is described in (Budaeva

and Makarov, 1998). Close verification of the model showed preservation of statistical properties of the real observations (Kochergin *et al.*, 2000). As for the prognostic models, the team of O.I. Zilbershtein used the 3D baroclinic model with the free surface and simulated the summary currents (Zilbershtein *et al.*, 2001).

4) The typical current profiles or reliable situations are used to calculate the average and the most probable parameters of the water column contamination. The tolerant criteria of vector characteristics (velocity and direction) that connect the corresponding velocity and direction intervals help to reveal the current profile belonging to a typical situation. Construction of a set of reliable situations is described by Rybalko (2000).

SEDIMENTATION

For the solid phase: the markers sedimentation velocity w_{S+Fl} is dependent on the natural sedimentation under the influence of gravity and resisting forces and additional effect of jet sinking and flocculation (in case there is a certain type of soil).

Velocity of the solid phase natural sedimentation in (1) is calculated over a balance equation of three forces made up for the ball-shaped particles of a given equivalent radius (diameter). The balance equation can be written down as the formula of Todes and Rozenbaum with empirical coefficients with account of irregular shape of a settling particle (Kurganov and Fedorov, 1973).

$$
W_s = \frac{g \cdot (\rho_i - \rho(z)) \cdot l_i^2 \cdot \sqrt{1 + 0.862 \lg k}}{\mu \cdot \rho(z) \cdot \left(18 + 0.61 \cdot \sqrt{\dfrac{g \cdot (\rho_i - \rho(z)) \cdot l_i^3}{\mu^2 \cdot \rho(z)}}\right)}, \qquad (4)
$$

where:

g – is the gravitational acceleration;

l_j – is a typical particle diameter;

ρ_i – is the particle specific weight;

$\rho(z)$ is the water density at a marker depth;

k – is the geometrical shape factor;

μ – is the viscosity coefficient (m²/sec) calculated over empirical equation (for fresh water):

$$
\mu = \frac{0.01775}{1 + 0.0337t + 0.000221t^2}, \qquad (5)
$$

where:

t – is the non-dimensional temperature in degrees Celsius.

The equivalent diameter l_i in (4) for irregularly shaped and rough particles is calculated as described in (Kurganov and Fedorov, 1973). For the purpose of engineering calculations the shape factor k (shows the ratio of the irregular particle area to the area of the equivalent sphere) is set according to the reference data of (Kurganov and Fedorov, 1973) and varies from 1.17 (for the rounded sands) to 1.5–1.67 (for the sharp-grained sands).

The flocculation effect describes the sticking of two solid particles and formation of particle combinations. (Winterwerp, 1997). Flocculation is typical for sludgy soils or colloidal solutions. The contaminant particles become covered with suspension, thus sticking to each other (Gavrilova, 1999). Sedimentation of a large particle, or floc, is faster. When calculating the drilling mud and cuttings discharges, it was admitted about 25-70% of particles are subject to flocculation. Flocculation effect lasted from 2 to 30 minutes.

The jet sinking effect described in (1) by w_{JS} parameter is observed under intensive discharges (*e.g.* dumping or instantaneous discharges) and shows itself in dragging the contaminant to the bottom with a much higher velocity as against a low-intensity discharge (Kurganov and Fedorov, 1973). The effect can be explained by the following processes. First, the jet is destructing due to the shear instability, turbulent pulsations and other factors. Second, the jet is sinking as its density is higher than the density of ambient waters. This is the jet sinking effect proper. Third, when the flow structure destructs due to decreasing concentration of the solid phase, the jet sinking effect stops and the particles settle according to the balance of gravity and other forces. VOSTOK 8.9 model takes account of all these processes and allows calculating an additional sedimentation velocity for the markers contained in heavy portions of the jet.

On average, the jet sinking effect lasts 0.5–1.5 minutes depending on the current velocity, discharge rate and other factors. The highest jet sinking effect is registered under instantaneous discharges.

It should be noted, there are not enough studies (some of them (O'Reily *et al.*, 1989; Caflish and Luke, 1985; etc.)) of flocculation and jet sinking effects to have the proper model verification tests. As a rule, the expert assessments of the above effects are used in calculations. These effects are to be incorporated in the model in the next versions.

Thus, the marker sedimentation velocity w_{S+Fl} and w_{SJ} can be calculated over eqns (4,5) taking the effects of increased amount and equivalent radius into account due to flocculation and jet sinking effects.

TURBULENCE PARAMETERS

The turbulent parameterization is based on the approach of (Ozmidov, 1986). The turbulence may be presented as the enclosed eddies of a different scale depending on oceanic processes. The calculation method described in (1) takes account of three scales of horizontal velocity turbulent pulsations that describe the mixing efficiency and one scale of vertical velocity turbulent pulsations.

Components of the turbulent pulsation velocity in (1) are determined using the standard deviation values σ_u, σ_v, σ_w and average velocity modules that are calculated over experimental data of current

observations or constructed by semi-empirical correlations. If basing on the hypothesis of normal spectral distribution of oceanic turbulent pulsations (Ozmidov, 1986), we can make up the following expressions of the velocity pulsation components in (1) for every statistical checking:

$$u' = P(\mu_u, \sigma_u),$$

$$v' = P(\mu_v, \sigma_v),\qquad(6)$$

$$w' = P(\mu_w, \sigma_w),$$

where:

$P(\mu, \sigma)$ – is a random value calculated over equation:

$$P(\mu, \sigma) = P_{sgn} \cdot P_{norm}(\mu, \sigma),\qquad(7)$$

where:

P_{sgn} – is a random value equal -1 or +1 with a density function of $f_{sgn}(x) = 0.5$ specified in the system of two points: $x = \{-1; +1\}$;

$P_{norm}(\mu, \sigma)$ – is a random value distributed by the normal law with μ (expectation) and σ (standard deviation) parameters and a distribution function of:

$$f_{norm}(x, \mu, \sigma) = \frac{1}{\sigma \cdot \sqrt{2\pi}} e^{-\left(\frac{(x-\mu)^2}{2\sigma^2}\right)}.\qquad(8)$$

The formula to get a random value distributed over the normal law (8) is easily made with the help of evenly distributed random numbers according to (Koonin, 1986):

$$P_{norm}(\mu, \sigma) = \sqrt{P_e} \cdot \cos(-2 \cdot \ln(1 - P_e)) \cdot \sigma + \mu,\qquad(9)$$

where:

P_e – is a random value distributed over the uniform distribution law and specified in $0 \le P_e < 1$ interval.

Thus, the function of distribution density $P(\mu, \sigma)$ has the form presented in Figure 1.
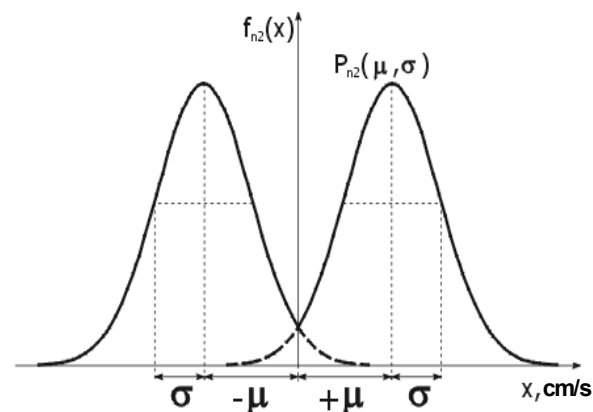
Figure 1. Distribution density of the turbulent velocity pulsations

It should be noted that by definition the stochastic nature of turbulent pulsations does not produce influence on the summary contaminant transport. Expectation of $P(\mu,\sigma)$ that determines velocity of turbulent pulsations equals 0. μ is the average module of the turbulent pulsation velocity that describes velocity of the specified spatial and temporal turbulent scale.

The discreteness of statistical tests depends on the temporal turbulent scale. In practical engineering calculations it is quite enough to specify the turbulence starting from about 0.5-minute scale. If velocity of turbulent pulsations amounts to 10 cm/sec, the minimum jet diameter should be not less than 3 m. This is possible within 10-30 m from the source. Unfortunately, there are no accurate less-than-10-minute-discreet measurements of current velocity in this range. Therefore, determination of the turbulent pulsation velocity in 0.5–15-minute range is based on available reference data and constructed semi-empirical engineering correlations shown below.

The next turbulent stage is marked for the range of 15–60 minutes. Here σ and μ from (6) can be calculated over instrumental current observations on the Sakhalin north-eastern shelf with 10 and more minutes discreteness. This kind of turbulence is found 150–500 m from the source. This is the proper control section required by Russian environmental law.

The last turbulent stage registered in 60–360-minute range is tied with horizontal eddy formations 300 and more meters in size. This kind of turbulence is found at the distance of more than 1 km from the source. Here, σ and μ parameters needed for calculation of turbulent pulsations in (6) are also determined over instrumental current observation series.

Calculation of turbulent current velocity in the range of 15–360 minutes was tested while processing instrumental current series for Piltun-Astokh and Arkutun-Dagi fields. Here, D_x, D_y dispersions were calculated for two temporal scales (Kochergin *et al.*, 1999).

The components of velocity of minimum-scale turbulent pulsations $u'_{0.5-15}$, $v'_{0.5-15}$, w' in (1) comparable with calculation discreteness under no or insufficient experimental data are calculated over the shear unsteadiness theory that ties the dispersion of velocity components and the Richardson criterion (Ozmidov, 1986; Natural conditions in Baydaratskaya Guba, 1997). In the simple form the turbulence and the flow rate are connected with formula of Pukhtyar and Osipov (1981). In practice this formula is used when there are no *in situ* measurements of the velocity dispersion for (6). Formula of Pukhtyar and Osipov and linearized dependencies of the boundary turbulent parameters (Ozmidov, 1986; Natural conditions in Baydaratskaya Guba, 1997) served the basis for establishing engineering formulas to calculate the

turbulent pulsation velocity (Bogdanovsky and Kochergin, 1998). Engineering formulas are constructed over assumption that primary dispersion meaning is dependent on the flow proper and additional wind and bottom corrections. The said corrections are the result of the series expansion and parameterization of the wind wave impact (τ) by turbulence:

$$\alpha \approx k_1 \cdot z \cdot \tau \cdot e^{-k_2 z} \qquad (10)$$

and parameterization of the bottom friction impact that is proportionate to $(z\text{-}h)^2$.

Thus, we can calculate the standard deviation over the following empirical equations:

$$\sigma_{u'} = \sqrt{2 + 0.196 \cdot v_x^2 + 0.076 \cdot v_y^2} \times$$

$$\times \left(K_1 + K_2 \cdot e^{-\alpha z} + \frac{K_3}{\beta \cdot (h-z)^2 + 1} \right),$$

$$\sigma_{v'} = \sqrt{2 + 0.196 \cdot v_y^2 + 0.076 \cdot v_x^2} \times$$

$$\times \left(K_1 + K_2 \cdot e^{-\alpha z} + \frac{K_3}{\beta \cdot (h-z)^2 + 1} \right), \qquad (11)$$

$$\sigma_{w'} = \gamma \cdot \sqrt{\sigma_u^2 + \sigma_v^2} \cdot f(Ri),$$

where:

v_x, v_y – are the typical flow rates (cm/sec);

K_1, K_2, K_3 – are non-dimensional coefficients of relative contribution of different processes into the turbulence;

φ is – the additional coefficient that takes account of m^2/sec^2 direction and usually valued at 1;

α – is the scale of surface impact (wind waves);

β – is the parameter of bottom impact (rough bottom) (m^{-2});

γ – is the transitional parameter describing the average ratio of horizontal and vertical diffusions (is equal to 0.083);

$f(Ri)$ – is the function dependent on Richardson criterion, it depresses the turbulent mixing under the steady stratification and intensifies it under unsteady stratification. Richardson criterion is the ratio of squared Brunt-Vaisalla and Kelvin-Helmholtz frequency and shows laminarity or turbulence of the flow.

The expectation value of the velocity module in (6) is calculated over the standard deviation taking account of empirical dependencies constructed for larger scales $\mu \approx 0.8 \sigma$.

Standard deviation of a latitudinal, zonal and vertical components of turbulent pulsations is calculated over (11) for the surface and the sea bottom in the range of 0.5–15 minutes. The following criteria were chosen for determination of empirical coefficients. α parameter is inversely proportional to the typical wind wave impact $0.25 L$, where L is the typical length of wind waves. In deep waters the wind wave length is calculated over $L = T^2 g / 2\pi$, where T is the period of

wind waves. β parameter describes the thickness of the bottom boundary layer and is assessed according to the theory of (Landau and Lifshits, 1986). For the average velocity of bottom currents β equals 0.16. Coefficient $K1$ is determined empirically and taking on value of 1.0–0.5 being in compliance with (Pukhtyar and Osipov, 1981). Coefficient $K2$ ranges from 0.1 to 0.5 by wind characteristics (0.03 of the wind velocity module). Coefficient $K3$ ranges from 0.1 to 0.2.

The following semi-empirical parameters are used to calculate the dispersion of vertical velocity. Transitional coefficient γ is calculated over correlations of the vertical and horizontal velocity scales. The chosen value 0.083 does not conflict with the assessments given in (Ozmidov, 1986) (the usual assessment is 0.1). In order to get a function of Richardson criterion the authors used different polynomial and exponential approaches (Ozmidov, 1986; Natural conditions in Baydaratskaya Guba, 1997). The exponential one for the steady stratification is the most reliable (Natural conditions in Baydaratskaya Guba, 1997). Thus, we have $F(Ri)= e^{-1.1Ri}$.

VERIFICATION AND COMPARATIVE TESTS

Verification testing of the model began in 1994. However, two activities should be emphasized that allowed enlarging the model features and specifying a number of coefficients. The first one is the discharge experiment organized by Exxon Neftegas Ltd., as operator of the Sakhalin-1 consortium, in 1998. The second is the comparative simulation on AKS model developed in Computing Centre of the Russian Academy of Sciences (CC RAS) and Ecocenter IFPA (Arkhipov *et al*., 2000) in 2002.

Environmental monitoring organized in 1998 at Arkutun-Dagi field involved assessing the potential environmental impact of experimental drilling mud and cutting discharges. Environmental observations (monitoring of hydromet and oceanographic parameters and discharges) were organized aboard two operating jack-up drilling rigs. *In situ* measurements of the suspended solids content in the water column were organized aboard R/V "Pavel Gordienko" and two Zodiak-type boats.

The actual discharge and hydrodynamics conditions were taken into account. Analysis of observation results showed the spatial distribution (vertically and horizontally) of the discharged contaminants and concentration fields of the drilling mud solid phase in specified location and time.

We made the detailed calculation of concentration of the drilling mud solid phase in the water column and compared calculated results with actual data observed from the research vessel and boats. Figure 2 presents the comparative diagrams of contaminant concentration (for three current types) determined over observed and modeled data.
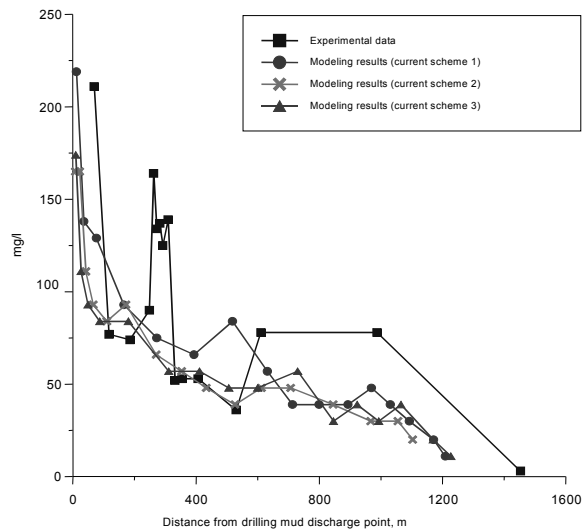
Figure 2. Distribution of maximum concentrations of suspended solids depending on the distance from the drilling mud discharge point (real observations and the modeling case)

Within TEOC stage of Sakhalin 1 project we used two independent models – VOSTOK 8.9 model of FERHRI and AKS-ECO model of CC RAS–Ecocenter IFPA – and compared the modeling results. Among the impacts simulated there is site leveling including the dredging and soil dumping (volume of soil 5,000 m^3) and construction of underwater pipeline including trenching, temporal storage of soil at the sea bottom and trench backfilling (volume of soil over 800,000 m^3). The input data in both models included the list of impact sources and their technical parameters (capacity, operation time, location of impact sources, granulametric composition of soils).

For the purpose of comparison, output results were prepared using the same gradations and units. The following output results were compared: the curves of the maximum extent of suspended solid concentration depending on the distance from the source, the average volumes of contaminated water by the concentration gradations, the lifetime of waters contaminated with a given concentration of suspended solids, and the size of formed bottom sediments by height gradations.

Comparison of modeling results shows their relatively good convergence. The highest convergence is achieved when calculating the sediments area at the sea bottom (relative difference within 0–35% for different gradations). This testifies to the use of approximately the same calculation parameters of solid particles sedimentation velocities. Comparison of calculated water column contamination parameters shows that both models produce almost the same results for the suspended solid concentration in the plume of more than 10 mg/l (10–30%), while results may be considerably different (up to 70%) if the concentration is low.

Thus, despite the difference in modeling approaches (VOSTOK model is based on Lagrange approach, while AKS-ECO model uses Euler approach) the models produce comparable results. The models may be considered adequate enough as they were tested under other different conditions and regimes.

CONCLUSION

The model described above is a quite finished methodical product having its own engineering solutions ensuring the model applicability for practical calculations. Engineering solutions allowed development of methods to set the sea current fields, calculate the turbulence, set parameters of contaminant interaction at the solid and atmospheric boundary and calculate the flocculation and jet sinking effects.

Computer realization of the contaminant transport computation process ensures forecasting the contaminant spread and sedimentation, the plume trajectory, the spread of contaminant concentrations and the sediment characteristics depending on the bottom dynamics etc.

ACKNOWLEDGMENTS

REFERENCES

Arkhipov B.V., Koterev V.N., Solbakov V.V. **2000**. AKS model for distribution prediction of discharges from marine drilling platforms. Report on applied mathematics, CC RAS, Moscow, p. 68–70. (In Russian).

Astrakhantsev G.P., Rukhovets L.A., Egorova N.B. **1988**. Mathematical modeling of admixture distribution in water. J. of Meteorology and Hydrology, 6, p. 71–79. (In Russian).

Beloshapkova S.G., **Beloshapkov** A.V. **1994a**. Mechanics of particle detachment under the action of coherent structures in water flow (filtration weighing model). J. Oceanology, v.34, 1, p. 127–132. (In Russian).

Beloshapkova S.G., **Beloshapkov** A.V. **1994b**. Mechanics of particle detachment under the action of coherent structures in water flow (turn over model). J. Oceanology, v.34, 4, p. 474–480.

Bogdanovsky A. A., Kochergin I. E. **1998**. Turbulent characteristics parameterization for typical conditions of north-eastern Sakhalin shelf. FERHRI Proceedings, Specialized Issue. 82–102. (In Russian).

Bogdanovsky A. A., **Kochergin** I. E. **1999**. Technique of contaminant transport modeling in marine environment applied to Sakhalin shelf conditions. Proceedings of Int. Forum on problems of science, technology and education. Science Academy of Earth, Moscow, p. 111–113. (In Russian).

Budaeva V.D., **Makarov** V.G. **1999**. A peculiar water regime of currents in the area of the Eastern Sakhalin shelf. Proceeding of the Second PICES Workshop on the Okhotsk Sea and Adjacent Areas, 131-138.

Caflish R.E., **Luke** J.H.C. **1985**. Variance in the sedimentation speed of a suspension. Phys. Fluids 28, p. 759.

Dmitriev N.V., **Dvurechenskaya** E.A. **1994.** Numerical analysis of admixture transport for top turbulent layers of seas and oceans. J. Meteorology and Hydrology, 12, p. 53–62. (In Russian).

Gavrilova T. A. **1999**. Physical-chemical characteristics of drilling mud used for Sakhalin shelf drilling. FERHRI Special Issue No. 2, Vladivostok, p. 204–217. (In Russian).

Kochergin I.E. **2000**. Calculation of zones with increased suspended solids concentration during construction of oil and gas facilities on the Sakhalin shelf. FERHRI Proceedings, 140, p. 40–51. (In Russian).

Kochergin I.E., Bogdanovsky A.A., Budaeva V.D., Varlamov S.M., Dashko N.A., Makarov V.G., Putov V.F., Rybalko S.I. **2000.** Construction of hydrometeorological scenarios for environmental impact assessments. FERHRI Special Issue, No. 3. Vladivostok, p. 223–240.

Kochergin I.E., **Bogdanovsky** A.A. **1999**. Transport and Turbulence Characteristics for the Northeastern Sakhalin Shelf Conditions. Proceeding of the Second PICES Workshop on the Okhotsk Sea and Adjacent Areas, p. 115–121.

Kochergin I.E., Bogdanovsky A.A. Rybalko S.I. **2000**. Modelling of pollution transport in the marine environment of Sakhalin shelf. WITpress proceeding "Environmental Coastal Regions III", 105-114.

Kochergin I.E., Rybalko S.I., Putov V.F., Shevchenko G.V. **1999**. Processing of the instrumental current data collected in the Piltun-Astokh and Arkutun-Dagi oil fields, North East Sakhalin shelf: some results. FERHRI Special Issue No. 2, Vladivostok, p. 96–113. (In Russian).

Kochergin V.P., **Bokovikov** A.G. **1980**. 3D numerical model of admixture distribution in coastal zone of deep water object. Proc. of USSR Academy of Science, Physics of Atmosphere and Ocean, v.16, 7, p. 729–737. (In Russian).

Koonin S. **1986**. Computational physics. Addison-Wesley Publishing Company.

Korotenko K.A., **Lelyavin** S.N. **1990**. Admixture transport calculation by particle method. J. Oceanology, v.30, 5, p. 930–936. (In Russian).

Kurganov A.M., **Fedorov** N.F. **1973**. Reference book on hydraulic calculations of water supplying and sewage systems, Leningrad, 408 p. (In Russian).

Landau L.D., **Lifshits** E.M. **1986**. Hydrodynamics, Moscow, 736 p. (In Russian).

Natural conditions of "Baydaratskaya Guba". **1997**. Main results of research for Yamal–Center pipeline construction, Moscow, 423 p. (In Russian).

Nikolskiy M.A., Fedorov A.L., Dorozhkin A.I. **1990**. Numeric solution of passive admixture distribution problem in sea coastal zone. J. Meteorology and Hydrology, 1, p. 57–56. (In Russian).

O'Reilly J.E., Sauer T.C., Ayers R.C., Brandsma M.G., Meek R. **1989**. Field verification of the OOC mud discharge model. Drilling wastes. New York, p. 647–665.

Ozmidov R.V. **1986**. Admixture diffusion in ocean, Leningrad, 280 p. (In Russian).

Patania F., Siracusa G., Gagliano A., Siracusa A. **2000**. Control and protection of marine environment by Acitrezza town sewage. WITpress proceeding "Environmental Coastal Regions III", p. 217–226.

Pukhtyar L.D., **Osipov** Yu.S. **1981**. Turbulent characteristics of sea coastal zone. SOI Proceedings, 158, p. 35–41. (In Russian).

Rybalko S.I. **2000**. Methods of instrumental wind and current series processing for NE Sakhalin shelf development projects. 50th Anniversary FERHRI Proceedings, p. 225–238. . (In Russian).

Sharp J.J., **Moore** E. **1989**. Marineoutfall design-computer models for initial dilution in a current. Proc.Inst.Civil.Eng., p. 953–961.

Voltsinger N.E., Klevanniy K.A., Tuzova O.I. **1990**. On problem of calculation of transport and diffusion of admixture in arbitrary field. J. Meteorology and Hydrology, 5, p. 56–58. (In Russian).

Winterwerp J.C. **1997**. A simple model for turbulence induced flocculation of cohesive sediment. J. Hydraulic Research, v.36, 3, p. 309–326.

Zagar D., Rajar R., Sirca A., Horvat M., Cetina M. **2000**. Three-dimensional model of dispersion of mercury in marine environment. WITpress proceeding "Environmental Coastal Regions III", 205-215.

Zaytsev O.V., **Zaytseva** T.V. **1984**. Modeling of admixture transport in coastal zone by Monte-Carlo method. FERHRI Proceedings, 131, p. 50–61. (In Russian).

Zilberstein O.I., Safronov G.F., Popov S.K., Lobov A.L., Verbitskaya O.A., Chumakov M.M., Elisov V.V. **2001**. Problems of surveys support with extreme and operative characteristics of sea level and currents. Proceedings of Fifth Int. Conference "Russian Arctic Offshore", Saint-Petersburg, p. 281–286. (In Russian).

OCEANOGRAPHY OF AREA CLOSE TO THE TUMANNAYA RIVER MOUTH (THE SEA OF JAPAN)

M.A. Danchenkov[1], D.G. Aubrey[2], K.L. Feldman[3]

[1] Far Eastern Regional Hydrometeorological Research Institute (FERHRI), Russia
Email: danchenk@fastmail.vladivostok.ru

[2] Woods Hole Group, USA

[3] Institute of Marine Biology, Far Eastern Branch of Russian Academy of Sciences (IMB FEBRAS), Russia

Tumannaya river mouth is the frontier area between PRC, North Korea and Russia. Marine area close to it is investigated on the base of unique field measurements. Northwest thermal front from this area to the Yamato Rise was found. To the south of it southeastward current was traced by salinity distribution and surface floats drift.

INTRODUCTION

The Tumannaya river (Tumangang, Tumenzyan) represents a prospective way for transport of the Chinese goods to the east. Now, because of low depth the river is not navigable, though under deepening of the waterway it can become navigable, similar to the majority of the area rivers. Under the intensive industrial development of the riverbed, its waters will transport pollutants to the Sea of Japan area directly to the adjacent marine reserve (around Furugelm island). Investigation of the problem "where the river drains would be transported to after flowing into the sea" is interesting from both the scientific and applied science point of view.

The river runs into the Sea of Japan (Figure 1) between Gashkevich Bay (Choson Bay) in the south and Possiet Bay in the north.

In present paper waters of the Sea of Japan close to the Tumannaya river mouth are investigated.

A few papers are devoted to the physical oceanography of the area (Vanin *et al.*, 1999; Vinokurova and Skokleneva, 1980; Grigorieva *et al.*, 1998; Podorvanova *et al.*, 1989; Rodionov, 1984). Relatively detailed analysis of oceanographic conditions of small area, close to the Tumannaya river mouth from the north, was published just recently (Moschenko *et al.*, 2000). There the conclusion on the northward transport of polluted water from the Tumannaya river mouth to the north was made.

But there is another source of contamination – non-treated waters of ports and cities (there are four seaports near the river mouth: Possiet, Zarubino, Slavyanka and Vladivostok). Ships coming into the ports can pollute the waters of local marine reserve as well.

Over primary water transport from the river mouth to the north (Moschenko *et al.*, 2000) the basic source of marine reserve water pollution would be the river run-off (from China). Under the primary water transport from the north into the area of marine reserve the basic source of water pollution would be the Russian industrial and household drains.
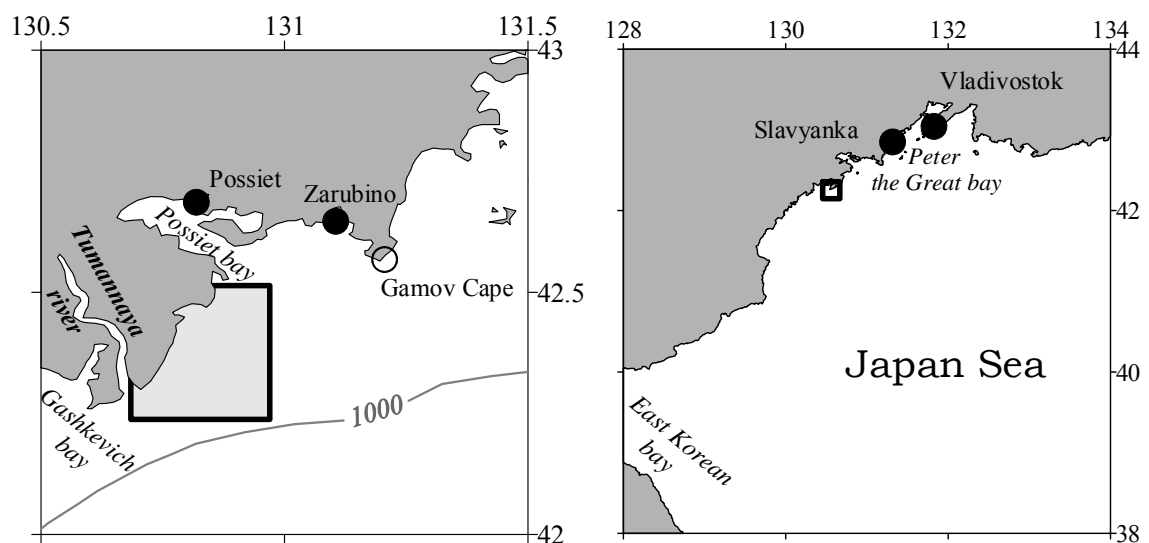

Figure 1. Tumannaya river mouth (left) and northwest Sea of Japan (right)

To estimate the possible ways of distribution of water pollution it is necessary to know the prevailing currents, and due to a small number of their measurements it is logical to attract comprehensive meteorological and oceanographic characteristics of the area.

DATA

In this work accessible oceanographic surveys for the last 15 years are used. The oceanographic data in the researched area were received during the following periods: January 11–12, 1986; July 27–28, 1989; March 1–7, 1995; August 28–31, 1996; September 27–30, 1996; April 4–6, 1997; July 26–29, 1997; August 21–26, 1997; September 20–23, 1997; October 12–15, 1997; May 28–31, 1998; July 4–5, 1998; August 23–26, 1998; April 14–16, 1999; November 23 – December 3, 1999; March 4–12, 2000.

Among them 10 surveys were executed by Institute of Marine Biology in a small area between the Tumannaya river mouth and Furugelma Island. (marked by square in Figure 1).

METEOROLOGICAL CHARACTERISTICS OF AREA

In a number of papers (Vanin *et al.*, 1999; Moschenko *et al.*, 2000; Moschenko *et al.*, 2001) the calculations of the wind currents are carried out with a wind speed that is not typical for the researched area. To be convinced of it, the monthly average characteristics of wind are necessary to be studied.

Within the limits of Peter the Great Bay the direction and speed of wind are measured only at three coastal meteorological stations. One of them (Vladivostok) is located far from the considered area. Another station (Possiet) is situated inside the bay. Only one station ("Gamov Cape") can be regarded as the typical one for this area. Here, westward wind prevails in winter and eastward wind prevails in summer. Meridional component of speed is rather insignificant (in cited papers meridional component is essential). Monthly average wind speed is not more than 5 m/s within year.

Comparatively big discharge of Tumannaya river (5.7 km^3 per year) was calculated (Vyshkvartsev, Lebedev, 1997) indirectly only (measurements of the river flow, as well as river level, have never been carried out) – on the base of volume of precipitation.

WATER MASSES

Water Mass (Water) is the homogeneous water typical for the large area and existing for enough long time. Sea waters close to the Tumannaya river mouth from the north were divided recently (Moschenko *et al.*, 2000) into the following types:

- Surface Water (temperature in core is 16.8°C, salinity – 33.17‰)
- Subsurface Water (16.3°C, 33.36‰, in August only)
- Deep Water (3.2°C, 33.95‰)
- Bottom Water (0.9°C, 34.03‰)

Let us note that parameters of so defined Subsurface Water are too close to parameters of Surface Water and pointed parameters of Bottom Water are not typical. And Water of low (33.4‰) salinity could not be called "Subsurface" (high salinity is a typical feature of Subsurface Water).

$T(S)$ – indices constructed on the same data as in the cited work give absolutely other values of Water cores indices (Figure 2):

- Surface Water (21°C, less than 33.0‰),
- Intermediate Water (17°C, 33.5–33.6‰),
- Deep Water (1-2°C, 33.96–34.07‰).

Because of rather small depths at these stations water parameters near the bottom in summer did not essentially differ from the characteristics of waters above, therefore Bottom Water was not distinguished in summer. Water with comparatively low salinity is named as Intermediate Water.

The core of Surface Water was positioned at surface, core of Intermediate Water was at 10-20 m deep and Deep Water spread near the bottom. Salinity of Surface Waters augmented with the increase of distance from the coast up to the values typical for Intermediate Water. From this the distance of restricting distribution of Surface coastal Water was determined as 12 miles. Behind this limit the surface layer and intermediate layer merged.
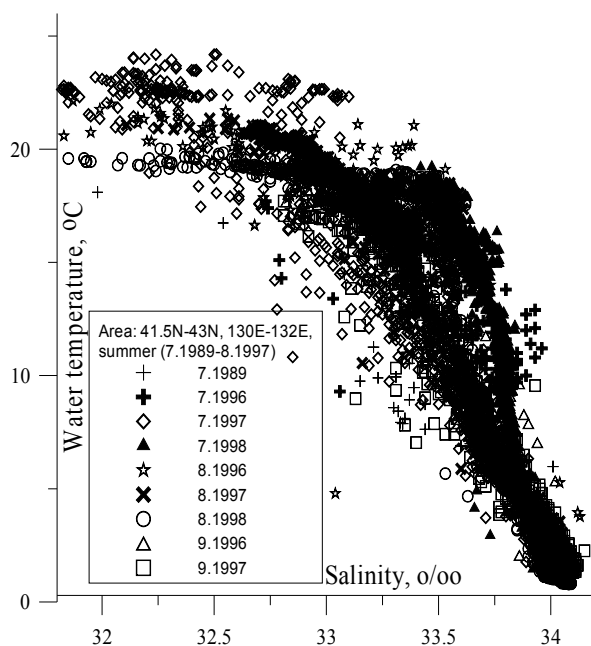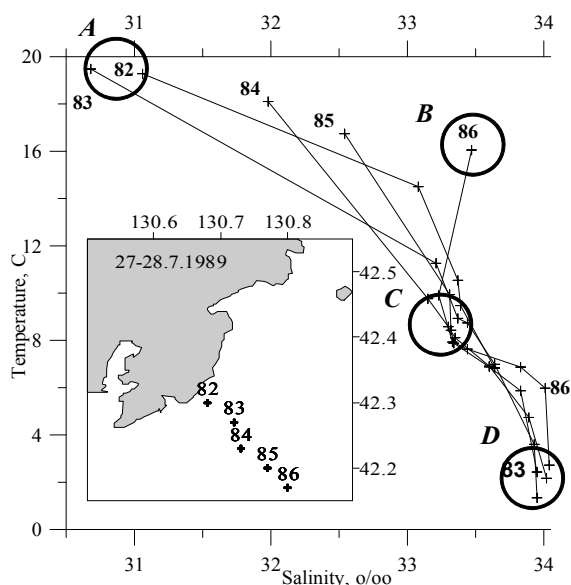

Figure 2. *T(S) – indices of waters in the northwest part of the Sea of Japan in summer*
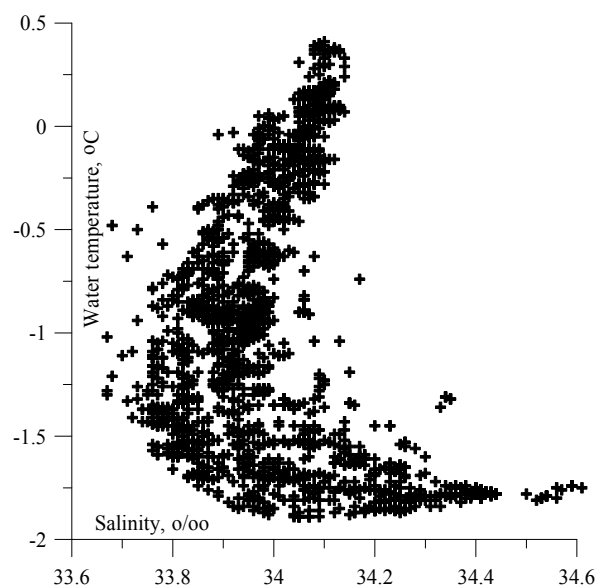
Figure 3. *T*(*S*) – curves for the section near the Tumannaya river mouth in summer of 1989. (By digit the number of station is designated, by circles – water core position)

Figure 4. *T*(*S*) – indices of Peter the Great Bay waters in winter (March of 2000)

There was similar vertical structure of waters in the area to the east of the mouth of Tumannaya river in summer of 1989 (Tkalin, 1999): below heated surface layer on coastal (A – st. 82–85) and offshore (B – st. 86) stations the Intermediate Water of low salinity (C) was observed, which core (temperature 7–10°C, salinity less than 33.5‰) was situated at 10 m deep (Figure 3).

The deep layer was occupied by the Sea of Japan Proper Water (D), its temperature was less than 2°C, and salinity was 33.95-34.08‰. The next station was located off the coast, the salinity of deep waters was higher.

SEASONAL VARIATIONS OF WATER STRUCTURE

The water structure in the researched area changes strongly vertically within a year. At surface (on the example of the section off Gamov Cape) it is possible to determine the Surface Coastal Water of low salinity (-0.6°C, 33.96‰) and Surface Offshore Water of increased temperature and high salinity (0.2°C, 34.08‰). Offshore water is characterized by the high uniformity from the surface to the bottom (to 120 m deep). Rather warm water is transported here from the east by large-scale gyre (Danchenkov *et al.*, 2000). It is interesting that within the considered area in spring the Cold Water of low temperature (characteristic for the areas with ice formation – for example, the Okhotsk Sea) was not found absolutely (though the ice here is formed every winter). The reason of its absence is the influence of warm subtropical water penetrating into Peter the Great Bay from the east.

In winter in upper 100 m layer (Figure 4) it is possible to locate three Waters:

- Surface Water (water temperature is more than 0°C, water salinity is 34.05–34.15‰), which core is located far from the coast

- Fresh Intermediate Water (water temperature is less than 0°C, salinity – 33.7–33.9‰) with a core located at surface

- Deep Water (temperature is less than 0°C, salinity is more than 34.1‰), which core is situated near the bottom

Salinity of Deep Water achieves very high values (up to 34.6‰).

In March the Surface Water was homogeneous by temperature (about 1°C), and in April the surface layer was warmed up to 3°C. Salinity of Surface Water in April increased by 0.02–0.08‰ compared with March values.

Intermediate Water became considerable in spring. This Water is known at least since 1953 (Miyazaki, 1953). But in Russian publications (Leonov, 1960; The basic features..., 1961; Yakunin, 1989) it was not mentioned prior to recent time. There was the supposition that Intermediate Water was formed by the downwelling of Surface Water at the Subarctic front (Miyazaki, 1953) and that it was transported from there to the south by North-Korean current (Kim and Kim, 1983).

In April of 1999 core of Intermediate Water lied close to the surface, its salinity did not exceed 33.98‰, and temperature was between 0.2°C and 3.5°C. In May of 1998 its core lowered, temperature increased, and salinity reduced. This Water requires the special

attention as it is formed in the researched area between Northwest and Subarctic fronts.

The signs of influence of warm subtropical waters in the researched area were described more than once. "In Peter the Great Bay there is a significant quantity of subtropical and boreal benthos. However, hydrological observations do not point to the direct indications of any branch of warm current influx into the bay" (Biryilin *et al.*, 1970). Near Possiet thermophilic fish were met usually in the end of August – beginning of September. The found species were: sharks, tuna, fish – saber and moonfish (Shmidt and Taranets, 1934; Taranets, 1938; Gorodnichiy, 1949; Rumyantsev, 1951; Novikov, 1957a; Novikov, 1957b). The constant congestions of flounder in winter near Gamov Cape and in the vicinity of Askold Island were remarked (Moiseev, 1937).

But subtropical waters of high temperature and high salinity (more than 34.05‰) also were not found here in 1989-1998. Water salinity in upper 200-meter layer in summer did not exceed 34.00‰. Only in August of 1996 the water of high salinity (34.12‰ at the depth of 45 m) was marked, but its temperature was rather low (4°C).

The way of subtropical waters penetration into Peter the Great Bay was identified for the first time recently (Danchenkov *et al.*, 1997a). Warm waters transport occurs like a chain of warm eddies running along 131.5°E. But such northward water transport was never traced to the north off Possiet. The existence of warm waters to the north off Possiet (in Ussuri Bay and near Askold isl.) is caused by their transport from the east by westward flow of subtropical waters from Hokkaido (Danchenkov *et al.*, 2000).

SPATIAL WATER STRUCTURE

Following the traditional concepts, according to which the Subarctic front in the Sea of Japan runs along 40°N, it is impossible to explain penetration of warm waters into the Possiet area. But lately (Danchenkov *et al.*, 1997b) another large-scale and non-zonal Northwest front (Figures 5, 6) alongside with the known thermal front along 40°N was discovered.

This front passes from the Tumannaya river mouth to the southeast also separating the cold subarctic water from the transformed subtropical one. The shift of temperature through the front equals 3°C-6°C. Between the fronts interfrontal area is situated. The temperature gradients across the Subarctic front are more than cross Northwest front. Non-zonality of this front is caused by the transport of subtropical origin water into the investigated area from the south. Due to it the farthest border between warm (from the south) and cold (from the north) waters removed to north in western part of the Sea – size of interfrontal area decreases from the west to the east. Northwest thermal front is noticeable down to 100 m deep. Together with the thermal shift across the Northwest front there are gradients of salinity. So, this front is traced by salinity gradients as well.

To the south of the Northwest front in winter the belt of fresh water is situated (Danchenkov *et al.*, 2000). The formation of this Water is well visible, for example, at the section along 130.5°E (Figure 7) and by the distribution of surface salinity in March of 1997 (Figure 8).
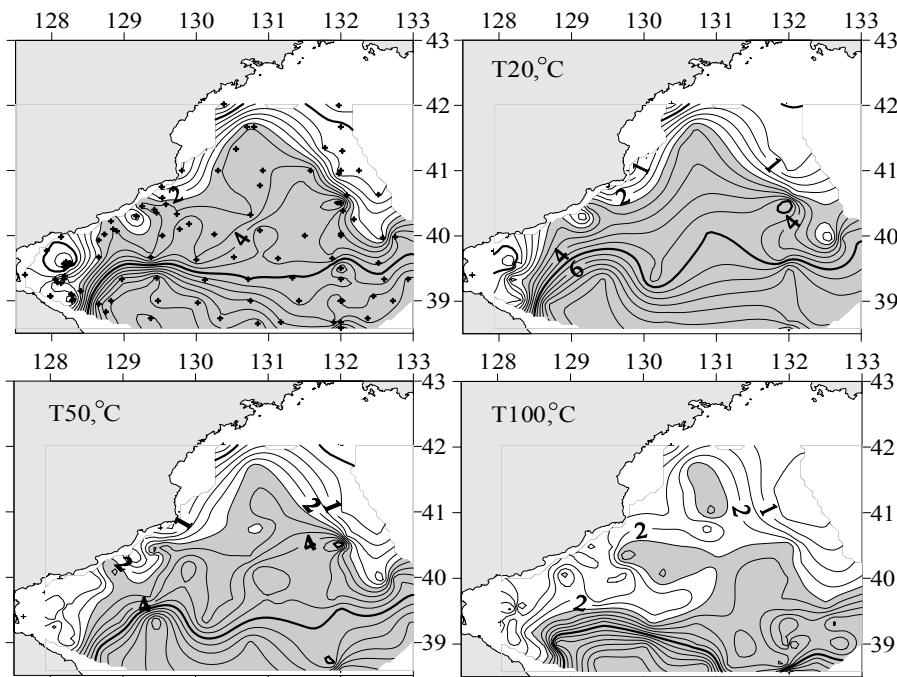

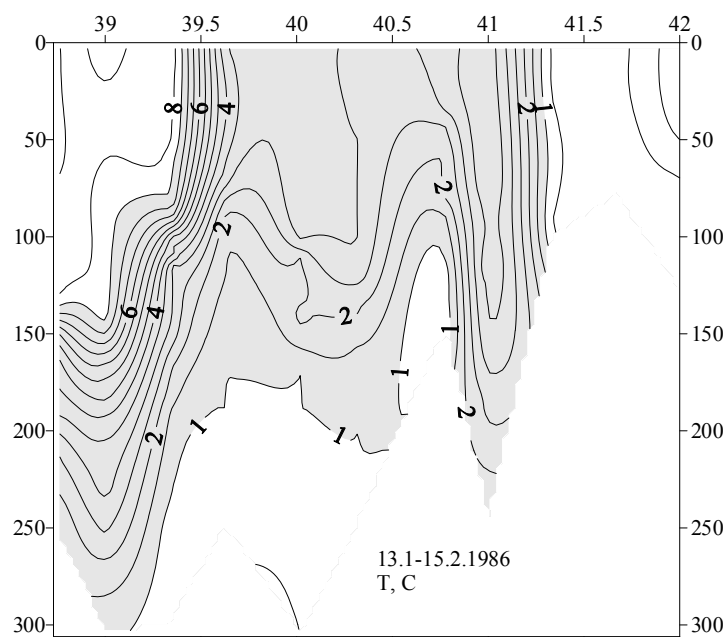**Figure 5. Water temperature at surface and 50 m deep in winter of 1986**

Figure 6. Water temperature at the section across two fronts in winter of 1986
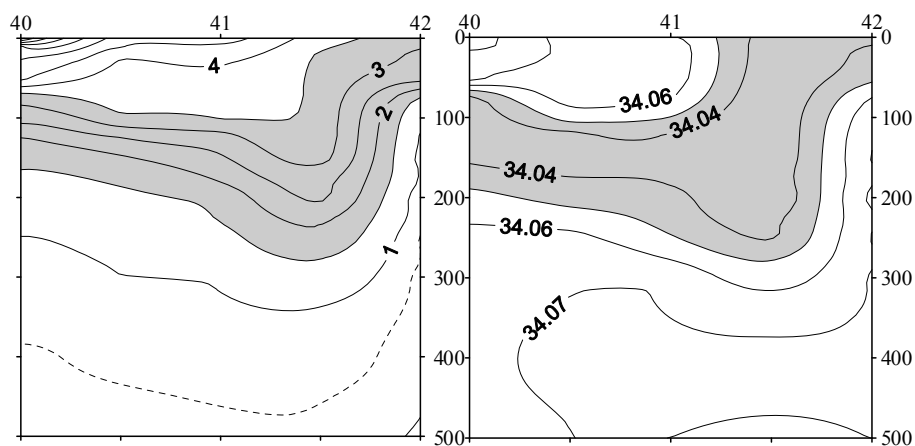

Figure 7. Vertical distribution of temperature and salinity along 130.5°E in March, 1997
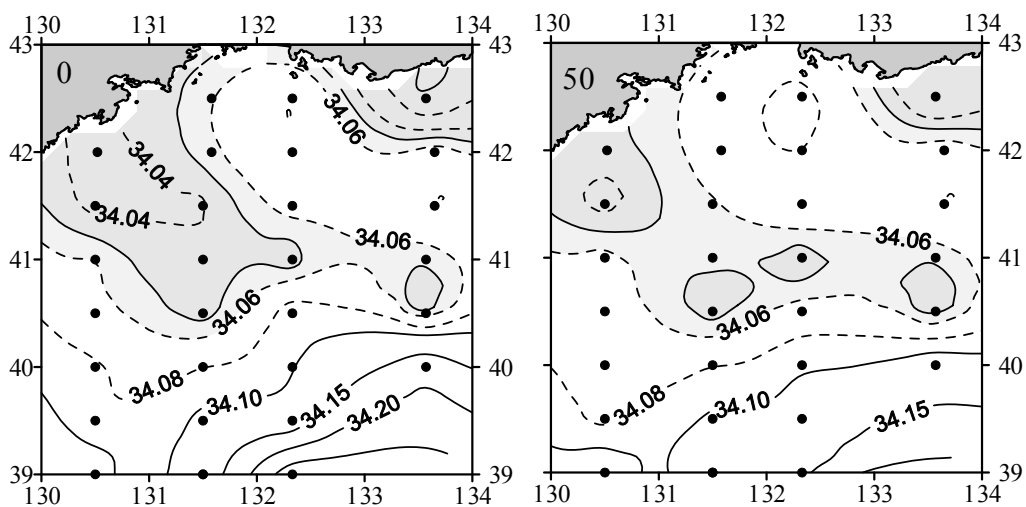

Figure 8. Distribution of salinity at surface and 50 m deep in March of 1997

When the surface waters begin to get warm, the tongue of cold fresh water at surface disappears, but water of low salinity does not disappear at all. Its presence in the intermediate layer in summer is marked across the wide water space from Possiet to the coast of South Korea. It is possible to assume that it is distributed in that intermediate layer from the place of its formation (between two fronts) to the south. Not only water of the river Tumannaya and rivers flowing into the Peter the Great Bay, but also coastal waters of Southern Primorye participate in its formation at surface in winter.

SEASONAL AND INTERANNUAL VARIATIONS OF NORTHWEST FRONT

The significant changes in oceanographic fields of northwest part of the Sea of Japan take place during a year. Though the Northwest front exists within the whole year, in summer the spatial gradients across the front at surface are considerably weakened. Along 131°E there is steady water transport to the north along a chain of eddies. As a result, in autumn near Possiet the extensive area of warm water appears. In October to the south of Vladivostok the steady northern winds cause the upwelling of cold subsurface water and their further quick (in one month) cooling. Cold waters spread to the south and southwest blocking the area of warm water at Possiet. The cooling of this area takes two months. After that Northwest front is promptly displaced to the south to 40°N. Subarctic front strengthens. Together with it a new Northwest front is formed between Tumannaya river estuary and Yamato Rise.

Transport of comparatively warm and salty waters from Hokkaido to the west along 42°N creates the obstacle to the ice spreading to the south.

Such winter structure is kept till April. Accordingly, degree of cooling and formation of dense water not February, but March can be supposed as the most typical winter month (Danchenkov and Goncharenko, 1994). In April the Subarctic front in the western Sea of Japan collapses and again the chain of eddies is restored.

Beyond the seasonal variations the year-to-year ones are significant as well. Disastrous sardine stock abundance in 1930s is the only example of interannual changes. Despite the fact that temperature of air continuously grew in the 20th century, oceanographic conditions exhibited the periods of warming and cooling. So till 1913 the heat-loved sardine and saury did not inhabit the coastal Primorye waters. And from the end of 1930s the arrival of sardine to the Russian coast constantly was late, and in 1942 the sardine practically disappeared (Gorodnichiy, 1949). On the contrary, catches of cryophilic herring in the southern Primorye in 1930s were sharply reduced and again increased in the beginning of 1940s. The next warming displayed in detection of the heat-loved

fishes near Possiet (Kos, 1969) began in 1949, and the next cooling happened in 1962.

DISCUSSION ON THE SOURCE OF WATER POLLUTION

Recently (Vyshkvartsev and Lebedev, 1997) it was declared about a new current directed to the north from the river Tumannaya mouth: "On the shelf of the Possiet bay besides Primorye current the current of opposite direction exists. It flows near the river Tumannaya mouth with the speed of 0.2–0.5 knots and is included in anti-cyclonic circulation in the open part of the Possiet bay. It testifies to the transport of polluting substances from China to Russia....". Any proofs of new current existence were not given. The desire of the authors is clear to show that the contamination of marine reserve waters (near Furugelma is.) occurs not from the wastes drain of Vladivostok or Zarubino, but from Tumannaya River.

In one paper (Grigorieva *et al.*, 1998) two maps of sea currents were published ("appropriate to tidal inflow and tide outflow"). The method of such division is not clear; the recognized opinion is (Sailing directions of the Sea of Japan, 1972) that tidal currents in this area are not almost registered at all. The authors of cited paper for some reason used to reference the data on the sea level in the narrow Possiet bay, where the tidal level variations strongly differ from those in the area of investigation. The data of measurements of currents from 6 buoy stations were not analyzed, probably due to "the measurements of currents are of isolated and casual character and do not give the complete picture of coastal water circulation" (Moschenko *et al.*, 2000).

In line of papers northward drift current was got from calculations based on the possible strong northward wind. The results of the same calculations (with the conclusions about water transport from the river mouth to the north) were published four times (Vanin *et al.*, 1999; Vanin *et al.*, 2000; Moschenko *et al.*, 2000; Moschenko *et al.*, 2001). The representations of currents are made concerning the results of calculations of wind currents by the assumption that the depth of area everywhere is small, and that "the wind was homogeneous in time and space".

But water depth just in the investigated area is very different (depth in the southeastern part is more than 500 m), in summer the wind has different direction and northward wind does not prevail. Any essential drift current could appear in case of long-term wind action only and it could be seen under the average speed values. Strong (with speed of 10 m/s and 20 m/s) wind is not typical for this area in summer at all (monthly average speed is about 5 m/s).

Let us look at the results of observation of currents in the investigated area. For the first time some strong (about 50 cm/s) flow transporting the sea grass and wood from the Tumannaya river mouth to the southwest was noticed in 1797 during English round-

the-world expedition. The transport of cold waters to the south along the western coast of the sea further (Shrenk, 1874) was described under the name of Liman current. Then (Uda, 1934) instead of one continuous current along the continent three separate currents were distinguished: Liman, Siberian and North Korean. Later Siberian current was renamed to Primorye current. One coastal cold current is torn into two pieces (Primorye current and North Korean current) just near Tumannaya river mouth. The southwestward current between Vladivostok and Possiet Gulf was marked by drift of vessels and bottles many times, for example in May – June of 1939 (Istoshin, 1950).

Results of observation of surface drift of ARGOS floats in 1993–1997 and PALACE floats in 1999–2000 did not show any northward drift north of Tumannaya river mouth.

In summer in the investigated area the southwestward current just near the coast was traced (Lee *et al.*, 1997) usually (Figure 9). In late fall current in opposite direction was traced many times as a curve of the chain of warm eddies (right).

But this current (and warm eddies) never penetrated north of Tumannaya river mouth.

In autumn (August – October of 1993 and August – October of 1994) the surface southwestward drift of floats took place near the coast (with average velocity of 10 cm/s). Surface drift of floats in the opposite

direction in October – December of 1993 and in 1994 passed with smaller velocity (up to 4 cm/s). In the last case the floats did not passed to the north of the Tumannaya river mouth and turned to the southeast without approaching the river mouth area.

Sometimes (July of 1997) the drift of float to the west along 42°N was marked. In winter water from the river mouth area is transported to the southeast usually.

The southeastward current along Northwest front is a more interesting and stable feature of water circulation. It is evident not only for the surface layer (Figure 10), but also for 300°m (Taira, 1997) and 800 m deep (Danchenkov *et al.*, 2000). The analysis of a number of drifting floats showed that from southwestern Peter the Great Bay the water was transported to the southeast along the above described (Figure 10) Northwest thermal front. And the drift in the southeast direction from area of Tumannaya river mouth to the Yamato Rise was traced by the drift of floats more often than to the northeast or southwest.

So it is possible to conclude that current measurements does not show any northward water transport from Tumannaya river mouth.

Any influence of the river run-off is traced not far from the river mouth (Sailing directions, 1972) with a very rare exception. Usually the distribution of fresh water is limited by narrow area close to the river mouth – Figure 11.
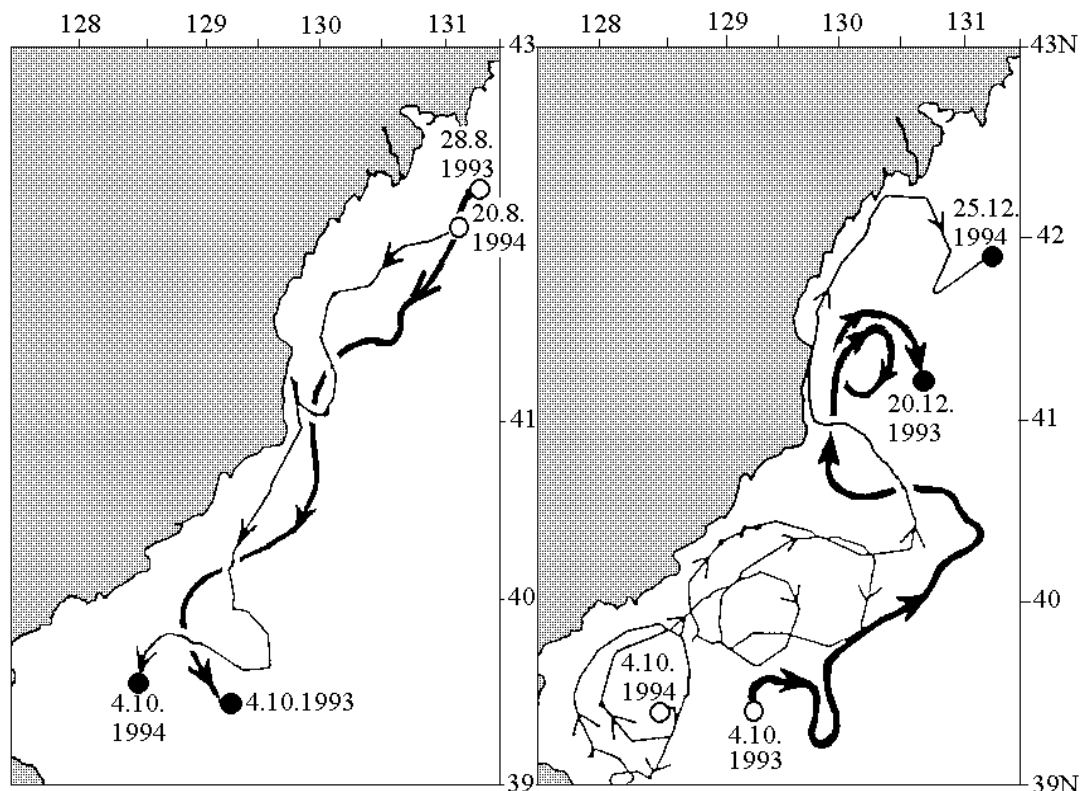

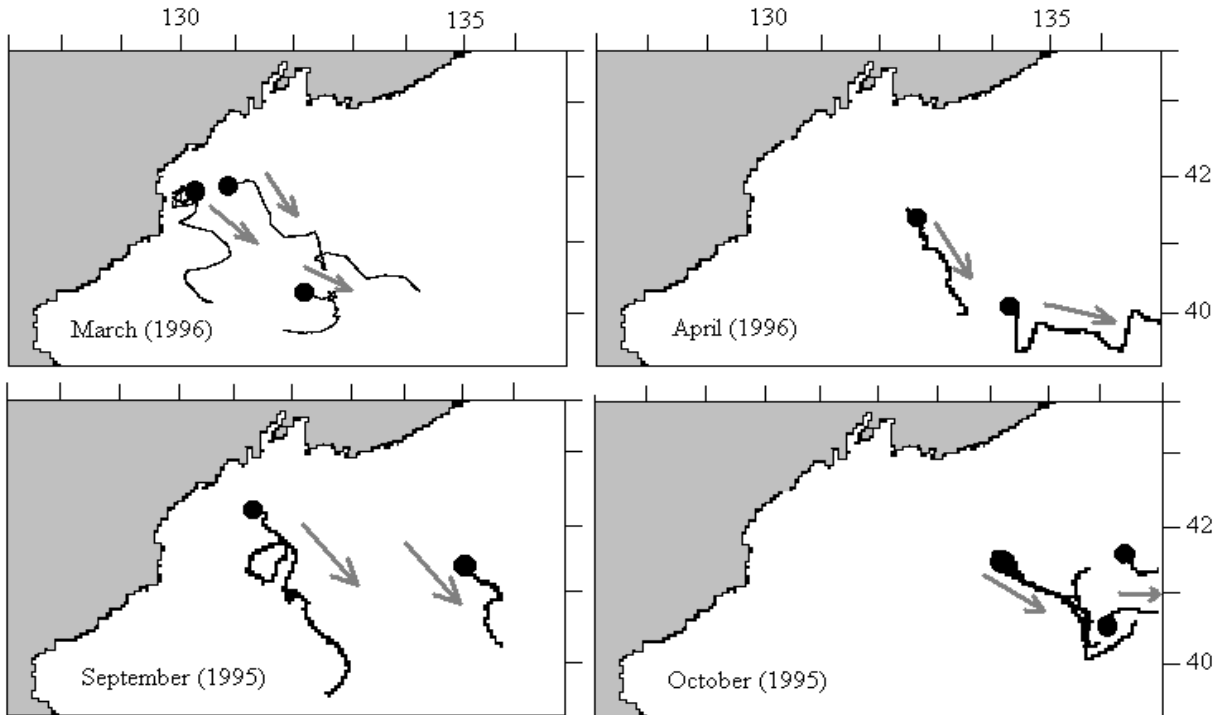**Figure 9. Drift of surface ARGOS floats in 1993-1994**

Figure 10. Drift of surface buoys to the southeast in 1995-1996 (Lee *et al.*, 1997)
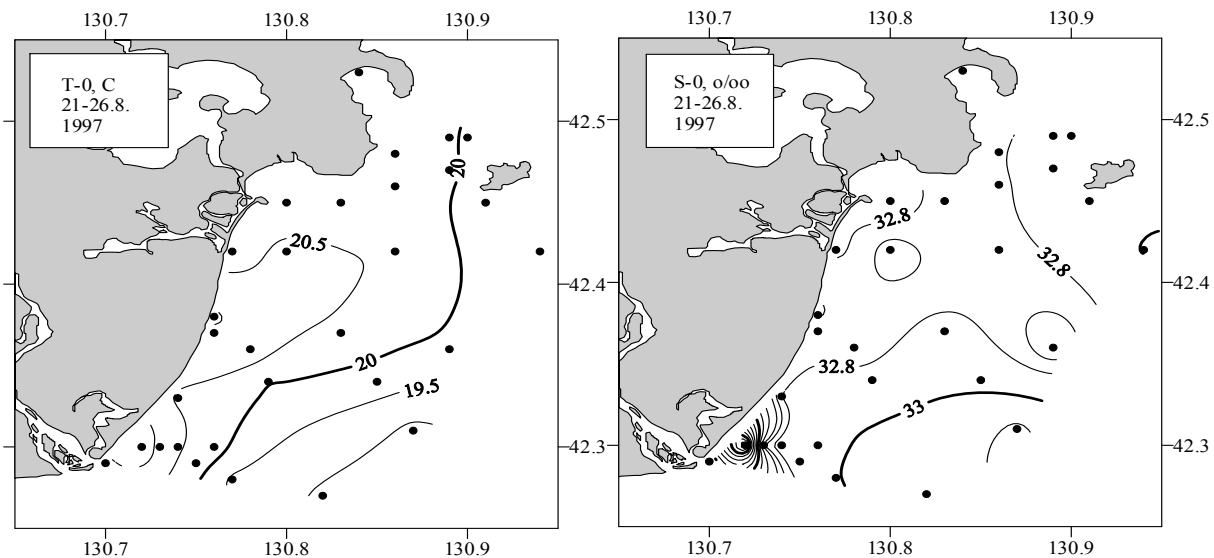

Figure 11. Typical temperature and salinity distribution at surface to the north of Tumannaya river mouth

Except the polluted flow of Tumannaya river there is another source of contamination – waste from numerous ships and from sea ports. In ports there are not any facilities for collection of oil-contaminated waters. There is not any control of ships that pollute the sea bottom Peter the Great bay. Polluted waters (both urban and industrial) are not purified. Any waste from Vladivostok, Slavyanka and Zarubino could be transported by the prevailing current (southwestward) into the investigated area. Concentration of organic matter between Vladivostok and Zarubino is high enough: 120-130 μg/l – in water and 20-30 mg/100 g – in sediments (Rodionov, 1984). Volume of oil-contained waste is about 18,000 t per year (Rodionov,

1984) and of urban polluted waters – about 13,000 t per year that is comparative with the discharge of Tumannaya river.

CONCLUSIONS

1. Basic feature of oceanographic water structure of the investigated area is Northwest thermal front situated between Tumannaya river estuary and Yamato Rise. Intermediate water of low salinity is formed in winter at surface of coastal area close to Tumannaya river estuary.

2. According to the floats drift and salinity distribution, any polluted water from Tumannaya river mouth could be transported mainly to the southeast.

REFERENCES

Danchenkov M.A., Aubrey D.G., Lobanov V.B. **2000**. Spatial water structure of the northwest Japan Sea in winter. FERHRI Special Issue, 3, p. 92–105.

Danchenkov M.A., **Goncharenko** I.A. **1994**. Variation of hydrological characteristics along 132°E in the Japan Sea. CREAMS Proceedings, Seoul, p. 19–22.

Danchenkov M.A., Lobanov V.B., Nikitin A.A. **1997a**. Mesoscale eddies in the Sea of Japan, their role in circulation and heat transport. CREAMS Proceedings, Fukuoka, p. 81–84.

Danchenkov M.A., Nikitin A.A., Volkov Yu.N. Goncharenko I.A. **1997b**. Surface thermal fronts of the Sea of Japan. CREAMS Proceedings, Fukuoka, p. 75–79.

Gorodnichiy A.E. **1949**. The variations of some Primorye fishes stocks in connection to oceanographic conditions. Rybnoye khozyaistvo, 1, p. 36–40.

Grigorieva N.I., Moschenko A.V., Propp L.N., Feldman K.L. **1998**. The study of water transport and oceanographic conditions of an area to the north of Tumannaya river estuary. TINRO Proceedings, v. 123, p. 423–430.

Istoshin Yu.V. **1950**. Currents of the Sea of Japan by bottle drift. Transactions of Central Institute of weather forecasts, 1950, p. 88–131.

Kim C.H., **Kim** K. **1983**. Characteristics and origin of the cold water mass along the east coast of Korea. J.Oceanol. Soc. Korea, v. 18, 1, p. 73–83.

Kos M.S. **1969**. The decreasing of heat-loved elements in plankton of the Possiet bay (the Sea of Japan). Reports of USSR Academy of Sciences, v. 184, 4, p. 951–954.

Lee D.K., Lee J.C., Lee S.R., Lie H.J. **1997**. A circulation study of the East Sea using satellite-tracked drifters. 1. Tsushima Current. J.Korean Fish. Society, v. 30, 6, p. 1021–1032.

Leonov A.K. **1960**. The Sea of Japan. Regional oceanography. Part 1. 291–463 pp.

Miyazaki M. **1953**. On the water masses of the Sea of Japan. B. Hokkaido Reg.Fish.Res.Laboratory, 7, p. 1–65.

Moiseev P.A. **1937**. Fishery of flounders by small-sizes ships in Ussuri bay in spring of 1935. Izvestiya TINRO, v. 12, p. 125–158.

Moschenko A.V., Feldman K.L., Vanin N.S., Yurasov G.I. **2001**. Solid run-off and contaminants distribution as a tracer of wind currents in the area north of the Tumen river mouth (Peter the Great bay, Sea of Japan). Rep. Int.Workshop on the Global change studies in the Far East. Part 1., p. 72–86.

Moschenko A.V., Vanin N.S., Lamykina A.E. **2000**. Bottom relief, bottom sediments and oceanographic conditions of Tumannaya river estuary (Russian EEZ). Ecological conditions and biota of southwestern part of Peter the Great bay and Tumannaya river estuary, p. 42–75.

Novikov N.P. **1957a**. The case of catching of Xesurus scalprum in Primorye waters. Izvestiya TINRO, v. 44, p. 245–246.

Novikov N.P. **1957b**. Diodon holocanthus in the Amurskii bay (the Sea of Japan). Izvestiya TINRO, v. 44, p. 246–247.

Podorvanova N.F., Ivashinnikova T.S., Petrenko V.S., Homichuk L.S. **1989**. Basic features of hydrochemistry of the Peter the Great bay (the Sea of Japan). 201 pp.

Rodionov N.P. **1984**. The Sea of Japan. The forecast of pollution in the USSR seas, p. 118–150.

Rumyantsev A.I. **1951**. New cases of the finding of rare specimen of fishes. Izvestiya TINRO, v. 35, p. 185–186.

Sailing directions of the Sea of Japan. Part 1. **1972**. 288 pp.

Shmidt P.Yu., **Taranets** A.Ya. **1934**. On new elements in ichtiofauna of the northern Sea of Japan. Reports of the USSR Academy of Sciences, v. 2, 9, p. 591–593.

Shrenk L.I. **1874**. On the currents of the Okhotsk, Japan and adjacent seas. **Notes of Russian Academy of Sciences**. Supplement to v. 23, 3. 112 pp.

Taira K. **1997**. Application of the ARGOS system to NEAR-GOOS. ARGOS Newsletter, 52, p. 13–15.

Taranets A.Ya. **1938**. On new findings of southern fishes of the northwestern Sea of Japan. B. Far Eastern branch of USSR Academy of Science, v. 28, 1, p. 113–126.

The basic features of geology and hysrology of the Japan Sea. Moscow, USSR Academy of Sciences. **1961**, 218 pp.

Tkalin A.V. **1999**. Marine environment contamination near Tumangang (Tumen) river mouth. Ocean Research, v. 21, 1, p. 81–86.

Uda M. **1934**. Hydrographical studies based on simultaneous oceanographical survey made in the Sea of Japan and its adjacent waters during May-June 1932. Rec.Oceanogr.Works in Japan, v. 6, 1, p. 19–107.

Vanin N.S., Moschenko A.V., Feldman K.L. **1999**. The modeling of wind currents to the north of Tumannaya river estuary (Peter the Great bay of the Sea of Japan). Marine Biology, v. 25, 2, p. 93–94.

Vanin N.S., Moschenko A.V., Feldman K.L., Yurasov G.I. **2000**. Simplified model of the wind-driven circulation with emphasis on distribution of the Tuman river solid run-off. Ocean Research, v. 22, 2, p. 81–90.

Vinokurova T.T., Skokleneva N.M. **1980**. Temporal variability of the oceanographic conditions in the Possiet bay. TINRO Proceedings, v. 104, p. 29–35.

Vyshkvartsev D.I., **Lebedev** E.B. **1997**. The project of economic development of the Tumangan river – a danger for shallow water bay ecosystem of Posyeta bay, Sea of Japan. Marine Biology, v. 23, 1, p. 51–55.

Yakunin L.P. **1989**. On the water masses of the Sea of Japan. Abstracts of International Conference on the Japan and the Okhotsk Seas, Nakhodka, p. 12–13.

DEVELOPMENT OF THE SUB-REGIONAL SEGMENT OF THE UNIFIED SYSTEM OF INFORMATION ON THE WORLD OCEAN CONDITION OF RUSSIA IN POI FEBRAS

I.D. Rostov, V.I. Rostov, E.V. Dmitrieva, N.I. Rudykh

V.I. Il'ichev Pacific Oceanological Institute, Far Eastern Branch of Russian Academy of Sciences (POI FEBRAS), Russia
Email: rostov@pacificinfo.ru

INTRODUCTION

For the last years, as a result of the wide spread of new computer devices, development of telecommunication networks and application of new information technologies many important problems of accumulation and integration of the large volumes of multi-discipline data sets, provision of the users access to this information and the effective use of information resources have been solved. Considerable progress in this field is provided at the expense of concentration and efficient coordination of studies under the Sub-Program of the Federal Target Program "The World Ocean" developed in 1999–2002 aimed at the creation of the National Unified System of Information on the World Ocean Condition (ESIMO). Functions of the first order for the ESIMO base module are:

- Collection of the operative and historical data and formation of the integrated data base "Oceanography"

- Integration of information resources (metadata, data and information products) on-line and off-line

- Maintenance of the remote user with the metadata and provision of access to data of different types and in different forms of presentation

- Providing the possibility to conduct the assigned list of calculations and acquisition of calculated data

- Preparation and supply of the remote user with the information products.

Such functions should be realized by both the regional centers of the ESIMO and other organizations that are the participants of the Sub-Program. Such information on the realization of this Sub-Program is placed on the official site: http://www.oceaninfo.ru.

Within the bounds of the conception of ESIMO construction in POI FEBRAS the work is being carried out on the creation of ESIMO sub-regional (departmental) segment for placing the general and special information resources to the FEBRAS network and Internet. The goal of the studies being performed is the formation of the regional information fund of ESIMO and provision of the telecommunication access of a wide circle of users to the initial information and products on the problems of studies and exploration of the sea water areas and coastal territories of the region on the basis of the web and GIS technologies. Main objectives of the studies are:

- Formation of the information fund of the sub-system, development and realization of the integrated data bases (DB) on oceanography in the Northern Pacific including the Far Eastern Seas of Russia

- Development of a specialized web-site of POI as an integrated base of the information resources on the sea water areas of the Far Eastern Region of Russia

- Development and realization of the subject electronic information-reference text-books and atlases for their distribution through the telecommunication network and on CDs

- Realization of the calculated-model block, construction of the complex information-analytical system on the state of marine media and resources of the Far Eastern Seas

- Development of GIS on regional oceanography, marine geology and geophysics

- Creation of bibliographical electronic data base.

Below we consider some results of POI activity under the first three objects of studies.

DATA BASE DEVELOPMENT

All available data sets on oceanography were determined and made the informative basis for the integrated DB. Using the relational database management system "Paradox", several local DB and electronic data sets including the comprehensive data base of the archival historical oceanographic data on the Northern Pacific and the DB of all POI cruises are created on the basis of the purposefully developed data model:

- Database of hydrographic observations (national and foreign) in the Northern Pacific (1887–2001, 2 million stations with temperature and salinity) – "Ocean-1"

- Database of observations in POI cruises (1969–2002, 23,000 stations with hydrography, hydrochemistry and hydrobiology) – "Ocean-2"

- Database of archival observations (national and foreign) of currents in the Northern Pacific (1958–

2000, currents velocity and direction, 1,700 moored buoys) – "Ocean-3"

- Data base of hydrographic observations (national and foreign) in the Bering Sea, Sea of Okhotsk and Sea of Japan (1925–2000, 530,000 stations with temperature and salinity) – "Ocean-4"

- POI NEAR-GOOS Delayed Mode data base (1925–2000 – archival hydrographic data, 1995–2002 – delayed mode data of 37 cruises) – "POI NEAR-GOOS DMDB"

- Satellite observation data base

- Sea ice, waves and atmospheric circulation data archives

- Bank of the marine geological-geophysical data – "BANKW"

The technology for integrating the local bases of oceanographic data has been developed. It is based on the principle of generalizing the data elements in the united bases. The complex of programs for executing the typical activities in DB media has been developed. By integrity of the data set completeness, the way of their organization and possibility of rapid access to the archival observation data, the integrated data bases of hydrographic observations ("Ocean-1") and current observations ("Ocean-3") developed at POI FEBRAS do not have analogues in the Far Eastern Region of Russia.

DB systems allow organizing direct access to all stored information and easy manipulation of data for the analysis and visualization. Executing various requests it is possible to receive any information that is presented in the DB to make various calculations, construct the diagrams and pictures illustrating outcomes of the requests and calculations. For the convenience of DB operation a special form for the survey and choice of necessary information is created.

DEVELOPMENT OF THE REGIONAL WEB SITE

As a result of work carried out under the second objective, a new version of the specialized web site of POI FEBRAS titled "Oceanography and Marine Environment of the Far Eastern Region of Russia", which is an independent component of ESIMO, has been developed and put onto Internet in domain www.pacificinfo.ru (Figure 1).

The site contains data on the databases maintained in POI FEBRAS, in the region and in the world, as well as on other available resources and information products on different aspects of regional oceanography, hydrometeorology and ecology of the Northern Pacific and the Far Eastern Seas of Russia. The subject base of access to the external resources on the studied area for obtaining the additional current, diagnostic, and prognostic information has been created.
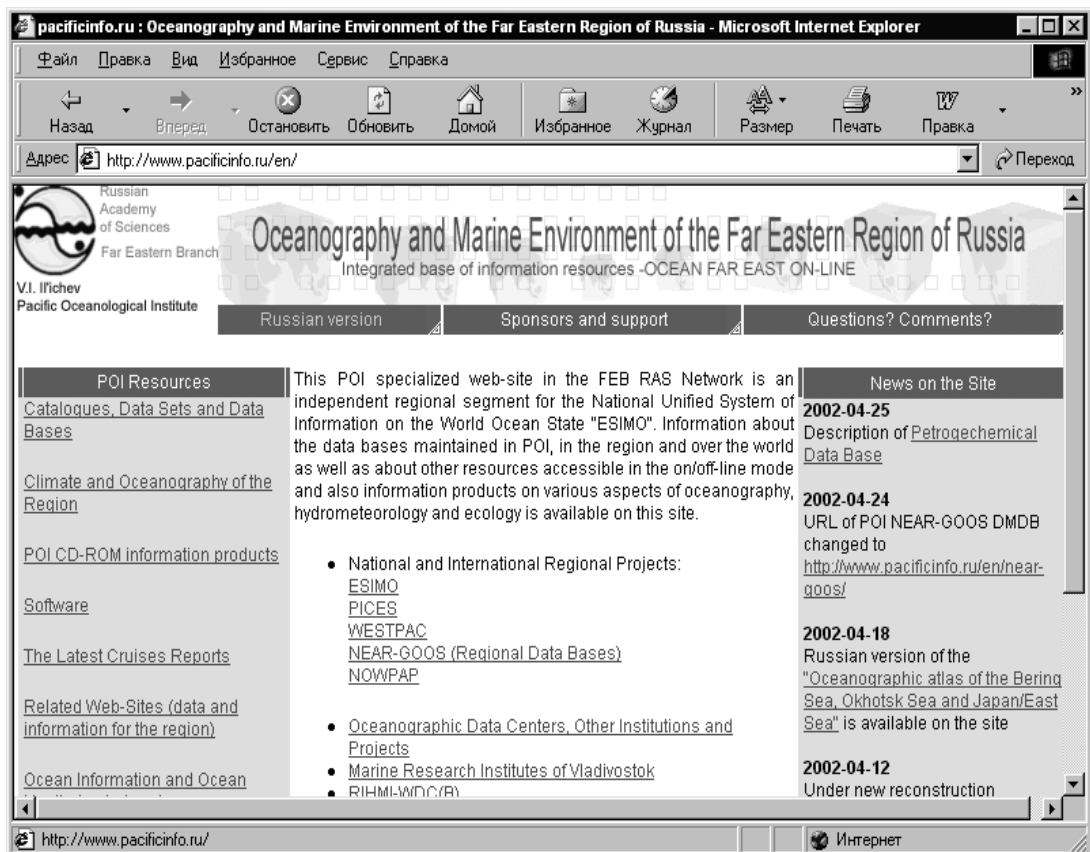

Figure 1. Main page of the POI regional web-site

A new version of the site is done in the fixed display resolution of 800 dots. To create the site the technologies of HTML, JavaScript, PHP, and the data bases of MySQL were used. Application of PHP scripts and MySQL DB gave the opportunity to select the best and the most reliable way of realization of the assigned problems. For instance, to update the information on the site the web-forms can be used.

SOFTWARE AND INFORMATION PRODUCTS

Within the bounds of the third objective the work is being carried out on the creation of special software for oceanographic data users and series of electronic information-reference systems and atlases on CD-ROM under the common title "Information Resources of POI. Oceanography":

- Archival data on cruise studies of POI (1969–2002). (Done in Russian).
- Atlas on oceanography of the Bering Sea, Sea of Okhotsk, and the Sea of Japan. (Done in Russian/English).
- Archival data of observations of currents by moored buoy stations in the Northern Pacific and the Far Eastern Seas. (Done in Russian).

- Atlas on Oceanography and marine environment in the coastal areas of Russia in the Sea of Japan. (In progress).
- Atlas of fishery invertebrates and algae in the seas of the Russian Far East. (Pacific Institute of Geography, POI, Institute of Marine Biology). (In progress).
- CD-ROM containing the components of the archival oceanographic database from all available sources on the Far Eastern Seas and the Northern Pacific. (In progress).

CONCLUSIONS

As a whole, the POI component of system being developed under ESIMO project is aimed at providing the information support and solving a wide circle of problems of fundamental and applied studies in the field of oceanography, hydrometeorology, ecology and the nature use. It can be applied by the system of education, scientific and producing organizations, administrative boards, which activities are related to the use of information on the environment state, exploration of resources of marine and coastal water areas, development of the nature preservation measures, including the force-major situations.

SEDIMENT AND BIOGENIC MATTER ACCUMULATION IN THE SEA OF OKHOTSK

G.-H. Hong

Korea Ocean Research and Development Institute (KORDI), Republic of Korea
Email: ghhong@kordi.re.kr

SUMMARY

Three sediment cores were collected at the western shelf and at the basin (1300 m deep) of the Sea of Okhotsk. Sediment accumulation and sediment parameters were obtained using vertical distribution of excess ^{210}Pb based on one dimensional, two-layer, steady-state constant ^{210}Pb flux, constant sedimentation rate model in which mixing occurs only in the surface mixed layer. Sediment accumulation rate varies from 115 to 212 and 13 mg/(cm^2·yr) in the western shelf and deep basin, respectively. Surface mixed layers varied from 11 to 12 and 10 cm in the shelf and basin, respectively. Mixing coefficient were 4 to 9 and 2 mg/(cm^2·yr) in the shelf and basin, respectively. Particle residence times in the surface mixed layer were *ca.* 50 and 80 years in the shelf and basin, respectively. Steady state excess ^{210}Pb flux to the sediment surface was about 2 to 3 dpm/(cm^2·yr). In the surface sediment, organic carbon concentration varied from 1.0 to 1.2% and 1.4–1.5% in the shelf and basin, respectively. Biogenic silica content varied from 3.4 to 4.2% and 16.5–19.1% in the shelf and basin, respectively. Sediment incorporation of particulate biogenic matter is estimated to be at least 1.8 mg C/(cm^2·yr) and 2.9 mg Si/(cm^2·yr) in the shelf and 0.2 mg C/(cm^2·yr) and 2.2 mg Si/(cm^2·yr) in the basin.

MAIN TEXT

Recent sediment accumulation and mixing rates are among the least known terms of chemical budgets of the Sea of Okhotsk. Knowledge of the chemical budget becomes increasingly important in the Sea of Okhotsk because of the environmental concern of the past Russian dumping of nuclear wastes and an increasing mining and oil exploration in the region. In this paper I report sediment accumulation and mixing rates calculated from excess ^{210}Pb activity profiles collected from 3 sites. These data should establish a set of recent sediment accumulation rates, mean residence times of ^{210}Pb associated particles in the surface mixed layer of the Sea of Okhotsk sediments. Mixing rates provide information on the response time of superficial sediment concentrations to changes in concentrations in the incoming particles.

Box core sediments were collected from the shelf and basin of the Sea of Okhotsk using the R/V "Ocean" (FERHRI, Russia) in August 1995. ^{210}Pb-derived sediment accumulation and mixing rates were calculated based on a one-dimensional, two-layer, steady-state constant ^{210}Pb flux/constant sedimentation model in which mixing occurs only in the surface mixed layer. The sediment accumulation rate of the study area is on the average 164 $\pm$ 68 mg/(cm^2·yr) on the shelf and 13 mg/(cm^2·yr) in the central basin. Accumulation rates are thus apparently up to 16 times greater in the shelf than in the central basin. Since ^{210}Pb-derived sediment accumulation is the combination of advective burial and mixing, ^{210}Pb derived sediment accumulation is usually larger than the long-term sediment accumulation rate beyond the ^{210}Pb-dateable time span due to the high sediment mixing rates.

The entire area of the Sea of Okhotsk is 1.52 x 10^6 km^2, and it is appears that shelf occupies about 30% of the total surface area. Although detailed measurements on the distribution of suspended particulate matter in the sea are poorly known, it is still instructive to establish the broad-brush sediment accumulation budget in the sea using the present data. Combining the areas with average sediment accumulation rates from August 1995 cores gives sediment fluxes of 74 and 14 x 10^{13} g/yr for shelf and basin, respectively. Total depositional flux of sediments over the basin is lower than on the shelf by nearly a factor of 4 due to the high sedimentation rates and extensive development of shelf area in the sea.

In the Sakhalin Shelf organic carbon, nitrogen, and biogenic silica contents are 1.1, 0.16, 3.5%, respectively for the top 25 cm of bottom sediments. There is no systematic downward decrease as observed in most coastal sediments in other regions. In the central basin, organic carbon, nitrogen, and biogenic silica are 1.5, 0.2, and 16.8%, respectively, for the top 25 cm of sediments. Organic carbon, nitrogen and biogenic silica concentrations in the surface sediments are higher in the basin than in the shelf. In the central basin, in situ biological particle formation contributes significantly to the total sediment as indicated by the high content of biogenic silica. Sediment mixing should contribute at least equal amount of advective burial, although diffusive burial could not be estimated due to the lack of decomposition of bulk biogenic matter properties in the upper 30 cm of the superficial sediment on the sea floor in the Sea of Okhotsk.

ARGO PROJECT IN RUSSIA (part 1)

M.A. Danchenkov

Far Eastern Regional Hydrometeorological Research Institute (FERHRI), Russia
Email: danchenk@fastmail.vladivostok.ru

INTRODUCTION

ARGO project is directed at creation of the global standing oceanographic network. For this purpose about 3,000 profiling floats will be deployed in the World Ocean. On coming to the surface from 2,000 m deep every ten days, the float measures pressure, temperature and electric conductivity. The satellite communications system ensures data transmission from the floats to coastal centers and then to the owners of floats. The latter convert data from floats, qualify and process it, calculate water salinity and density and visualize the results. Within 24 hours data are distributed to GTS to be used by operational communities. Within several months the delayed-mode quality control of the collected data is carried out and data are transmitted to one of the two Global ARGO Centers. In every country participating in the project the collected data are available through the ARGO national site and ARGO national center.

Before creation of ARGO system oceanographic data were mostly non-synchronous by time (most of data were obtained in summer) and heterogeneous by location (most of data were collected by the developed countries). Like the new changes introduced in meteorology after the creation of meteorological network, considerable changes are expected in oceanography as well. The creation of the global standing oceanographic network is directed at new science – on-line oceanography. Annually, homogeneous and high-quality data from about 100,000 stations will be included in oceanographic data funds, and this is 10 times as much as the current data flow from oceanographic vessels. It should also be noted that available oceanographic observational data are of different quality depending on the accepted data verification methods and calibration rigs.

ARGO data can be used in all kinds of the ocean conditions research, but they do open fundamentally new possibilities in the long-term weather forecasts.

ARGO FLOATS

Floats of a different origin (manufactured in different countries and time) are used in ARGO project. The older ones allow measuring the water temperature and salinity only, while the newer ones account for the difference in drifting horizon and the lower depth of measurements (2,000 m). In the near future the floats controlled by the onshore computer (to change the surfacing frequency, drifting horizon, measurement discreetness and surfacing duration). There are three kinds of floats used in the project: APEKS, PROVOR and SOLO. Japan is now manufacturing NINZIA floats, while DPRK is developing and India is producing their own floats. All the floats are equipped with sensors of pressure, temperature and electric conductivity, the data being transmitted to the same satellites. The main difference is in the floatability system.

ARGO floats measure the seawater parameters at 2,000 m deep to the surface every ten days. They transmit collected data to the satellite (IRIDIUM satellites are probably to be used soon) and produce 100–150 stations. The float recovery and re-use are not planned.

ARGO DATA

Before the float deployment ARGOS tele-communication system assigns a unique number to it. This number, as well as all necessary parameters (vertical discreetness of observations, drifting time and depth), is entered into the float specifications. The owner of the float determines the deployment location. Collected coded data (pressure, temperature and electric conductivity) are transmitted in portions to several ARGOS satellites. The float is located. The coastal center accumulates data and transmits it to ARGOS center where data are converted, checked and distributed to the owner of the float who is the ARGOS service user. The latter (or ARGO national center) is to carry out the delayed-mode data quality control (using climatic and historical data) within several months. The data are processed, visualized (drifting trajectory, vertical and temporal diagrams) and transported to ARGO regional center. Here they are tested again and distributed to one of the two ARGO global centers.

WORLD ARGO NETWORK

The planned ARGO system is to consist of 3,000 floats. The whole network was expected to be created by the end of 2003, but currently only one third of floats are in operation. As a result, the creation of network is delayed till the end of 2006. The floats distribution in the world ocean is not homogeneous (data are renewed daily by M. Belbokh on ARGO information site www.jcommops.org), floats lacking in southeastern Pacific, around Antarctica and ice-bound seas in the northern hemisphere.

National ARGO Center team

ARGO PROJECT IN RUSSIA

Application of the deep-water profiling floats started in Russia within joint expeditions (Russia-Japan expeditions in the Sea of Japan in 1999 and 2000, Russia-USA expedition in the Sea of Japan in 1999 and Russia-Japan expedition in the Sea of Okhotsk in 2000 and 2001). School of oceanography, University of Washington, USA (prof. S.C. Riser, D. Swift) rendered us great assistance in training and data processing. Thus, even before ARGO project beginning Russia has got necessary knowledge and experience and laid the foundation of the national center of the float data processing.

Since 2001 Russia has taken part in all the meetings of ARGO Scientific Committee and Data Committee.

In 2002 the Russian ARGO national center was established in Vladivostok. Two Russian floats (owned by Russia) were deployed to the east off Kamchatka. The floats were manufactured by WEBB company and tested in University of Washington.

However, the Russian government has not started financing ARGO project yet, thus being different from other developed and developing countries participating in the project (13 countries on the whole). All the activities are performed by the single research institute (FERHRI) supported by Russian federal service for hydrometeorology and environmental monitoring.

RUSSIAN ARGO CENTER

The Russian ARGO center carries out both real (float deployment, connection with ARGOS center, primary control and data processing, site maintenance) and delayed-mode (using the existing database) data quality control.

The national center group is shown in the photo: from left to right – Novikov D.V. (oceanographic calculation), Stadnik V.S. (delayed-mode quality control), Danchenkov M.A. (site maintenance, float deployment, data analysis, connection with ARGO committees), Uraevsky E.P. (head of the Russian ARGO data center), Fadeeva L.A. (software support), Chayka D.D. (database administrator), Uraevsky S.E. (software support). Unfortunately, Volkov Yu.N., who is FERHRI director and the main enthusiast of ARGO project development in Russia, is not in the photo, being searching funds for the project.

VISION FOR THE FUTURE

What are the future prospects of ARGO project in Russia?

We believe they are good. The project is advantageous without any controversy and we hope it will attract other authorities and investments from government. Fishery authorities have already declared their intention to participate in the project. The national ARGO program is considered by governmental bodies.

MODELING OF POTENTIAL OIL SPILL FATE BETWEEN HOKKAIDO AND SAKHALIN ISLANDS

A.A. Bogdanovsky[1], I.E. Kochergin[1], I.A. Arshinov[1], V.D. Budaeva[1], V.G. Makarov[1,2], V.F. Mishukov[3], S.I. Rybalko[1] and V.P. Tunegolovets[1]

[1] Far Eastern Regional Hydrometeorological Research Institute (FERHRI), Russia.
Email: abogdanovsky@hydromet.com

[2] National Politechnic Institute, Mexico

[3] V.I. Il'ichev Pacific Oceanological Institute, Far Eastern Branch of Russian Academy of Sciences (POI FEBRAS), Russia

In 2002-2003 oil spill modeling was carried out for four potential oil spill scenarios in Aniva Bay and La Perouse Strait areas (Table 1). The oil spills near Prigorodnoe village are regarded as a potential result of increasing emergency probability under Sakhalin-2 project development with the planned construction of the oil-refining plant and marine terminal. La Perouse Strait is the area of on-going and projected tanker operations with a higher risk of navigation due to intensive hydrodynamics and strong winds. Korsakov is the largest Russian port in Aniva Bay and here the risk of emergencies is also high. The areas specified are included in the Regional oil spill response plan and regarded as the highly dangerous sites.

The typical hydromet scenarios were constructed using the specific method that had already been successfully applied for the oil spill statistic modeling on the eastern Sakhalin shelf (Kochergin *et al.* 2000a). The method incorporates typification of wind situations at the coastal hydromet stations, reconstruction of wind fields with the help of re-analysis data, calculation of non-tidal currents by a liner baroclinic model, calculation of tidal currents by instrumental data and the final composition of hydromet conditions for the trajectory oil spill modeling.

The typical wind fields were constructed by 15-year data from five coastal hydromet stations (Krilion Cape, Novikovo, Salmon Bay, Korsakov and Kirilovo) and data of the surface wind retrospective analysis (NCEP NOAA). Typical wind situations were chosen by the occurrence table constructed for the hydromet station closest to the oil release point. Typification is based on the combined wind direction and velocity gradations taking into account the regional climatic features, influence of the surface wind on the surface currents formation, frequency of a given situation, oil transport specificity and expert assessments (Table 2). In addition situations with extremely strong wind velocity and rare occurrence were defined. Every wind situation is supported with the average vectors calculated in the points with synchronous measurement series and subsequent interpolation of those vectors in the regular grid for the investigated area.

Table 1

Potential oil spill scenarios in the region of Aniva Bay and La Perouse Straight

##	Spill source	Vol. (t/ths. bar.)	Spill duration (hour)	Oil type	Spill location	Hydrometeo conditions	Quantity of calculated variants
1	tanker accident	5500 /41	0.083 (instantaneous)	crude oil typical for Piltun-Astokh oil&gas field	nearby vil. Prigorodnoye	November climatic conditions and light north wind situation	4 three-day trajectories for different tide phases, 1 ten-day trajectory for light wind situation
2	– // –	– // –	– // –	– // –	region of La Perouse Strait	November climatic conditions	4 three-day trajectories for different tide phases
3	ship accident	300 /2.2	1	mazut, diesel	water area of Korsakov harbour	summer, autumn and winter typical conditions	14 six-day trajectories for typical wind situations, 1 trajectory for extremely strong winds
4	tanker accident	3000 /22	6	crude oil typical for Chayvo oil&gas field	region of La Perouse Strait	summer, autumn and winter typical conditions	16 six-day trajectories for typical wind situations, 1 trajectory for extremely strong winds

Table 2

Example of wind probability table (%) with the wind situations selected for modeling

Grada-tions	Winter								Summer								Autumn							
	N	NE	E	SE	S	SW	W	NW	N	NE	E	SE	S	SW	W	NW	N	NE	E	SE	S	SW	W	NW
Calm	7								10[1]								6							
1-4 m/s	43[1]		8[3]	0.5	1.2	0.4	10[4]	(1)	24[2]			4	19[4]	15[6]		1.6	31[5]			1.4	16[1]			14[2]
5-9 m/s	24[2]			0.2	1.1	0.8		(2)	12[3]			0.8	11[5]			0.3				1.2		3.8	18[3]	2.3
10-14 m/s			0.4		0.1	0.1	1.8		0.2	0.2	0.5			0.3		0.2	0.6	0.5	1.0	0.4	0.9	1.2		0.3
15-19 m/s	0.3	0.3	0.2			0.2						0.1						0.1				0.1		0.1
20-24 m/s	0.1	0.1	0.1									0.1											0.4[4]	
25-29 m/s																								

Notes:
wind situations selected for modeling are marked with gray background;
wind situation #4 for autumn period is not typical and is selected to assess oil spill fate in extremely strong wind conditions;
the wind situations codes are presented in parentheses, names of situations are:

	Winter		Summer		Autumn
(1)	light NW-N-NE winds	(1)	calm	(1)	light and moderate S winds
(2)	moderate and strong NW-N-NE winds	(2)	light N-NE-E winds	(2)	light SW-W-NW winds
(3)	light and moderate E winds	(3)	moderate N-NE-E winds	(3)	moderate and strong W winds
(4)	light and moderate W winds	(4)	light S winds	(4)	extreme strong W winds
		(5)	moderate S winds	(5)	light and moderate N-NE-E winds
		(6)	light and moderate SW-S winds		

Hydrodynamic calculations using the Ekhman-type linear baroclinic model (Budaeva and Makarov, 1999) resulted in the construction of diagnostic current schemes for each selected wind situation. Water density fields were constructed by the historical oceanographic data sets (RODC FERHRI, 1948-1992) and data of the hydrological surveys in Aniva Bay conducted by SakhNIRO in 2002.

Tidal current fields were calculated by extracting harmonic constants out of the series of instrumental current observations and interpolating them into the regular grid with account of spatial variability of 6 main harmonics amplitude and phase.

The oil fate in the sea was modeled by VOS 3 model developed in FERHRI (Kochergin *et al.* 2000b). Output results include the oil transport trajectories with oil location specified in time (Figure 1) and other characteristics. The modeling results allow estimating the most probable oil transport trajectories under the summer, autumn and winter (no ice case only) conditions. Oil weathering processes (evaporation, dispersion, emulsification, etc.) were assessed using POI FEBRAS model (Michoukov and Abramova, 1997) and ADIOS II model developed in NOAA and MMS.

The following conclusions were made by the modeling results for the statistically reliable situations. In case of the oil spilled in the northern part of Aniva Bay in summer, the oil will be transported to the open sea waters to the south (over 60% probability), though the oil beaching under the southern winds is also likely (about 30% probability). In autumn the oil will be transported either to the east of the bay under the western winds (over 30% probability) or to the south under the northern winds (about 30% probability). Oil beaching in the north of the bay is also probable (about 15% probability) under the southern winds. In winter the oil will be transported to the south (75%) and the south-east (10%). The current tidal phase is not significant for the oil spills in the north of Aniva Bay as the tidal current velocity is low.

Modeling of the potential oil spills in La Perouse Strait shows that in summer the oil will be transported towards the Sea of Okhotsk with the oil transport along Hokkaido Island or oil beaching on it (50%) or oil transport to the south of Aniva Bay (35%). In autumn the oil may be transported towards the Sea of Japan (30%) or to the east (60%) but unlike the summer results the oil is not transported to the coastal zone of Hokkaido Island within 6 days. Oil transport to Aniva Bay is 9% probable only, in rest of the cases oil is transported to the east. In winter the oil is transported to the Sea of Japan (about 35% probability), in rest of the cases the oil is transported to the south-east parallel to the coast of Hokkaido Island. It should be noted that the current tidal phase is of great significance here as the tidal current velocity may amount to 2 m/s (both in the eastern and western direction). This is especially critical for oil spill response plan development.
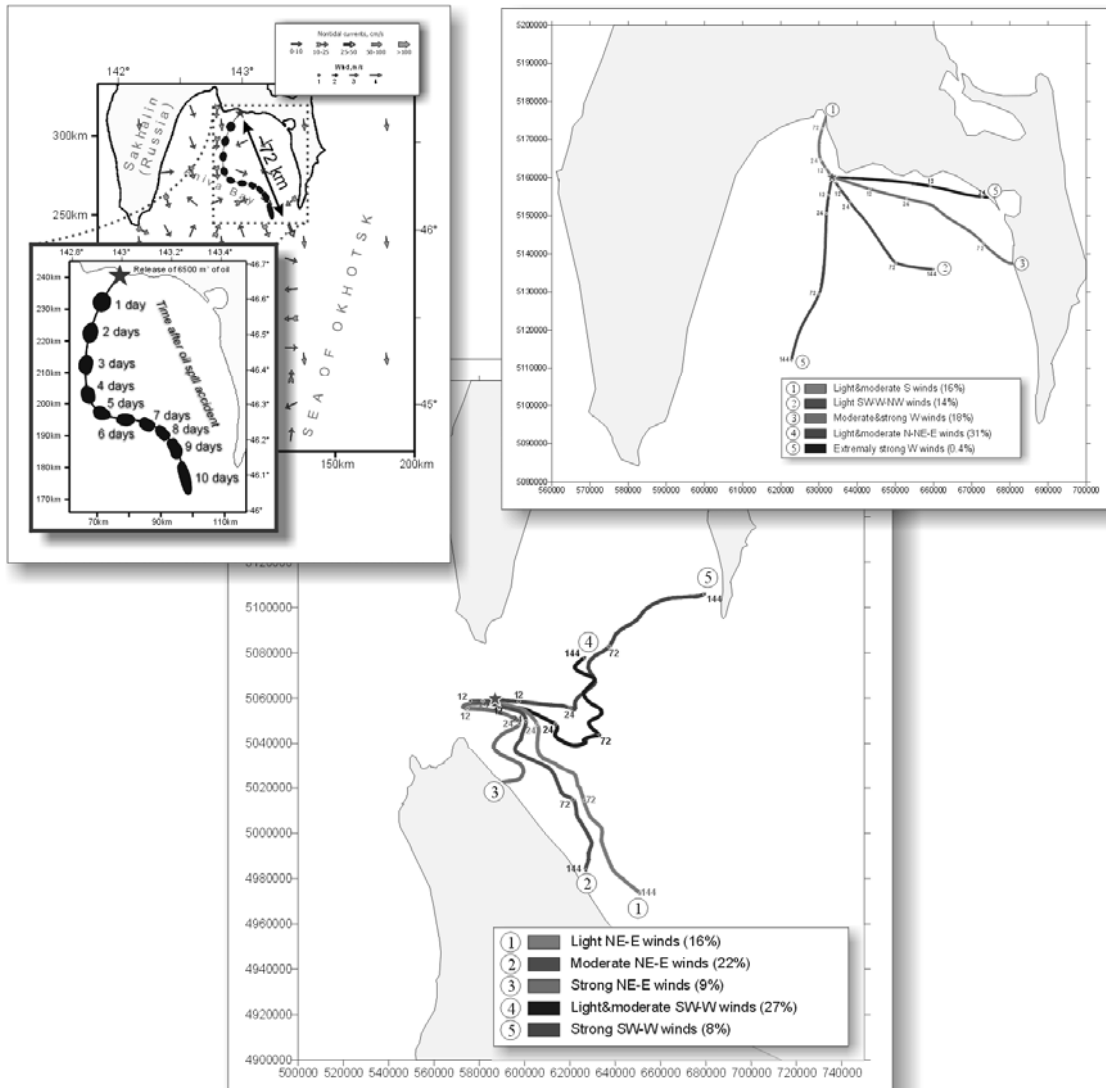
Figure 1. Example of potential oil spill trajectory modeling results: (a) spill nearby vil. Prigorodnoe (light north winds situation), (b) spill in the water area of Korsakov harbour (autumn typical and extremely strong winds situations) and (c) tanker accident in the La Perouse Strait (summer typical winds)

REFERENCES

Budaeva V. D., **Makarov** V. G. **1999**. Peculiar water regime of currents in the area of Eastern Sakhalin shelf. Proceeding of the Second PICES Workshop on the Okhotsk Sea and Adjacent Areas. 12, p. 131–138.

Kochergin I. E., Bogdanovsky A. A., Budaeva V. D., Varlamov S. M., Dashko N. A., Makarov V. G., Putov V. F., Rybalko S. I. **2000a**. Construction of hydrometeorological scenarios for environmental impact assessments. FERHRI Special Issue No. 3. Vladivostok: Dalnauka, p. 223–240.

Kochergin I.E., Bogdanovsky A.A., Mishukov V.F. & Putov V.F. **2000b**. Oil spill scenario modeling for Sakhalin shelf. Proceedings of WITpress "Oil and Hydrocarbon Spills II", p. 39–50.

Michoukov V., **Abramova** O. **1997**. Experimental Study of Oil Degradation in the Sea of Okhotsk. Proceedings of International Marine Science Symposium on "Biogeochemical Processes in the North Pacific" (1996), Mutsu, Japan, November 12-14, 1996, Published by Japan Marine Science Foundation, Tokyo, March, 1997, p. 376–391.

THE CURRENTS MODELING FOR PETER THE GREAT BAY
ON THE BASE OF FERHRI SURVEY, 2001

P.A. Fayman

Far Eastern Regional Hydrometeorological Research Institute (FERHRI), Russia
Email: pfayman@hydromet.com

Peter the Great Bay PGB of the Japan Sea (Figure 1) is distinguished with the intensive cargo and passenger shipping and active coastal activities. Therefore, the area draws continuous attention to the study of water physical and chemical parameters and sea currents.

The first attempts to calculate the sea currents in PGB by instrumental observation series started in the 19th and early 20th centuries, the results being generalized in (Belinsky and Istoshin, 1950). The current schemes constructed over instrumental data of 1930–2000 period are summarized in sailing directions and described in (Yurasov and Yarichin, 1991). Mathematic modeling of Peter the Great Bay currents is shown in (Savelieva, 1989). Here she used a linear nonstationary model based on the shallow water equations and calculated currents for Ussuriyskiy and Amurskiy Bays. Savelieva made the conclusion about the Ussuriyskiy Bay anticyclonic circulation under the constant northern winds (in winter) and cyclonic circulation under the constant southern winds (in summer). In Amurskiy Bay the surface currents structure depends on the wind direction: southern wind causes flowing to the north, and vice versa. The specialists of the Institute of Marine Biology FEBRAS also investigated the currents in PGB under Tumen river project.

Thus, there are no enough data on the currents structure in Peter the Great Bay that would depict the synoptic variations of wind, tides, river discharge, baroclinic effects, etc. For the purpose of filling this gap the Far Eastern Regional Hydrometeorological Research Institute (FERHRI) developed the program on experimental hydrological observations under differing atmospheric conditions and seasons. The water circulation scheme is supposed to be modeled over the registered hydrological parameters and instrumental current observations.

The present report informs of the PGB currents modeled over instrumental data of two surveys (summer and autumn 2001). The surveys were made under steady wind regime (homogeneous wind situation 2–3 days before and during the survey) to calculate exact currents that form under the influence of typical summer and autumn winds.

The expedition was aimed at getting the sea water temperature and salinity profiles at 113 oceanographic stations and making short-term current instrumental observations. Two research vessels – "Pavel Gordienko" and "Hydrobiolog" – were involved. The summer survey was organized on August 15–19, 2001 under the steady southern winds and the autumn one – on November 14–18, 2001 under the steady northern winds. Hydrochemical water parameters were measured with CTD AST-1000S, CTD FSI and CTD NEIL BROWN sones.
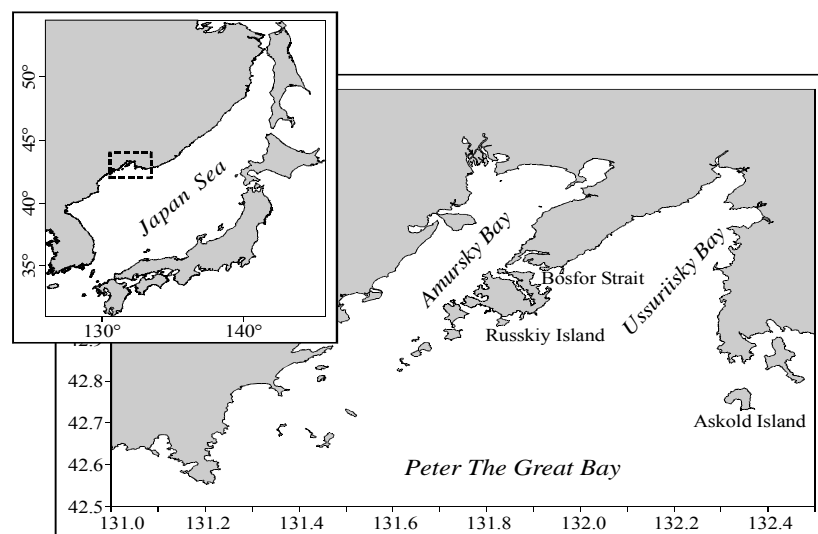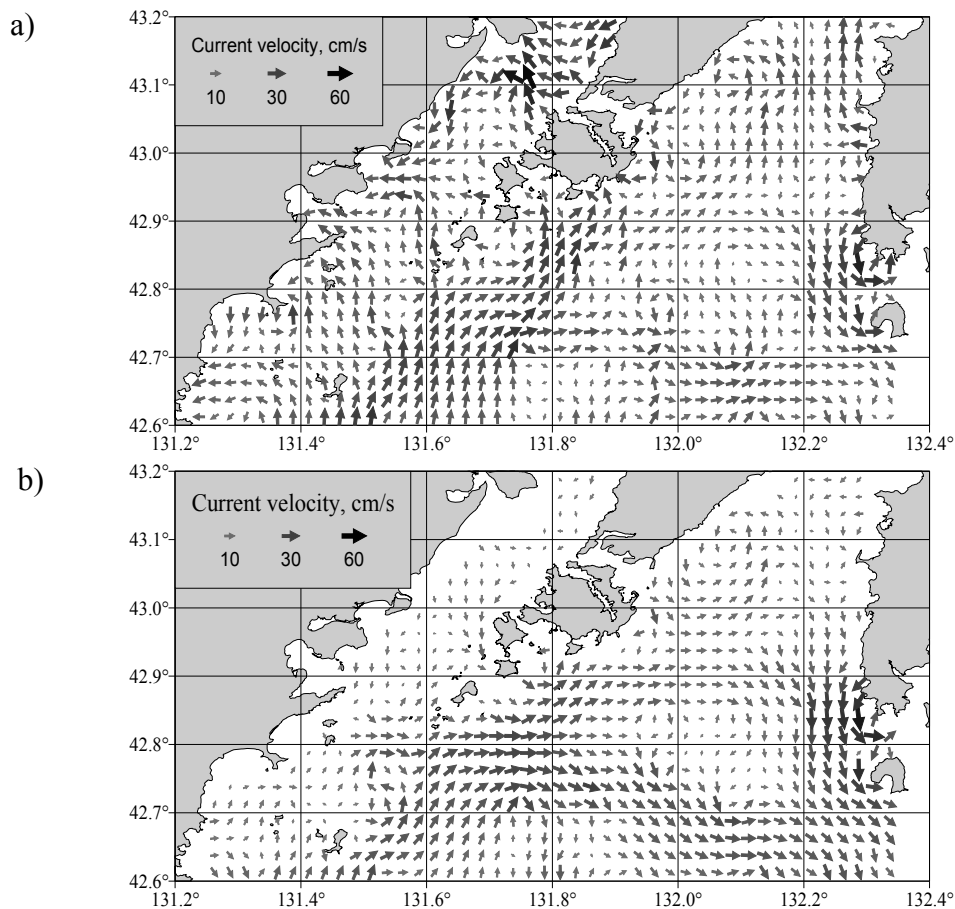

Figure 1. Peter the Great Bay

a)

b)

Figure 2. Sea currents in August (a – at the surface, b – at the depth of 10 m).
Velocity scale (cm/s) is on the left

In the sea currents modeling over the reconstructed density fields the Sarkisyan's diagnostic and baroclinic D1 model was used (Marchuk and Sarkisyan, 1988; Sarkisyan, 1977). The modeling equations had the numerical solution that is the second order accurate, data being extrapolating according to Richardson (Marchuk and Shaidurov, 1979; Marchuk, 1989). Components of the sea current velocity were calculated in every point of orthogonal grid and every one meter deep.

The water circulation schemes modeled for 0 and 10-meter horizons over experimental data are shown in Figures 2 and 3.

The summer current structure is the following: the flow of water enters PGB from the south, the flow velocity amounting to 20–25 cm/s. One part of the flow enters Amurskiy Bay, while another one goes to Ussuriyskiy Bay and branches out.

The first branch deviates in the center of PGB, turns to the south-east and goes along the southern boundary of investigated area, velocity of the flow amounting to 10–15 cm/s. The second branch deviates southward of Russkiy Island, turns to the east to Askold Island (velocity of this flow amounts to 10 cm/sec) and comes across the first

branch. The rest of the flow turns to the north (15 cm/s) and forms the cyclonic ring in Ussuriyskiy Bay. Part of the flow enters Bosfor Strait and goes to Amurskiy Bay. In northeastern part of Ussuriyskiy Bay the density field becomes adjusted to the southern wind and the currents flow to the north (10–20 cm/s). In Amurskiy Bay northward of 43°NL the currents flow to the south, except the intensive stream (up to 30 cm/s) along the western coast of the bay. The latter is formed by the flow from Bosfor Strait (Figure 2).

Currents reconstruction in November survey shows that the anticyclonic eddy found in the center of investigated area moves to the north-east and is observed in the eastern part of PGB. The depth of the eddy is 50 meters like in summer. The current velocity in the eddy ranges from 15 to 30 cm/s. The strongest currents are registered around Askold Island, the flow velocity amounting to 40 cm/sec. The branch of this eddy forms the anticyclonic circulation in Ussuriyskiy Bay with the flow velocity at surface of 10-20 cm/s and 30 m depth. In Amurskiy Bay the predominant surface currents are the southern currents under the northern winds with the flow velocity of 10-15 cm/s (Figure 3).
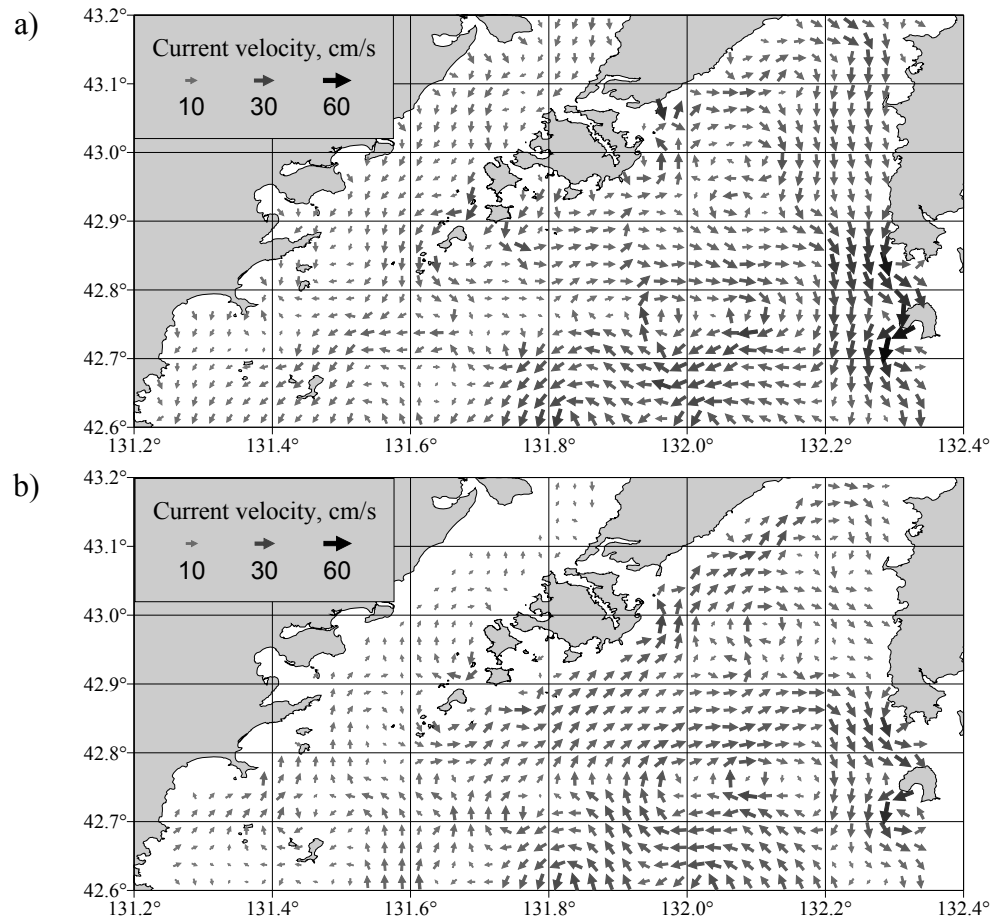
Figure 3. Sea currents in November (a – at the surface, b – at the depth of 10 m).
Velocity scale (cm/s) is on the left

CONCLUSION

The surface currents in PGB are largely subject to the influence of wind. Deep currents structure is dependent on water discharge at water boundary of investigated area. The primary features of PGB circulation are the anticyclonic ring with the center being located in the central part of the bay in August and westward of Askold Island in November; and circulation ring in Ussuriyskiy Bay that changes it direction from cyclonic to anticyclonic under the changing predominant wind. The obtained results are in compliance with the generally accepted water circulation structure in PGB.

The following FERHRI specialists participated in the development of the research program and organization of the expedition: Yu.N. Volkov, A.F. Scherbinin, I.E. Kochergin, V.A. Luchin, A.E. Rumyantsev, V.N. Kraynev, S.I. Rybalko, V.D. Budaeva and crew members. The author expresses his sincerest gratitude to Vitaliy G. Yarichin, Senior researcher of IACP FEB RAS, for brief information on the main Peter the Great Bay water circulation elements.

REFERENCES

Belinsky N.A., **Istoshin** Yu.V. **1950**. The Primorsky Current by data from Rossinante schooner expedition 1936. Proceedings of CIP, 017, p. 132-143 (In Russian).

Marchuk G.I., **Sarkisyan** A.S. **1988**. Mathematic models of the ocean circulation. (In Russian).

Matchuk G.I., **Shaidurov** V.V. **1979**. Increasing the accuracy of difference scheme solution. (In Russian).

Marchuk G.I. **1989**. Calculus mathematics methods. (In Russian).

Savelieva N.I. **1989**. The general water circulation scheme for Amurskiy and Ussuriyskiy Bays made over numerical modeling results. (In Russian).

Sarkisyan A.S. **1977**. Numerical analysis and forecast of the sea currents. (In Russian).

Yurasov G.I., **Yarichin** V.G. **1991**. The currents of the Sea of Japan.

THE FORGOTTEN NAMES

M.A. Danchenkov[1], A.A. Bobkov[2]

[1] *Far Eastern Regional Hydrometeorological Research Institute (FERHRI), Russia*
   Email: danchenk@fastmail.vladivostok.ru

[2] *Saint-Petersburg State University (SPSU), Russia*

INTRODUCTION

Among the bitter heritage of the past the lost connection of generations is the most grievous, especially in the field of scientific researches. For example, FERHRI considers its history from 1950 (see 50th Anniversary FERHRI Proceedings, 2000). However, in 1929-1934 its predecessor – Far Eastern Geophysical Institute (DALGEOPHYZIN) – was located in that same building. It dealt with the scientific problems FERHRI is engaged in now, but also conducted researches on geophysics and geology of Russian Far Eastern seas. DALGEOPHYZIN published the scientific journal "Geophysics". Stalin's repressions not only stopped the oceanographic researches in Vladivostok, but also put an end to the connection of two institutes. As a result, many regional oceanographers are forgotten.

Even FERHRI research vessels are named mostly either after the specialists and scientists from Moscow and Leningrad (Korolev, Shirshov, Voeikov, Shokalsky, Khromov, Frolov, Gordienko) or bear inanimate names: Priliv (tide), Priboy (surf), Okean (ocean), Volna (wave).

Sharing the belief of the Russian national poet Pushkin A.S. ("the relation to the past distinguishes a cultural man from a wild one"), we do not want to refuse from our scientific heritage. For this purpose there is the scientific museum created in FERHRI and we are trying to restore the institute history.

In the historical section of Pacific Oceanography journal we are going to remember the Russian scientists who investigated the Russian Far Eastern seas. Special papers will be devoted to oceanographers of DALGEOPHYZIN (Gomoyunov K.A.) and FERHRI (Batalin A.M., Biryulin G.M., Veselova L.E., Supranovich T.I.). Our journal is open for memories of scientists of other institutes as well. Such papers will require more time for preparation than professional papers but our duty to the forerunners obliges us to do that.

We begin the history section by our first paper about the oldest regional oceanographer Maidell E.V.

EDUARD VLADIMIROVICH MAIDELL

Maidell E.V. – major-general of the Corps of the Naval Navigators – was the first Russian Far Eastern oceanographer. He was born in Nemirov of Podolsk province and died in Gelsingfors (Helsinki) far from his native land. For 36 years of his activities (he retired on a pension because of illness) he either himself or among other activists founded the Russian weather forecasting service and meteorological stations in the Russian Far East and prepared the navigation maps for the Japan, Black, White, and Baltic seas.

Brief biography:

08.11.1842:	born
1856:	entered the Naval cadet Corps
1862:	graduated with the promotion in naval cadet rank
1862–1864:	participated in navigation in the Baltic Sea
1864:	entered the midshipman rank
1864–1866:	participated in navigation in the Atlantic ocean
1866–1868:	studied the academic course of marine sciences (predecessor of the present Naval academy)
1868:	entered the lieutenant rank
1870:	carried out the meteorological and magnetic measurements in the Barents and North Seas
1872–1874:	organized the Russian service of weather forecast
1874:	appointed to the Siberian small fleet
1875:	founded meteorological stations in Vladivostok, Nikolaevsk and Korsakov
1876–1878:	as the head of hydrographic party investigated the Amur river gulf, the northern part of Tartar Strait, currents in the Japan Sea, Peter the Great Bay, and La Perouse Strait
1878:	entered the lieutenant-captain rank; the head of hydrographic survey of the whole Russian coast of the Japan Sea
1879:	transferred to the Baltic Sea fleet
1880:	transferred to the Black Sea fleet (Nikolaev)
1883–1885:	the head of hydrographic survey of the Caucasian coast of the Black Sea
1885:	entered the captain 2 rank
1885–1887:	the head of hydrographic survey of the northern coast of the Black Sea
1887–1991:	the head of hydrographic survey of the White Sea
1890:	entered the colonel rank of Admiralty
1892–1893:	served in the Corps of the Naval Navigators

1894–1897:   the head of hydrographic survey of the Russian Pacific

1896:   became the major-general

1897:   transferred to the Baltic Sea fleet

1898:   retired

12.06.1918:   died

Maidell E.V. left his wife and two sons in revolutionary Russia (37 and 31 years old, both got education in Naval cadet Corps like their father). Their destiny is unknown (in 1928 Maidell's wife was living in of the Soviet villages) but, most likely, is sad.

Though Maidell is often referred to as the first Russian weather forecaster (Ioselev, 1969) or meteorologist (Khisamutdinov, 2001), his papers on regional oceanography allow us to regard him as the first Russian Far Eastern oceanographer. He was supervising the hydrographic surveys in primary Russian Seas as the oceanographer and all his life he was writing papers on oceanography.

Maidell wrote about 50 papers and short notes that were published in the basic Russian oceanographic journals ("Notes on hydrography" and "Marine bulletin"). Even now his papers on water upwelling, Kuroshio, Peru, Liman currents and North Polar ocean navigation are of great interest. It is Maidell (and not Makarov S.O. according to Batalin, 1968) who investigated in details the origin of Liman Current and showed that it had no connection with Amur river run-off.

Maidell's works devoted to Krillion Current are especially interesting. Even today Krillion Current is poorly investigated. Onatsevich M.L. (1877), for example, refutes its existence: "low water temperature in northern La Perouse Strait is the consequence of the cooling influence of the coast". The well-known book of the famous oceanographer Makarov S.O. describing La Perouse Strait contains no references to Maidell's papers. Therefore, we think it appropriate to cite here Maidell's main conclusions about Krillion Current:

- "When approaching to Krillion Cape the bottom waters gradually go from the depth of 80 fathom up to 25 fathom and consequently will show that water temperature near Krillion Cape is lower than near Aniva Cape".

- "There are two currents in La Perouse Strait. The warm one washes the Soya Cape and occupies a wide part of La Perouse Strait to the south off the Stone of Danger. The second current is the cold one, it goes from the Okhotsk Sea into the Japan Sea between the Stone of Danger and the Krillion Cape. When turning round the cape, it quickly turns to the north. The tidal currents change the strength and direction of the constant cold current".

Main Maidell's papers about the Krillion Current:

Magnetic and hydrological works in the East ocean. Morskoi sbornik, 1877.

Additional data on the cold current in La Perouse Strait. Morskoi sbornik, 1879.

Cold water spots in La Perouse Strait. Morskoi sbornik, 1880.

Meteorological and hydrological observations in the East ocean. Morskoi sbornik, 1880.

Papers and short notes about Maidell E.V.:

Das freiherrliche Geschlecht von Maidell. Helsingfors, 1868, p. 385–396.

Das freiherrliche Geschlecht von Maidell. Neval, 1895, p. 106–108.

Ioselev Ya.Kh. The first Russian weather forecaster. Meteorology and hydrology, 1969, 10, p. 109–113.

Maslennikov B.G. The first Russian weather forecaster. Krasnoye znamya, 27.1.1972.

Tcherkashin V. The first Russian weather forecaster. Vodnyi transport, 21.11.1987.

Bolgurtsev B.N. The name on a map of Pacific ocean. Vinnitskaya pravda, 17.8.1988.

Gruzdev A.I. Coastal line: the name on a map. Vladivostok, Dalnauka, 1996, p. 116–117.

History of hydrographic service of the Russian navy. Saint-Petersburg, 1997, p. 205–206.

Khisamutdinov A.A. Meteorologist baron Maidell. "White sails on the East Pomorye". Vladivostok, FESU, 2001, p. 125–128.

REFERENCES

Batalin A.M. **1968**. Scientific results in the Russian Far East for 50 years of the Soviet authority. Oceanography. Vladivostok, Siberian branch of USSR Academy of Sciences, 103 pp. (In Russian)

Onatsevich M. **1877**. On currents in La Perouse Strait. Marine bulletin, 2, p.25–32.

50th Anniversary FERHRI Proceedings. **2000**. Vladivostok, Dalnauka, 257 pp. (In Russian)

FOR AUTHORS

GENERAL

- Papers submitted must not been published previously and not be under consideration for publication elsewhere.
- Materials submitted must be in English only. The Editors have the right to reject the paper in case its level of English is poor.
- Publication in 2003 is free of charge, but any financial support is welcome (to cover partially the costs on paper review, technical editing and publication).
- Authors should submit an electronic copy of their paper, as well as two hardcopies to the Editorial Office.
- Authors should subscribe the paper for publication.
- The paper should start with Title and Authors and Abstract.
- The following information about authors should be attached: Name, Degree, Institution, Postal Address, Telephone Number (with Country and Region code), E-mail Address. The corresponding author should also be identified.
- Paper Length, including figures and tables, should be confined to no more than 10 pages. Papers, the length of which exceeds 10 pages, will be accepted for publication upon Editors' decision.
- References to unpublished results that are used for argumentation are not permitted.
- The Editors reserve the right to adjust style to certain standards of uniformity. The papers are reviewed and may be accepted for publication, recommended for revision, or rejected upon Editors' decision.

FORMAT INSTRUCTION

- Hardcopy of the paper must be of A4 sheet size. Font size of no less than 12 pt, 1.5 line interval and left and right margins of 3 cm are required.
- Electronic copy of the paper should be provided on a 3.5" diskette, CD-R, CD-RW etc. or submitted by e-mail.
- Text and Tables – Text and tables should be provided in any of the following formats: Microsoft Word (.DOC), Rich-Text Format (.RTF), TeX Format (.TEX).
- Formulas and Equations – Formulas and equations should be provided as Microsoft Equation objects in Microsoft Word, RTF, or TeX Formats (with rare exception, formulas and equations are allowed to be written down on paper by hand but in distinct block letters).
- Illustrations – All figures, charts and photographs should be provided in electronic form and must be of a good quality, suitable for a high-resolution grayscale print.
- Units – International System of Units (SI System) should be used as far as possible. If other units are used, the metric equivalents must be given in parentheses, or the correct conversion factor must be presented in a footnote.
- Fractional part is separated from integer one with a dot.
- A list of references should be arranged alphabetically following the text of the paper. References should be given in the following form:

  > **Boetius** A., **Lochte** K. **1994**. Regulation of microbial enzymatic degradation of organic matter in deep-sea sediments. Marine Ecology Progress Series, vol. 104, p. 299–307.

  > **Green** A. **1991**. Deformations in Acanthaster planci from the Coral Sea, observed during UEA Special Project 7, July 1978. Journal of Pollution Research, vol. 14, 7.

  > **James** Z. **1997**. Ecological effects of sea wall construction during 1994 at Bridlington, UK. Listserver Message, Eco-list, 20 October 1995.

  > **Jones** P. **1996**. Research activities at Smith Technology Institute. WWW Page, http://www.sti.com/about_us/research.

  > **Leonov** A.K. **1960**. The Japan Sea. Regional oceanography. Moscow: Hydrometeoizdat. p. 292–463. (In Russian)

  > **Moustakas** N. **1990**. Relationships of morphological and physicochemical properties of Vertisols under Greek climate conditions. Ph.D. Thesis, Agricultural Univ., Athens, Greece.

- In the text refer to the author's name (without initials) and year of publication, for example:
  (Boetius and Lochte, 1994; Walker *et al.*, 1999; Jones, 1996; Green, 1991).